Università degli Studi della Tuscia di Viterbo

Dipartimento per la innovazione dei sistemi biologici, agroalimentari e forestali

Corso di Dottorato di Ricerca in

Scienze, tecnologie e biotecnologie per la sostenibilità - **XXXIV ciclo**

Extraction and characterization of lignins and their application in the development of biobased products

Settore scientifico-disciplinare
SSD AGR/06

Tesi di dottorato di:
Dott. Sara Bergamasco

Cordinatore del corso
Prof. Andrea Vannini

Tutore
Prof. Manuela Romagnoli

Cotutore

Prof. Giuseppe Scarascia Mugnozza

A.A. 2023/24

UNIVERSITÀ DEGLI STUDI DELLA TUSCIA

DEPARTMENT FOR INNOVATION IN BIOLOGICAL, AGRO-FOOD AND FOREST SYSTEMS

PhD course in

Sciences, Technologies and Biotechnologies for Sustainable

XXXVI° Cycle

Extraction and characterization of lignins and their application in the development of biobased products

SSD AGR/06 – Wood Science and Harvesting

PhD candidate

Sara Bergamasco

Phd course coordinator

Prof. Andrea Vannini

Supervisor

Prof. Manuela Romagnoli

A.Y. 2023/2024

Summary

Extended abstract

Abstract

With the advent of biorefineries, the valorization of lignins has become an integral part of a more sustainable approach to the production of bio-based chemicals and high-value materials. Long considered a waste stream of the pulp and paper industry, this doctoral work aims to highlight industrial lignin isolation processes and green biomass fractionation techniques that are more environmentally friendly in order to obtain a lignin product with the highest achievable degree of purity. The lignins used in this study include an industrial Organosolv lignin from beech wood supplied by Fraunhofer Center for Chemical-Biotechnological Processes CBP (Leuna, Germany) and two lignins extracted in the laboratory using two different isolation techniques, namely acidolysis and ionic liquids, respectively. The comparison between these two methodologies allowed to highlight structural differences resulting from the different isolation techniques. Another important aspect of this work concerns the application of both industrial and extracted lignins. For this purpose, lignins have been used in the development of coating materials, specifically for wood coatings. Organosolv lignin was employed as a structural analogue of a polyol for the synthesis of polyurethane materials. In the second nanotechnological application, acidolysis lignin was used to create a nanocoating via electrospraying for the control of wettability and antibacterial activity of polycaprolactone (PCL) membrane surfaces produced via electrospinning technology. These membranes are intended for water treatment applications.

Keywords: lignin, organosolv, acidolysis, ionic liquid, chemical characterization, coatings, polyurethane, electrospinning

Structure of thesis

Chapter 1: Synthesis and Characterizations of Eco-Friendly Organosolv Lignin-Based Polyurethane Coating Films for the Coating Industry.

This work served as a screening phase to assess the feasibility of using lignin in the production of polyurethane-based coatings. An Organosolv lignin was employed as a polyol in the polyaddition reaction with Desmodur®L75, a mixture of aromatic polyisocyanates. By varying the weight ratios between lignin and the isocyanate mixture, three different formulations were created. The polyurethane coatings were then applied on beech wood specimens measuring 15 x 15 x 3 mm. Subsequent analyses were conducted to evaluate coating thickness, color, and material wettability through contact angle measurements. Additionally, a morphological study was carried out using scanning electron microscopy (SEM) image acquisition, along with Fourier-transform infrared

spectroscopy (FTIR) spectroscopy and FTIR mapping studies. Finally, pyrolysis-gas chromatography-mass spectrometry (Py-GCMS) confirmed the formation of urethane bonds between the hydroxyl groups of lignin and the isocyanate (NCO) groups of the isocyanates.

Chapter 2: Extraction and Characterization of Acidolysis Lignin from Turkey Oak (*Quercus cerris* L.) and Eucalypt (*Eucalyptus camaldulensis* Dehnh.) Wood from Population Stands in Italy.

This is one of two articles highlighting how extraction methods influence the chemical structure of the extracted lignin. Using the acidolysis method, lignins are extracted from the wood of two local Italian tree species. The first is Turkey oak (*Quercus cerris* L.), one of the most common deciduous oak species in Italy, while the second investigated species is *Eucalyptus camaldulensis* Dehnh., found in windbreak belts. The detailed study of these lignins is essential for future applications. The main analyses conducted allowed the assessment of molecular weight, with the evaluation of the dispersity of the molar mass distribution (Đ) through high-performance size-exclusion chromatography (HP-SEC). Investigations were also carried out using FTIR spectroscopy, Py-GCMS, and 2D NMR spectroscopy. All analytical techniques converge with the same results in terms of structural characteristics for each extracted lignin.

Chapter 3: Fractionation of Eucalyptus and Oak Wood Biomass through 1-Ethyl-3-Methylimidazolium Acetate: Recovery and Characterization of Lignin

In this second study on lignin extraction from the wood of *Quercus cerris* L. and *Eucalyptus camaldulensis* Dehnh., the ionic liquid 1-ethyl-3-methylimidazolium acetate [C2mim]OAc was used as a solvent. Ionic liquids are considered green solvents due to their excellent properties, such as low toxicity, non-flammability, and chemical and thermal stability. They demonstrated remarkable capabilities as solvents for biomass delignification and lignin recovery. Similar to the previous chapter, investigations were conducted to study the structure after treatment. The obtained information was then compared with the results from lignins extracted using the acidolysis method. The comparison highlighted how the extraction treatment influences the structure of the recovered lignin. Furthermore, while the characteristics of eucalyptus lignin appear almost identical, in the case of oak lignin, acidolysis treatment and treatment with ionic liquid yield lignins with different structures. These differences will be the subject of further study.

Chapter 4: Electrospun PCL filtration membranes enhanced with an electrosprayed lignin coating to control wettability and anti-bacterial properties

In this final chapter, a technological application of lignin as a nanocoating via electrospray on electrospun PCL membranes is presented. For this application, the oak and eucalyptus lignins extracted using the acidolysis method were used. The coating time of the deposited lignin on the PCL membranes was also varied. The results show that even for short lignin deposition times, it can alter the wettability characteristics of PCL, known for its hydrophobic behavior, imparting hydrophilicity to the membrane. Furthermore, lignin imparts new structural properties in terms of membrane porosity, permeability, and thickness. A morphological study was conducted using SEM, wettability tests using both hydrophilic and hydrophobic liquids, and infrared spectroscopy analysis conducted with ATR-FTIR spectroscopy. Additionally, these PCL membranes coated with lignins were evaluated for their antibacterial properties against *Staphylococcus aureus* and *Escherichia coli*.

Conclusion

Following extraction through acidolysis, oak and eucalyptus lignins exhibit structural differences confirmed by analyses such as FTIR spectroscopy, Py-GCMS, and NMR spectroscopy. The oak lignin demonstrates a higher syringyl-to-guaiacyl (S/G) ratio compared to eucalyptus lignin. NMR spectroscopy indicates a homogeneous lignin structure, while FTIR spectroscopy highlights acidolysis lignin (AL) fractions with few carbohydrate impurities. Molar mass analysis suggests suitability for applications such as antioxidants. Initial investigations into lignin extracted using ionic liquid reveal differences, particularly greater polymer fragmentation, as evidenced by molar mass analysis. There are also a lower abundance of β-O-4' structures and as well as fewer carbohydrate residues. Regarding applications, the increase in lignin concentration in polyurethane-based coating formulations imparts more intense coloration to the final product, contrasting with the coloration of commercial polyurethane coatings that are typically colorless. Analyses conducted through FTIR spectroscopy and Py-GCMS highlight the formation of urethane bonds between the functional groups of lignin and the isocyanate mixture used. Wettability measurements demonstrate that the presence of lignin leads to an increase in material hydrophilicity, attributed to the presence and abundance of lignin hydroxyl groups. This aspect is confirmed in the electrospinning experiment by wettability tests on PCL membranes coated with lignin electrospray, where, depending on the amount of deposited lignin, changes in the surface properties of PCL membranes are observed, known for their intrinsic hydrophobic characteristics, eventually exhibiting hydrophilic properties depending on the amount of deposited lignin. By using the two lignins extracted through acidolysis, it was demonstrated that electrosprayed lignin could create a functional coating with modifiable properties tailored for specific engineering applications.

Introduction

Lignin is the second most abundant organic polymer in nature, initially considered a waste product obtained from cellulose production for the paper and wood pulp industry. The estimated global production of lignin is around 1.65 million tons per year, with almost all of it being used in the energy sector through the combustion of the material itself. Only 2% is valorized, finding applications in the production of high-value-added chemical products [1]. It is projected that by 2030, the compound's annual growth rate (CAGR) will reach 4.9% [2]. Given these data, it is imperative to conceive ideas and processes aimed at valorizing this new raw material. It can serve as both a structural analogue for traditional fossil-based raw materials and an innovative component in biorefineries. The latter aims to use and valorize lignocellulosic biomass from various sources. The goal is to valorize new biological "building blocks," including lignin, cellulose, hemicelluloses, and secondary products. These materials are intended to undergo bioconversion to obtain sustainable products more environmental friendly [3]. The development of sustainable processes not only addresses the severe shortage of non-renewable fossil fuels caused by industrialization and globalization in recent decades but also helps counter greenhouse gas emissions and the various phenomena contributing to current climate change.

Lignin is a heterogeneous and amorphous polymer, among the principal constituents of lignocellulosic biomass. It is present in varying percentages, approximately ranging from 17-24% by weight in grass, 18-25% in softwood, and 27-33% in hardwood [4]. Moreover, this percentage is influenced by multiple factors such as the species' origin [5], age [6], and exposure to climatic and environmental conditions [7]. Its primary role, aside from providing strength and structure, is to protect the plant from atmospheric and microbial agents [8]. Its recalcitrant nature is well-known, manifesting during extraction treatment processes [9]. From a chemical standpoint, lignin consists of three different repetitive units or monolignols hydroxyl and methoxyl phenylpropanoid derivatives originating from the aromatic alcohols coniferyl, sinapyl, and p-coumaryl alcohol [10]. These units respectively make up the guaiacyl (G), syringyl (S), and p-hydroxyphenyl (H) lignin subunits. The relative quantities of these units vary depending on the plant biomass. Furthermore, the heterogeneity of the bonds between these various units results in a diverse array of aromatic byproducts [11].

The methodologies applied for the fractionation and recovery of lignin influence the chemical, physical, and structural properties of the material, as well as its degree of purity. Indeed, not all technical lignins, i.e., those obtained from industrial processes, can provide the same level of purity [12-15]. Furthermore, lignins can be classified based on the presence or absence of sulfur in their structure, which is due to the use of sulfur-based reagents. Below, the four main treatments applied at

an industrial level are described: the Kraft process, the sulfite process, soda pulping, and finally, the Organosolv process.

The Kraft process is one of the oldest treatments applied in the wood and pulp industry and precedes the treatment of woody biomass with agents such as sodium sulfide (Na_2S) and sodium hydroxide (NaOH), which act on the bonds between lignin and cellulose, breaking them. The use of agents containing sulfur atoms is crucial, as these atoms become part of the final chemical structure of the extracted lignin, with a percentage ranging from 1.5% to 5.0% [16,17], while its ash content varies from 0.5% to 9.74% [18,19]. One of the main industrial processes is known as LignoBoost®, developed by Chalmers University of Technology, which from black liquor obtains Kraft lignin [20]. The waste black liquor is a byproduct from the pulp and paper industry and is otherwise mostly used as fuel for heat generation [21]. Kraft lignin is primarily used in fertilizers, pesticides, and the production of carbon fibers, but it also finds niche applications such as in the production of vanillin in the food industry [4,22].

The sulfite process is also related to the paper industry [23]. As the name suggests, it involves the use of reagents containing sulfur, such as aqueous sulfur dioxide, along with sulfite-based salts of sodium, calcium, ammonium, and magnesium. The reactions governing the extraction process are hydrolysis and sulfonation, which help solubilize the extracted lignin. In this case as well, the chemical structure of the produced lignin will contain sulfur atoms, with a degree of substitution ranging from 0.4 to 0.5 mol of sulfonate per C9 unit [24]. Major companies that market lignosulfonate include Borregaard in Norway, Tembec in Canada, and Nippon Paper Industries in Japan. Lignosulfonate is a commercially traded product that is impure and requires additional purification treatments for use. Furthermore, there is observed a decrease in the availability of lignosulfonate. Similar to Kraft lignin, the sulfur content is high, ranging around 3.5-8%, while the ash content is much higher (4.0-8.0%) [4]. It is used in the production of various products such as colloidal suspending agents, detergents, feed additives, and additives for cements [12,25,26].

The soda pulping process involves the use of sodium hydroxide (NaOH), and unlike the Kraft process and lignosulfonate, the chemical structure of the obtained lignin will not contain sulfur atoms [27], with a low ash content, approximately ranging from 0.7% to 2.3% [4]. However, soda lignin is characterized by the presence of nitrogen and silica atoms because this process is applied to agricultural crops such as bagasse, flax, etc.[28], rather than woody biomass. The presence of silica affects the purity of lignin, leading to post-treatment and, therefore, a more costly process [29].

The Organosolv process is a method that involves the fractionation and recovery of lignin from biomass using organic solvents such as ethanol, acetone, methanol, solvent mixtures, or any solvents with a low boiling point. The extraction is carried out at a temperature between 100 and 250°C. During the extraction phase, acids like sulfuric acid, hydrochloric acid, formic acid, or other organic acids are added to facilitate lignin recovery [30,31]. Subsequently, the lignin is precipitated using other solvents or simply water. The lignin obtained from this process is free of sulfur atoms or any other contaminants, and compared to the previously described three lignins, it exhibits a higher degree of purity. Additionally, it has the lowest ash content, around 1.75% [4]. All these positive characteristics make Organosolv lignin one of the best technical lignins, finding numerous applications in creating high-value-added products.

In recent years, new methodologies for biomass conversion are being developed, focusing on the refinement of innovative and sustainable processes. The development of these new fractionation techniques will contribute to making the transition to biorefineries more tangible. Biomass pretreatment technologies encompass chemical, physical, physicochemical, and biological methods. Among the chemical treatments are ionic liquids (IL) and acidolysis (AL), which are the main protagonists of this doctoral work and will be extensively discussed in their respective chapters. In addition to ionic liquids, other green solvents that have found broad application in lignocellulosic biomass (LCB) treatment are deep eutectic solvents (DES). These are eutectic mixtures composed of two to three components in specific molar ratios. Similar to ILs, DES exhibit excellent properties such as low toxicity and good degradability [32]. Xu et al. [33] studied the mechanism underlying biomass delignification using a chlorine-based DES. In fact, hydrogen bonds are formed between halogen anions and OH groups of lignin, leading to its dissolution.

Regarding physical pretreatment methods, fractionation through milling, involving mechanical processing to reduce dimensions, finds application. Additionally, irradiation techniques using gamma rays, electron beams, or microwave radiation are employed [34,35]. Among these methods is steam explosion pretreatment, where biomass is subjected to high pressures (3.5 MPa) at temperatures ranging from 150-230 °C. This treatment induces a reduction in β-O-4 bonds [36]. All these pretreatment methods aim to enhance lignin availability and the biodegradability of lignocellulosic biomass, facilitating subsequent treatment steps such as organic and/or enzymatic hydrolysis [37].

Chemical-physical treatments are processes that combine both characteristics (chemical and physical) within the treatment, such as ammonia fiber explosion (AFEX) and ammonia recycle. In AFEX, lignocellulosic biomass is exploded with liquid ammonia at high temperatures and pressures. This technology is very similar to steam explosion, as mentioned earlier, but in this process, a dose of

ammonia is used, typically around 1-2 kg per kg of dry biomass. This treatment causes decrystallization of cellulose and partial depolymerization of hemicelluloses, along with the cleavage of the lignin-carbohydrate complex (LCC) [3]. An advantage of this technique is the complete recycling of the used ammonia, aiming to reduce treatment costs and make the system environmentally efficient. Another chemical-physical treatment that is widely applied is extraction using supercritical carbon dioxide (Sc-CO_2), which has shown excellent results. Extraction occurs with solvents brought into a supercritical condition, such as CO_2 in this case, but water or ammonia can also be used. Typically, CO_2 is preferred due to its non-toxic, low-cost, non-flammable, and recyclable nature. Moreover, it can be easily brought into supercritical conditions (31.1 °C and 73.6 bar). Sc-CO_2 treatment leads to the delignification of lignocellulosic biomass as CO_2 molecules can penetrate the porous matrix, making the structure more accessible to for an eventual enzymatic hydrolysis [38]. The advantage of this technique, besides the efficiency of a closed system allowing CO_2 recycling, lies in achieving decrystallization of biomass, cellulose removal, and, most importantly, it does not bring about any changes in the chemical structure of lignin [39,40].

Scientific studies regarding the applications of lignin to develop new high-value products have been ongoing for a long time; however, discoveries still remain confined to the realm of research. In the near future, it is hoped to witness much more established realities in the landscape of industrial research and development. Imagining the categorization of the main applications into two major sectors, we can identify the first sector as involving lignin used as a constituent element within macromolecular compounds [41], while another sector of application concerns the production of low molecular weight chemicals [42] following lignin depolymerization through thermochemical and catalytic conversion. In the field of macromolecular science and polymers, lignin can be employed as an analogue to traditional fossil-derived structural monomers to develop biocomposites as final products, which are more sustainable. Implicitly, this makes the synthesis process of the product and the end-of-life phase, i.e., disposal, more sustainable as well. One possible application of lignin, thanks to its abundance of phenolic and hydroxyl groups, allows it to be used as a structural analogue for the synthesis of phenol-formaldehyde resins [43], developing adhesives with good bonding strength without the formation, and subsequent release, of formaldehyde. Formaldehyde is a molecule responsible for both indoor and outdoor pollution and has been classified as a type 1B carcinogen since 2016 [44]. As also described in the first chapter of this thesis, lignin has been used as a structural analogue to petrochemical polyols for the synthesis, following reaction with isocyanate mixtures, of polyurethane materials in order to evaluate them as wood coating materials [45]. Another very interesting application concerns the use of lignin to produce high-performance concrete [46] as it provides better resistance and ease of manipulation, mitigating possible surface damage caused by

acid rain and humidity. Furthermore, through a sulfonation process, lignin acts as a dispersing agent in the cementitious matrix due to its high zeta potential value. Another important application concerns the development of carbon fibers [47], serving as a natural precursor due to its high carbon content and the high carbon yield after carbonization. Carbon fiber finds extensive use in the automotive and aerospace sectors due to its high strength-to-weight ratio and remarkable performance, potentially replacing steel used in these industries. Regarding the production of high-value-added products through the depolymerization of lignin via thermochemical transformation in the absence of catalysts, the pyrolysis process conducted in an inert atmosphere at temperatures between 250°C and 500°C yields fractions consisting of water, a solid part referred to as char, and bio-oil, which is the liquid fraction [42]. The composition of the produced fractions not only depends on the type of lignin used but also on the process conditions. Another non-catalytic thermochemical transformation enables the synthesis and production of syngas [48], composed of CO and H_2 molecules along with small amounts of CO_2. These syngas gases find extensive applications in the synthesis of DME (dimethyl ether) and biodiesel. Regarding catalytic transformation processes, catalytic reduction involves converting lignin into simpler molecules such as phenols and BTX (benzene, toluene, and xylene) [49], which can then be further processed for the synthesis of fine chemical products, utilizing well-established technology from the chemical industry. The technology for lignin conversion into BTX comprises two distinct phases: (I) depolymerization and (II) hydrodeoxygenation. Finally, catalytic oxidation enables the transformation of lignin into more complex molecules. Among these, a notable application involves the oxidation of technical lignin in an alkaline environment to produce vanillin [50], commonly used as a flavoring agent in the food and cosmetic industries, as well as an inhibitor of vulcanization and a chemical precursor in the agro-food and pharmaceutical industries.

In addition to these two main sectors described so far, another class of innovative processes involves the micro and nano-transformations of lignin to produce nanomaterials such as lignin nanoparticles for controlled release of active ingredients and essential oils [51,52], or nanofibers/nanosprays through electrospinning technology to create coating materials for applications in membrane filtration for wastewater treatment [53]. The application technologies are diverse and span across many sectors, all characterized by being emerging and innovative. The synthesis of these new bioproducts will represent a significant opportunity for the development of lignocellulosic biorefineries, aiming to shift from petroleum-based production to non-edible biological resources. This shift involves the development of efficient and sustainable industrial processes.

The most sustainable treatment of lignocellulosic biomass aims to obtain a lignin product of high purity, giving it a more significant role compared to previous applications where it was primarily used

as an energy source. With the increasing number of proposals for new technological applications, it is imperative to ensure pathways with reduced environmental impact. The transformation of the final product through these sustainable approaches will promote the adoption of a circular economy model based on lignin. This transition, lifting lignin from a low-value waste status to a new resource, has the potential to increase the circularity rate in the global economy [1]. A shift is expected from direct energy use towards high-value-added materials, such as bioplastics, coatings, adhesives, controlled drug release systems, and fine chemical products, equipped with chemical, physical, and mechanical properties that extend their lifespan.

Reference

1. Tardy, B.L.; Lizundia, E.; Guizani, C.; Hakkarainen, M.; Sipponen, M.H. Prospects for the integration of lignin materials into the circular economy. Materials Today 2023, https://doi.org/10.1016/j.mattod.2023.04.001

2. Lignin Market Size, Share & Trends Analysis Report By Product (Lingo-sulfonates, Kraft Lignin, Organosolv Lignin, Others), By Application, By Region, And Segment Forecasts, 2023 - 2030. Available online: https://www.grandviewresearch.com/industry-analysis/lignin-market#.

3. Menon, V.; Rao, M. Trends in bioconversion of lignocellulose: biofuels, platform chemicals & biorefinery concept. Progress in energy and combustion science 2012, 38, 522-550, https://doi.org/10.1016/j.pecs.2012.02.002

4. Bajwa, D.; Pourhashem, G.; Ullah, A.H.; Bajwa, S. A concise review of current lignin production, applications, products and their environmental impact. Industrial Crops and Products 2019, 139, 111526, https://doi.org/10.1016/j.indcrop.2019.111526

5. Santos, R.B.; Capanema, E.A.; Balakshin, M.Y.; Chang, H.-m.; Jameel, H. Lignin structural variation in hardwood species. Journal of agricultural and food chemistry 2012, 60, 4923-4930, https://doi.org/10.1021/jf301276a

6. Morrison, I. Changes in the lignin and hemicellulose concentrations of ten varieties of temperate grasses with increasing maturity. Grass and Forage Science 1980, 35, 287-293, https://doi.org/10.1111/j.1365-2494.1980.tb01525.x

7. Thevenot, M.; Dignac, M.-F.; Rumpel, C. Fate of lignins in soils: a review. Soil Biology and Biochemistry 2010, 42, 1200-1211, https://doi.org/10.1016/j.soilbio.2010.03.017

8. Frei, M. Lignin: characterization of a multifaceted crop component. The Scientific World Journal 2013, 2013, https://doi.org/10.1155/2013/436517

9. Cabana, H.; Jones, J.; Agathos, S.N. Elimination of endocrine disrupting chemicals using white rot fungi and their lignin modifying enzymes: a review. Engineering in Life Sciences 2007, 7, 429-456, https://doi.org/10.1002/elsc.200700017

10. Whetten, R.; Sederoff, R. Lignin biosynthesis. The plant cell 1995, 7, 1001, https://doi.org/10.1105/tpc.7.7.1001

11. Banu, J.R.; Kavitha, S.; Kannah, R.Y.; Devi, T.P.; Gunasekaran, M.; Kim, S.-H.; Kumar, G. A review on biopolymer production via lignin valorization. Bioresource technology 2019, 290, 121790, https://doi.org/10.1016/j.biortech.2019.121790

12. Tribot, A.; Amer, G.; Alio, M.A.; de Baynast, H.; Delattre, C.; Pons, A.; Mathias, J.-D.; Callois, J.-M.; Vial, C.; Michaud, P. Wood-lignin: Supply, extraction processes and use as bio-based material. European Polymer Journal 2019, 112, 228-240, https://doi.org/10.1016/j.eurpolymj.2019.01.007

13. Ferreira, J.A.; Taherzadeh, M.J. Improving the economy of lignocellulose-based biorefineries with organosolv pretreatment. Bioresource technology 2020, 299, 122695, https://doi.org/10.1016/j.biortech.2019.122695

14. Schutyser, W.; Renders, a.T.; Van den Bosch, S.; Koelewijn, S.-F.; Beckham, G.; Sels, B.F. Chemicals from lignin: an interplay of lignocellulose fractionation, depolymerisation, and upgrading. Chemical society reviews 2018, 47, 852-908, https://doi.org/10.1039/C7CS00566K

15. Passoni, V.; Scarica, C.; Levi, M.; Turri, S.; Griffini, G. Fractionation of industrial softwood kraft lignin: Solvent selection as a tool for tailored material properties. ACS Sustainable Chemistry & Engineering 2016, 4, 2232-2242, https://doi.org/10.1021/acssuschemeng.5b01722

16. Gellerstedt, G. Softwood kraft lignin: Raw material for the future. Industrial Crops and Products 2015, 77, 845-854, https://doi.org/10.1016/j.indcrop.2015.09.040

17. Evdokimov, A.N.; Kurzin, A.V.; Fedorova, O.V.; Lukanin, P.V.; Kazakov, V.G.; Trifonova, A.D. Desulfurization of kraft lignin. Wood Science and Technology 2018, 52, 1165-1174, https://doi.org/10.1007/s00226-018-1014-1

18. Maitz, S.; Schlemmer, W.; Hobisch, M.A.; Hobisch, J.; Kienberger, M. Preparation and Characterization of a Water-Soluble Kraft Lignin. Advanced Sustainable Systems 2020, 4, 2000052, https://doi.org/10.1002/adsu.202000052

19. da Silva, P.M.; Pasa, V.M.D. Upgrading of kraft lignin with phosphoric acid purification: A promising route for the synthesis of renewable epoxy resins. Industrial Crops and Products 2023, 204, 117202, https://doi.org/10.1016/j.indcrop.2023.117202

20. Tomani, P. The lignoboost process. Cellulose Chemistry & Technology 2010, 44, 53.

21. Kim, C.-H.; Lee, J.-Y.; Park, S.-H.; Moon, S.-O. Global trends and prospects of black liquor as bioenergy. Journal of Korea TAPPI 2019, 51, 3-15, https://doi.org/10.7584/JKTAPPI.2019.10.51.5.3

22. Agrawal, A.; Kaushik, N.; Biswas, S. Derivatives and applications of lignin–an insight. SciTech J 2014, 1, 30-36.

23. Fatehi, P.; Ni, Y. Integrated forest biorefinery− sulfite process. In Sustainable production of fuels, chemicals, and fibers from forest biomass; ACS Publications: 2011; pp. 409-441.

24. Demuner, I.F.; Colodette, J.L.; Demuner, A.J.; Jardim, C.M. Biorefinery review: Wide-reaching products through kraft lignin. BioResources 2019, 14, 7543-7581, https://doi.org/10.15376/biores.14.3.Demuner

25. Alwadani, N.; Fatehi, P. Carbon Resources Conversion, 1. 2018, https://doi.org/10.1016/j.crcon.2018.07.006

26. Browning, W.C. Lignosulfonate challenge. In Proceedings of the Applied polymer symposia, 1975; pp. 109-124.

27. Potůček, F.; Gurung, B.; Hájková, K. Soda pulping of rapeseed straw. Cellulose chemistry and technology 2014, 48, 683-691

28. Gan, M.J.; Niu, Y.Q.; Qu, X.J.; Zhou, C.H. Lignin to value-added chemicals and advanced materials: extraction, degradation, and functionalization. Green Chemistry 2022, https://doi.org/10.1039/D2GC00092J

29. Mousavioun, P.; Doherty, W.O. Chemical and thermal properties of fractionated bagasse soda lignin. Industrial crops and products 2010, 31, 52-58, https://doi.org/10.1016/j.indcrop.2009.09.001 .

30. Thoresen, P.P.; Matsakas, L.; Rova, U.; Christakopoulos, P. Recent advances in organosolv fractionation: Towards biomass fractionation technology of the future. Bioresource technology 2020, 306, 123189, https://doi.org/10.1016/j.biortech.2020.123189

31. Qian, Q.; Luo, Z.; Sun, H.; Wei, Q.; Shi, J.; Li, S. Comparing physicochemical characteristics and depolymerization behaviors of lignins derived from different pretreatment processes. Fuel Processing Technology 2023, 250, 107921, https://doi.org/10.1016/j.fuproc.2023.107921

32. Wang, W.; Lee, D.-J. Lignocellulosic biomass pretreatment by deep eutectic solvents on lignin extraction and saccharification enhancement: A review. Bioresource technology 2021, 339, 125587, https://doi.org/10.1016/j.biortech.2021.125587

33. Xu, H.; Kong, Y.; Peng, J.; Song, X.; Liu, Y.; Su, Z.; Li, B.; Gao, C.; Tian, W. Comprehensive analysis of important parameters of choline chloride-based deep eutectic solvent pretreatment of lignocellulosic biomass. Bioresource Technology 2021, 319, 124209, https://doi.org/10.1016/j.biortech.2020.124209

34. Khan, M.U.; Usman, M.; Ashraf, M.A.; Dutta, N.; Luo, G.; Zhang, S. A review of recent advancements in pretreatment techniques of lignocellulosic materials for biogas production: Opportunities and Limitations. Chemical Engineering Journal Advances 2022, 10, 100263, https://doi.org/10.1016/j.ceja.2022.100263

35. Kumar, B.; Bhardwaj, N.; Agrawal, K.; Chaturvedi, V.; Verma, P. Current perspective on pretreatment technologies using lignocellulosic biomass: An emerging biorefinery concept. Fuel Processing Technology 2020, 199, 106244, https://doi.org/10.1016/j.fuproc.2019.106244

36. Maniet, G.; Schmetz, Q.; Jacquet, N.; Temmerman, M.; Gofflot, S.; Richel, A. Effect of steam explosion treatment on chemical composition and characteristic of organosolv fescue lignin. Industrial Crops and Products 2017, 99, 79-85, https://doi.org/10.1016/j.indcrop.2017.01.015

37. Ziegler-Devin, I.; Chrusciel, L.; Brosse, N. Steam explosion pretreatment of lignocellulosic biomass: a mini-review of theorical and experimental approaches. Frontiers in Chemistry 2021, 9, 705358, https://doi.org/10.3389/fchem.2021.705358

38. Sohni, S.; Hashim, R.; Nidaullah, H.; Sulaiman, O.; Leh, C.P.; Lamaming, J.; Arai, T.; Kosugi, A. Enhancing the enzymatic digestibility of oil palm biomass using supercritical carbon dioxide-based pretreatment towards biorefinery application. Industrial Crops and Products 2020, 157, 112923, https://doi.org/10.1016/j.indcrop.2020.112923

39. Dharmaraja, J.; Shobana, S.; Arvindnarayan, S.; Francis, R.R.; Jeyakumar, R.B.; Saratale, R.G.; Ashokkumar, V.; Bhatia, S.K.; Kumar, V.; Kumar, G. Lignocellulosic biomass conversion via greener pretreatment methods towards biorefinery applications. Bioresource technology 2023, 369, 128328, https://doi.org/10.1016/j.biortech.2022.128328

40. Badgujar, K.C.; Dange, R.; Bhanage, B.M. Recent advances of use of the supercritical carbon dioxide for the biomass pre-treatment and extraction: A mini-review. Journal of the Indian Chemical Society 2021, 98, 100018, https://doi.org/10.1016/j.jics.2021.100018

41. Duval, A.; Lawoko, M. A review on lignin-based polymeric, micro-and nano-structured materials. Reactive and Functional Polymers 2014, 85, 78-96, https://doi.org/10.1016/j.reactfunctpolym.2014.09.017

42. Torres, L.A.Z.; Woiciechowski, A.L.; de Andrade Tanobe, V.O.; Karp, S.G.; Lorenci, L.C.G.; Faulds, C.; Soccol, C.R. Lignin as a potential source of high-added value compounds: A review. Journal of Cleaner Production 2020, 263, 121499, https://doi.org/10.1016/j.jclepro.2020.121499

43. Gao, Z.; Lang, X.; Chen, S.; Zhao, C. Mini-review on the synthesis of lignin-based phenolic resin. Energy & Fuels 2021, 35, 18385-18395, https://doi.org/10.1021/acs.energyfuels.1c03177

44. ECHA- European chemicals agency. Available online: https://echa.europa.eu/it/substance-information/-/substanceinfo/100.000.002

45. Bergamasco, S.; Tamantini, S.; Zikeli, F.; Vinciguerra, V.; Scarascia Mugnozza, G.; Romagnoli, M. Synthesis and characterizations of eco-friendly organosolv lignin-based polyurethane coating films for the coating industry. Polymers 2022, 14, 416, https://doi.org/10.3390/polym14030416

46. Breilly, D.; Fadlallah, S.; Froidevaux, V.; Colas, A.; Allais, F. Origin and industrial applications of lignosulfonates with a focus on their use as superplasticizers in concrete. Construction and Building Materials 2021, 301, 124065, https://doi.org/10.1016/j.conbuildmat.2021.124065

47. Fang, W.; Yang, S.; Wang, X.-L.; Yuan, T.-Q.; Sun, R.-C. Manufacture and application of lignin-based carbon fibers (LCFs) and lignin-based carbon nanofibers (LCNFs). Green Chemistry 2017, 19, 1794-1827, https://doi.org/10.1039/C6GC03206K

48. Li, C.; Zhao, X.; Wang, A.; Huber, G.W.; Zhang, T. Catalytic transformation of lignin for the production of chemicals and fuels. Chemical reviews 2015, 115, 11559-11624, https://doi.org/10.1021/acs.chemrev.5b00155

49. Ramirez Brenes, R.G.; Alhadeff, E.M.; Bojorge, N.; Trales, L.E.; Pazos, G.A. BTX production by breaking down lignin: Current status and future prospects. Biofuels, Bioproducts and Biorefining 2023, 17, 664-681, https://doi.org/10.1002/bbb.2460

50. Fache, M.; Boutevin, B.; Caillol, S. Vanillin production from lignin and its use as a renewable chemical. ACS sustainable chemistry & engineering 2016, 4, 35-46, https://doi.org/10.1021/acssuschemeng.5b01344

51. Zikeli, F.; Vinciguerra, V.; D'Annibale, A.; Capitani, D.; Romagnoli, M.; Scarascia Mugnozza, G. Preparation of lignin nanoparticles from wood waste for wood surface treatment. Nanomaterials 2019, 9, 281, https://doi.org/10.3390/nano9020281

52. Zikeli, F.; Vettraino, A.M.; Biscontri, M.; Bergamasco, S.; Palocci, C.; Humar, M.; Romagnoli, M. Lignin nanoparticles with entrapped Thymus spp. essential oils for the control of wood-rot fungi. Polymers 2023, 15, 2713, https://doi.org/10.3390/polym15122713

53. Bergamasco, S.; Fiaschini, N.; Hein, L.A.; Brecciaroli, M.; Vitali, R.; Romagnoli, M.; Rinaldi, A. Electrospun PCL Filtration Membranes Enhanced with an Electrosprayed Lignin Coating to Control Wettability and Anti-Bacterial Properties. Polymers 2024, 16, 674, https://doi.org/10.3390/polym16050674

CHAPTER 1: Synthesis and Characterizations of Eco-Friendly Organosolv Lignin-Based Polyurethane Coating Films for the Coating Industry

Sara Bergamasco, Swati Tamantini *, Florian Zikeli *, Vittorio Vinciguerra, Giuseppe Scarascia Mugnozza and Manuela Romagnoli *

Polymers **2022**, *14*(3), 416; https://doi.org/10.3390/polym14030416

Abstract

Three different formulations of bio-based polyurethane (PU), varying the weight ratio between Organosolv lignin and a commercial isocyanate, were synthesized. The coating formulations were characterized by SEM, pyrolysis-GC/MS, FTIR spectroscopy and FTIR mapping, which confirmed the successful formation of urethane bonds between commercial isocyanate and hydroxyl groups deriving from lignin. The coatings were applied on beech wood samples to measure color and contact angles, and eventually FTIR mapping of the coated wood samples was performed. FTIR mapping is an interesting tool to monitor the distribution of PU chemical bonds on the coating surface and to evaluate the homogeneity of the applied coating films. Increasing the lignin content of the PU coatings results in more red-yellow and darker tones, while the commercial PU coating is transparent. For a higher lignin concentration, the solid content as well as the weight gain of the applied coatings increase. A higher percentage of lignin in the prepared PU formulations leads to superficial cracks and therefore higher coating permeability compared to the commercial PU, but the prepared lignin-based PU coating still makes a raw wood surface significantly more hydro-phobic. Apparently, additives such as film-formers with low surface tension to counteract cracks' formation are necessary to improve the performance of lignin-based PU coatings.

Keyword: wood coating; wood color; contact angle; SEM; Py-GC/MS; FTIR mapping; beech; bio-circular economy

Introduction

Wood materials and wood-based products are increasingly considered the mate-rials of the future, fully in line with modern concepts of a bio-circular economy [1,2]. However, the intrinsic biodegradability of wood is the most important weakness, which limits a wider end use, and thus the improvement of wood durability is still one of the major challenges [3,4]. This challenge can be tackled by different means, such as thermo-treatments [5,6] or fossil-based and natural wood coatings with protective or biocidal functions [7–10]. A definition of "coating material" is given by the European Standard EN 971-1 [11]: "A product, in liquid, in paste or powder form, that, when applied to a substrate, forms a film possessing protective, decorative and/or other specific properties". Various types of organic substances have been used in the preparation of coating materials for wood. In ancient times, only natural products such as oils or resins were available [12,13]. Later on, the application of thermal or chemical modifications improved the performance of natural products. A continuously developing chemical industry in the first half of the 20th century produced a wide range of synthetic coating films, such as alkyds, polyurethanes and polyesters, which were successfully applied in many fields, including wood technology [14–18]. For the modern coating industry, polyurethanes (PUs) present an important class of polymers due to outstanding mechanical, chemical and physical properties. Thus, they find application in many industrial sectors in the form of flexible or rigid foams, coatings, adhesives, elastomers, thermoplasts or thermosets [8,19]. Modern PU coating applications include self-healing coating films that can also be applied to rather rough surfaces, such as wood [6]. Polyurethanes are available as solvent or water-borne formulations, and polymer curing may be brought about at ambient or elevated temperatures. One of the major issues of polyurethanes is their fossil-based origin and the toxicity of reactants and pre-cursors such as isocyanates, which act as a modifier or crosslinking agent, rather than the main film former. Conventional PUs are usually synthesized by a polyaddition reaction between polyols and poly-isocyanates. These two, when reacted together, form the urethane linkages observed in a cross-linked polymer. Recently, several attempts were reported to substitute fossil-based building blocks of PU coatings with bio-based compounds because the versatility in chemistry and processing enables wide opportunities for introducing new raw materials into various PU products [20]. Recent research utilizes castor oil for the preparation of a hyperbranched polyol that was further used for a bio-based PU coating with self-cleaning abilities [21]. Besides vegetable oils (i.e., from soybean) or starch, which have been extensively applied as natural and renewable polyol sources for PUs, lignin has emerged as a promising alternative polyol source for application in resins, adhesives and foams [22,23]. After cellulose, lignin is the second most abundant natural polymer, containing a broad range and high contents of chemical functional groups such as hydroxyls, carbonyls and carboxyls [24],

which allow for its utilization as an alternative for polymer development, especially as a substitute for petroleum-based polyols in polyurethane systems. Scientific contributions regarding the substitution of polyols by lignin in polyurethanes involve, in general, kraft lignins [25], while the performance of other technical lignins, i.e., Organosolv lignins, has not yet been evaluated. Thus, the objective of this article is to examine the use of technical Organosolv lignin, a waste stream from the pulping industry, as a polyol substitute to produce bio-based polyurethane coatings, which eventually provide a more sustainable alternative with less risk for human and environmental health by reducing the content of synthetic and fossil-based components. The lignin derives from species of short supply chain, which is one of the main topics of a bio-circular economy where alternative uses of wood waste in the substitution of synthetic compounds in coating or adhesive formulations are envisioned [1,26].

Materials and Methods

Materials

Flat-grained beech (Fagus sylvatica L.) wood samples, 15 mm × 15 mm × 3 mm (L × T × R), were taken in tangential direction from one cut board. Wood samples were con-ditioned in the lab at 65% relative humidity (RH) and 21 °C for one year. The commercial PU coating provided by the company Finedin S.r.l. (Taviano, Italy) is a PU-based synthetic flattener for wood. Hardwood (Beech) Organosolv lignin (OL) was supplied by Fraunhofer Italia S.c.r.l. (Bolzano, Italy). Desmodur®L75 is an aromatic polyisocyanate containing an isomeric mix of toluene diisocyanate (TDI), diethylene glycol and trimethylolpropane, and it was supplied by Covestro LLC (Leverkusen, Germany). 2-Methyltetrahydrofuran (2-MeTHF) was obtained from Carlo Erba Reagents (Cornaredo, Italy). The different formulations and relative abbreviations used in the text are explained in Table 1.

Table 1. Formulations of the different coatings and corresponding abbreviations used in the text.

Abbreviation	Formulation
PU-R	Reference sample: commercial polyurethane-based coating
PU-3:1	Lignin-based polyurethane, isocyanate:lignin ratio = 3:1
PU-1:1	Lignin-based polyurethane, isocyanate:lignin ratio = 1:1
PU-1:3	Lignin-based polyurethane, isocyanate:lignin ratio = 1:3
W-R	Reference sample: uncoated beech wood
WPU-R	Reference sample: beech wood coated with PU-R
WPU-3:1	Beech wood coated with PU-3:1
WPU-1:1	Beech wood coated with PU-1:1
WPU-1:3	Beech wood coated with PU-1:3

Polyurethane Synthesis

Three formulations of bio-based polyurethane, varying the weight ratio between lignin and isocyanate, were synthesized and eventually named as PU-3:1, PU-1:1 and PU-1:3. The lignin was

dispersed in 5 mL of 2-MeTHF (2-Methyltetrahydrofuran) with a dispersion degree equal to 20%, 40% and 60% (wt/vol) and stirred magnetically for 30 min at room temperature. After that, Desmodur®L75 equal to 60%, 40% and 20% (wt/vol) was added to the lignin solutions. For a complete dissolution of isocyanate and eventual polyurethane formation, the solutions were left under magnetic stirring for an additional 60 min at room temperature. Subsequently, the PU formulations were applied as coatings on the wood samples. Aliquots of the three formulations were poured in aluminum plates for subsequent heat-induced finalization of the crosslink-ing reaction in a drying oven (60 °C, 72 h) and eventual solid content determination (see below). The NCO /OH molar ratio was calculated based on the equation 1 below [27]:

$$\frac{\mathrm{NCO}}{\mathrm{OH}} = \frac{W_{TDI}[NCO]_{TDI}}{W_{OL}[OH]_{OL}} \quad (1)$$

where W_{TDI} is the weight (g) of isocyanate contained in Desmodur®L75 and W_{OL} is the weight of lignin, respectively. $[NCO]_{TDI}$ is the molar content of isocyanate groups in TDI and $[OH]_{OL}$ is the molar content of the total hydroxyl groups (phenolic, aliphatic and carboxylic) in lignin. For the determination of $[NCO]_{TDI}$, the real aromatic polyisocyanate composition present in the Desmodur®L75 was considered. In this way, it was possible to calculate the molar ratio starting from the weight ratio. Molar ratios equal to 1.96, 0.65 and 0.21 were obtained for the formulations PU-3:1, PU-1:1 and PU-1:3, respectively.

Coating Application

Coatings were applied onto one side of the beech wood samples using a brush (size 8) with synthetic bristles. Three layers of varnish were applied for each sample with a drying time of 1 h between each application.

Pyrolysis-GC/MS

About 1.5 mg of the sample PU-3:1 was pressed in a special syringe and directly pyrolyzed at 450 °C in a Pyrojector II (SGE Analytical Science, Trajan Scientific and Medical, Victoria, Australia). The pyrolysis chamber was maintained at 450 °C. Pyrolysis products were separated in a GCMS-QP5050 instrument (Shimadzu Corporation, Kyoto, Japan). Helium was the carrier gas at a pressure of 100 kPa in the pyrolyzer and 70 kPa in the GC injector (280 °C, 1–20 split ratio). The initial temperature in the oven was 45 °C for 4 min, then increased to 240 °C at a rate of 4 °C min^{-1} and finally until 280 °C at a rate of 39 °C min^{-1}. Pyrolysis products were identified by mass spectra interpretation and comparison with NIST and Wiley computer libraries and reference literature [28,29]. For each pyrogram, normalized at the most intense peak, the relative peak areas of 26 principal phenolic lignin pyrolysis products as well as the respective PU pyrolysis products were determined.

SEM

One representative sample (PU-3:1) was used for a morphological characteriza-tion of the coating by Scanning Electron Microscope (SEM) analysis. The sample was attached to aluminum stubs by carbon tape and sputter-coated with gold in a Balzers MED 010 unit (Oerlikon Balzers, Balzers, Liechtenstein). A JEOL JSM 6010LA SEM was used (JEOL Limited, Tokyo, Japan). The sample to be analyzed was selected after observation on a FTIR microscope.

Weight Gain and Coating Film Thickness

The weight of 12 samples for each formulation was measured before and after coating application using the electronic analytical balance JA503 (Fulltech Instruments S.r.l., Rome, Italy). The second weight was taken after one week of drying (168 h). The percentage of weight gain was calculated using Equation 2 below:

$$W_{gain} = \frac{W_2 - W_1}{W_1} \cdot 100 \quad (2)$$

where W_{gain} is the weight gain of the wooden sample after coating application, W_1 is the weight of uncoated samples and W_2 is the weight of coated samples. For determination of coating thickness, three samples per coating were halved and the coating layer was measured in five spots/sample using a stereomicroscope (model MZ 16A, Leica Microsystems AG, Wetzlar, Germany).

Solid Content Analysis

Samples of fresh varnishes were weighed using the electronic analytical balance JA503 (Fulltech Instruments S.r.l., Rome, Italy) and left in the oven (FD 115, Binder GmbH, Tuttlingen, Germany) at 60 °C for 72 h. After drying, the samples were weighed again and solid content (SC) in percentage was calculated using Equation 3:

$$SC = \frac{W_{dry}}{W_{fresh}} \cdot 100 \quad (3)$$

where SC is the solid content, W_{dry} is the weight after the drying period and W_{fresh} is the weight of fresh varnish before oven-drying.

Color Measurements

Digital images of the samples were taken using an HP Scanjet 4800 scanner, in order to analyze their CIELAB coordinates using the open-source graphics software GNU Image Manipulation Program (GIMP v2.10.12). According to UNI EN ISO/CIE-11664-4:2019 [30] and UNI EN 927-6:2019 [31], five different spots per sample were selected and three samples per coating formulation were analyzed. The coordinates L^*, a^* and b^* were measured on the tangential plane. The total color difference (ΔE^*) represents the difference in color between virgin wood and the samples coated with PU formulations and the commercial PU coating. ΔE^* was calculated according to Equation 4:

$$\Delta E^* = \sqrt{(L_2^* - L_1^*)^2 + (a_2^* - a_1^*)^2 + (b_2^* - b_1^*)^2} \quad (4)$$

where L^* is the lightness (0 to 100), a^* is the coordinate for red/green values (− 120 to 120), b^* is the coordinate for blue/yellow values (−120 to 120), Index 1 stands for the reference sample and Index 2 stands for the sample to analyze.

Optical Contact Angle

Optical contact angle (CA) measurements on the PU film were performed at room temperature using the optical tensiometer Attension Theta Flex (Biolin Scientific Group, Västra Frölunda, Sweden). Three samples per treatment were chosen, and two spots per specimen were analyzed. A droplet of deionized water (5 µL) was released on the three PU formulations, on the commercial PU and on three control samples. CA measurements after water drop release (CA-T0), after 10 s (CA-T10) and after 600 s (CA-T600) of drop deposition were recorded. Data elaborations were conducted using the software OneAttension v4.1.2 (r9576), provided by Biolin Scientific Group (Västra Frölunda, Sweden).

FTIR Spectroscopy and Mapping

After oven-drying at 60 °C for 72 h (FD 115, Binder GmbH, Tuttlingen, Germany), potassium bromide (KBr) pellets (Ø = 7 mm) were prepared for each coating formulation with a sample concentration of 2 wt.% using a Specac mini-pellets press at 2 bar for 5 min (Specac Inc., Orpington, UK). FTIR spectra were recorded in absorbance mode in the range of 4000–400 cm^{-1} with a FTIR-4100 Fourier Transform Infrared spectrometer (Jasco Corp., MD, USA). All FTIR spectra were smoothed, base-line-corrected and normalized for the most intense peak of the spectra using Spectra Manager software v2.15.01 (Jasco Corp., MD, USA). One representative wood sample per coating formulation was analyzed using a Jasco IRT-7000 Irtron Infrared micro-scope (Jasco Corp., MD, USA) in order to investigate the surface of the coated samples using FTIR imaging. The number of scans was 500 per measurement point and the analyzed area was 270 µm × 270 µm.

Statistical Analysis

After verifying the normal distribution of data with the Anderson–Darling method, the differences among formulations were investigated by ANOVA (Minitab® v18.1, Minitab Inc., State College, PA, USA). ANOVA was carried out on color change, weight gain and contact angle measurements. The statis-tical analysis considered a 95% confidence interval (CI). If significant differences were detected in the ANOVA (F test with $p \leq 0.05$), the Tukey test ($p \leq 0.05$) was applied to compare the series.

Results and Discussion

Commercial coating is transparent, soft to touch and has a shiny appearance. New formulations, with lignin-based PU, resulted shiny, but neither smooth nor transparent. The general procedure of the presented research is illustrated in Scheme 1.

Scheme 1. Overview of the general procedure for the preparation of the Organosolv lignin-based PU coating.

Macroscopic aspects of the prepared PU coatings, such as color, weight gain, coating film thickness and contact angle, are presented first, followed by microscopic investigations of the coating surface and finally chemical analysis of the prepared PU by FTIR spectroscopy and Py-GC/MS, respectively.

Color Measurements

Figure 1 shows the beech wood samples coated with the different PU formulations, and their respective color coordinates are listed in Table 2.

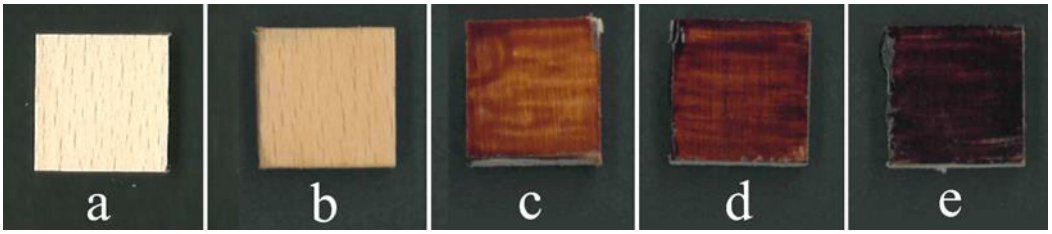

Figure 1. Beech wood samples before (a) and after coating application (b–e). (a) W-R, (b) WPU-R, (c) WPU-3:1, (d) WPU-1:1 and (e) WPU-1:3.

Table 2. Color coordinates based on CIELAB color space of wooden samples before coating application (W-R) and after coating application. ΔE* was calculated using the difference between uncoated (W-R) and coated wood samples. Statistical differences are reported as: *** $p < 0.001$, ** $p < 0.01$ and * $p < 0.05$.

	Before Coating (W-R)			After Coating			
	L*	a*	b*	L*	a*	b*	ΔE*
WPU-R	85.8 ± 3.8	6.4 ± 2.2	19.8 ± 2.0	71.8 ± 2.0 ***	11.3 ± 1.1	31.4 ± 2.6	19.5 ± 4.9 ***
WPU-3:1	85.6 ± 6.7	6.0 ± 2.4	20.3 ± 2.6	37.6 ± 5.3 ***	26.4 ± 2.6 ***	30.0 ± 5.5	54.7 ± 7.6 ***
WPU-1:1	86.2 ± 3.5	5.9 ± 2.0	21.3 ± 2.0	21.0 ± 4.3 ***	21.1 ± 4.2 ***	11.4 ± 5.8 ***	68.7 ± 5.7 ***
WPU-1:3	90.1 ± 2.4	4.0 ± 1.8	19.7 ± 2.4	10.8 ± 2.5 ***	7.8 ± 5.7	0.3 ± 1.0 ***	82.3 ± 3.9 ***
Mean W-R	86.9 ± 7.3	5.6 ± 2.9	20.3 ± 3.0				

Virgin wood (W-R) color coordinates are quite homogeneous, but after coating application, the color strongly changes. Commercial coating (WPU-R) is transparent, so the color variations compared to raw solid wood are the lowest among the other PU formulations, and wood structural elements such as rays can still be identified (Figure 1a, b). In all cases, L^* is lower, which means a darker color and less transparent coating, as seen in Figure 1c–e. The coordinate a^* increases for all coatings, meaning a redder color than virgin wood. For the CIELAB coordinate b^*, the situation is different. In WPU-R and WPU-3:1, b^* increases, rendering the color more yellow, while in WPU-1:1 and WPU-1:3, b^* changes the color to a bluer tone. This could be explained by the fact that in the first two samples (Figure 1a,b), wood underneath the coating is still visible, while the last two provide a less transparent coating (Figure 1c,d), where lignin covers the surface the most. Additionally, Jusic et al. [7] and Klein et al. [32] found a gradual color change at increasing lignin content. Changing color due to all formulations is always statistically significant (ΔE^*).

Weight, Coating Film Thickness and Solid Content

In Table 3, the measured sample weights and their respective weight gains are re-ported as well as the determined solid contents (SC). Weight gain was much lower for the prepared PU coatings compared to the commercial reference (WPU-R), and the difference is statistically significant. The decrease of weight gain in increasing lignin concentration is consistent with the low values of SC for the prepared PU formulations, which could be explained by the presence of other additives in the commercial products increasing its SC. Regarding the prepared formulations, an increasing lignin content led to higher SC. The coating thicknesses of the three prepared formulations are quite similar (Table 3). It is noteworthy that WPU-R shows a very high standard deviation, which might be due to higher viscosity and the presence of additives, as can be deduced by the SC.

Table 3. Weight of the samples before and after application of the different coating formulations and respective weight gain, solid content (SC) of the pure formulations (1 PU-R, 2 PU-3:1, 3 PU-1:1, 4 PU-1:3). Statistical differences are reported as: *** $p < 0.001$, ** $p < 0.01$ and * $p < 0.05$.

	Weight Gain (%)	Thickness (μm)	SC (%)
WPU-R	5.2 ± 1.7	28.2 ± 20.6	57.1 [1]
WPU-3:1	0.6 ± 1.7 ***	25.9 ± 7.0	45.1 [2]
WPU-1:1	0.8 ± 1.6 ***	28.1 ± 7.1	47.1 [3]
WPU-1:3	0.7 ± 1.3 ***	27.8 ± 9.2	51.0 [4]

Optical Contact Angle

In Table 4, the contact angle (CA) values are reported. As expected, the commercial coating had the highest CAs (Figure 2a), while higher lignin contents in the pre-pared PU coating led to lower CAs (Figure 2b). The CA of W-R changes strongly within the first 10 s after droplet deposition, while for WPU-R it remains stable, meaning that the water drop was adsorbed in the first case while in the latter the film is waterproof, as expected. In the coatings of the other PU formulations, the differences are not pronounced, which is why they are considered as waterproof as well, even if the CAs of the prepared PU formulations are lower than WPU-R. In the case of WPU-1:3, the water drop was completely absorbed within 10 min, as occurred with W-R. Standard deviations of prepared PU formulations are a little high, which might depend on the irregularity of the substrate, which in turn depends on the coating application. In fact, during brush application, PU formulations dried as they were applied, making the surface not flat. To summarize, it seems that the hydrophobicity of the prepared PU formulations decreased when lignin content increased. Griffini et al. [33] address this behavior to the presence of hydroxyl groups in lignin, which are higher for increasing lignin content in PU materials, leading to lower CAs. Another reason for this behavior could be explained by the cracks visible on the prepared PU surfaces (Figure 3a–c), which let the water pass through the coating film. CA values are significant only when the lignin concentration is the highest.

Table 4. Contact angle (CA) measured for different prepared PU formulations. Values of CA after waterdrop deposition (CA-T0), CA after 10 s (CA-T10) and CA after 10 min (600 s) after waterdrop deposition (CA-T600) are reported. Statistical differences are reported as: *** $p < 0.001$, ** $p < 0.01$ and * $p < 0.05$.

	CA-T0 (°)	CA-T10 (°)	CA-T600 (°)
W-R	93.9 ± 4.0	76.6 ± 5.9	-
WPU-R	89.5 ± 6.1	89.1 ± 6.2	79.9 ± 6.6
WPU-3:1	82.0 ± 8.2	79.7 ± 7.8	69.1 ± 9.6
WPU-1:1	79.8 ± 8.1	77.3 ± 8.5	54.7 ± 10.7 **
WPU-1:3	79.0 ± 7.7	70.4 ± 5.4 **	-

Figure 2 shows how the instrument extrapolates CA values by contrast between the white background and the dark droplet.

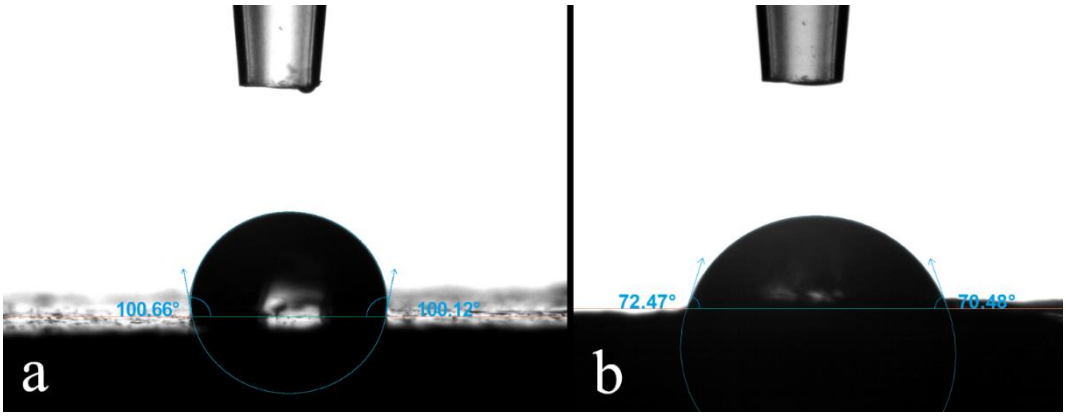

Figure 2. Two examples of CA measurement after drop release. In (a) a WPU-R sample, with a high CA, and in (b) a WPU-1:3 sample, with a low CA. Blue angle indicate how the instrument ex-trapolates the data from the images.

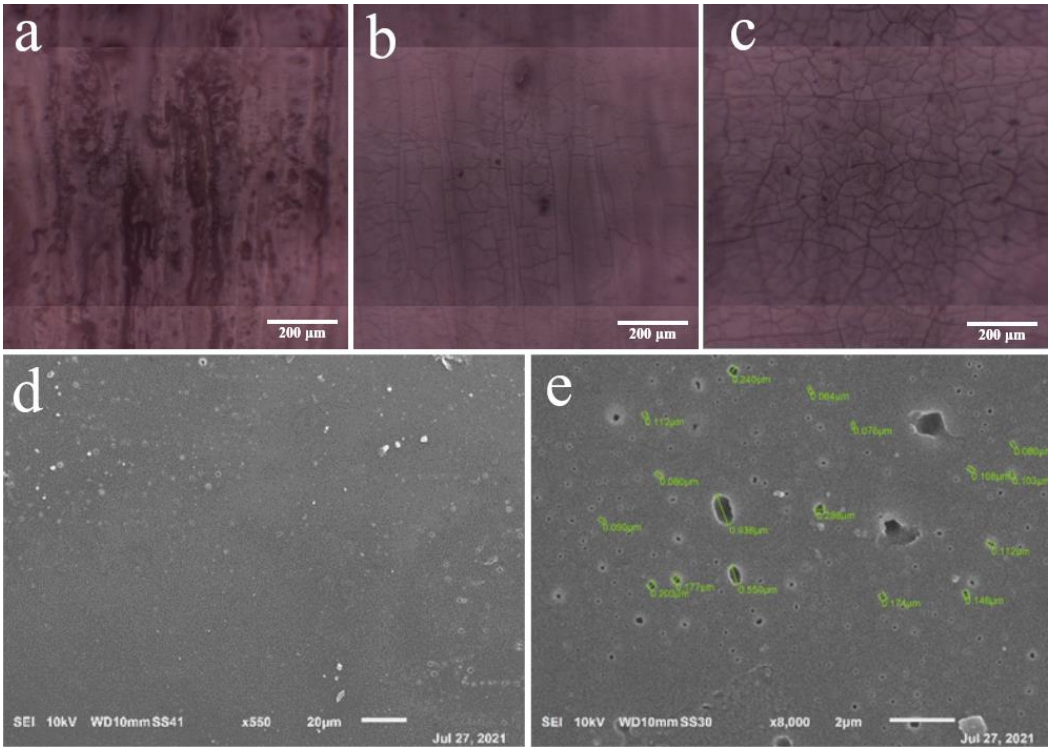

Figure 3. Pictures of measurement areas: (a) WPU-3:1, (b) WPU-1:1 and (c) WPU-1:3. SEM images of PU-3:1 (d, e).

FTIR Microscopy and Scanning Electron Microscopy (SEM)

The pictures of the measurement zones of the FTIR mapping of the three PU formulations were captured using the multi-channel Jasco infrared microscope IRT-7000 and a Cassegrain × 16 objective. These pictures show that with the in-creasing lignin concentration, changes in the morphology of the material occur, causing the formation of cracks in the coating. Hence, in the image of the sample WPU-3:1, the coating surface is less cracked (Figure 3a) than WPU-1:1 (Figure 3b) and WPU-1:3 (Figure 3c). This condition was confirmed by the acquisition of scanning electron

microscope (SEM) images, where a smooth and homogeneous structure (Figure 3d) was observed with the presence of a few porosities with an average diameter of 0.25 µm (Figure 3e) and a minimal presence of lignin aggregates. In contrast to other works in the literature, where significant lignin aggregation was observed using SEM [34], the PU formulations prepared in this work were rather free from lignin aggregates, as il-lustrated in Figure 3d, e.

FTIR Spectroscopy and Imaging

In order to investigate the chemistry behind the preparation of the PU formulations, FTIR analysis was performed on samples of the three different PU formulations after both spontaneous (room temperature) and temperature-induced (60 °C for 72 h) crosslinking. The formation of urethane bonds was evaluated by studying the respective IR bands of the specific involved functional groups. The absorption band at 2270 cm^{-1} is associated to the stretching modes of the unreacted isocyanate NCO groups in the three different formulations (Figure 4a). The signal intensity of this band depends on the presence of excessive NCO groups after the formation of urethane bonds in the respective formulations. The disappearance of the isocyanate band in the sample PU-1:3 indicates a rather complete reaction between NCO and lignin OH groups, while the more intense absorption band in the spectra of the samples PU-3:1 and PU-1:1 reveals residual unreacted isocyanate in the respective formulations.

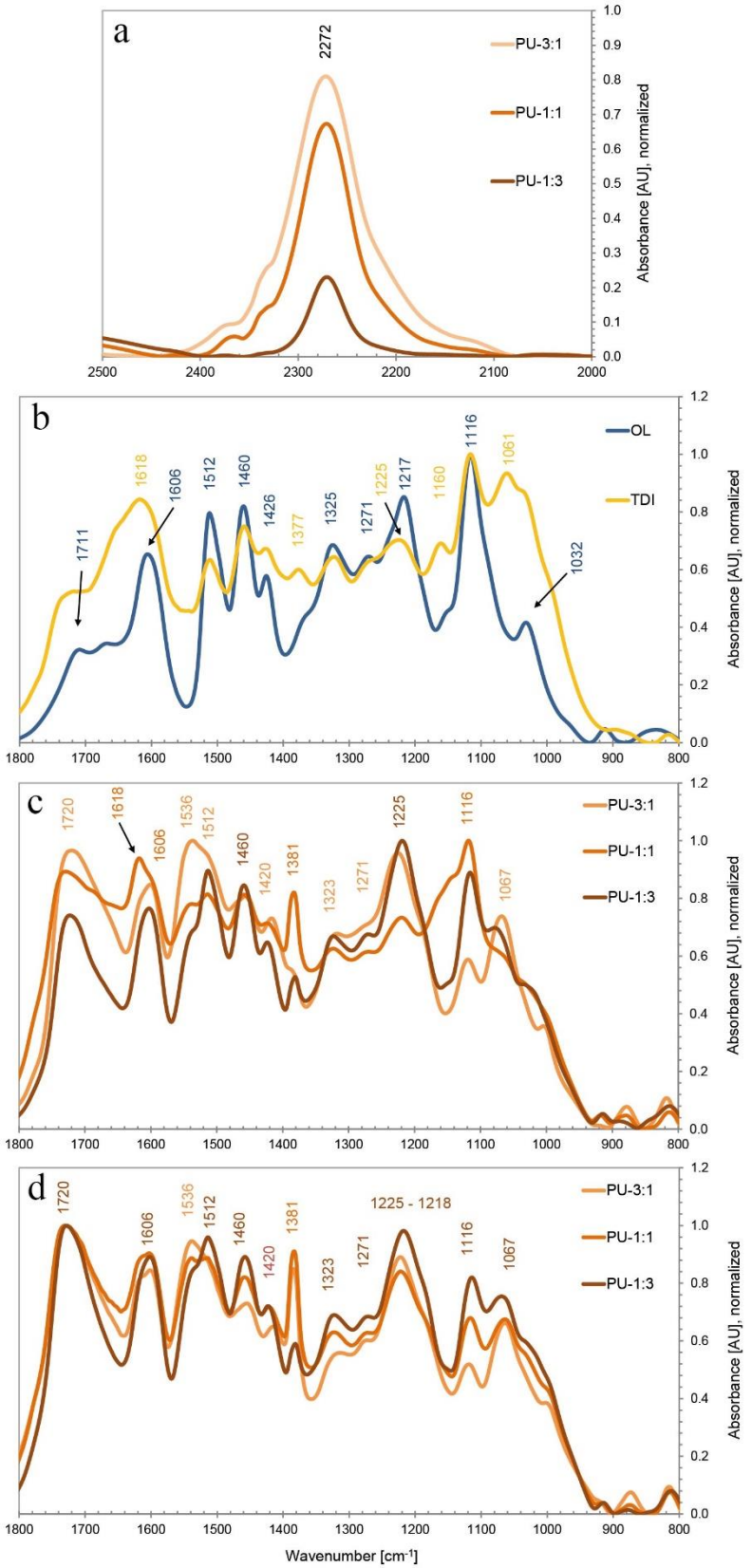

Figure 4. (a) Absorbance band of free isocyanate groups in the three different pre-pared PU formulations PU-3:1, PU-1:1 and PU-1:3. (b) FTIR spectra of Desmodur®L75 and Or-ganosolv lignin (OL). The three different prepared PU formulations PU-3:1, PU-1:1 and PU-1:3 after air-drying at room temperature (c) and after oven-drying at 60 °C for 72 h (d).

Figure 4b–d show the FTIR spectra of the three crosslinked PU formulations at room temperature (c), and the respective FTIR spectra of the cross-linked samples after post-curing under controlled conditions (60 °C for 72 h, d). The strong absorption band at 1720 cm^{-1} is attributable to the C=O group in the formed urethane linkages. Comparing the trends of the three different formulations, it was observed that the band is strongest in the formulation PU-3:1, followed by the formulations PU-1:1 and PU-1:3, respectively, in the case of crosslinking at room temperature. On the other hand, after crosslinking under controlled conditions, it is possible to note that the C=O band in all three different formulations in-creases and becomes the maximum in all three respective FTIR spectra. This indicates that the more hydroxyl groups were available with higher lignin concentration, the bigger the need for a temperature-induced crosslinking for the completion of urethane bonds' formation. In the range 1536–1512 cm^{-1}, similar trends can be found between the three formulations, with an increase in absorption in the case of crosslinking conducted under controlled conditions. The absorption peak at 1512 cm^{-1} is related to the stretching vibrations of the aromatic skeleton C=C [35], which characterizes both the chemical structure of lignin and of the isocyanate used (TDI). On the other hand, the absorption at 1536 cm^{-1} is attributed to the bending deformations related to the NH group of the formed urethane bond [32]. Thus, this absorption band is absent in the spectra of lignin, while it is found in the spectrum of TDI, respectively, which is a urethane prepolymer containing TDI. In Figure 4d, the band intensities at 1536 and 1512 cm^{-1}, respectively, therefore well-represent the ratio between TDI and OL in the three different formulations. The stretching vibration at 1225–1218 cm^{-1} corresponds to the C-N linkage [33,36] in the urethane group, while the band at 1218 cm^{-1} is assigned to S and G ring breathing in lignin [37], with both bands visible in all three formulations and under both crosslinking conditions. An increase of the absorbance at 1225 cm−1 can be observed in the formulation PU-1:3, especially in the case of controlled crosslinking (Figure 4c), indicating increased urethane bond formation with higher lignin content and temperature-induced curing of the respective formulation. The presence of an ab-sorption band at around 1067 cm^{-1} indicates the stretching deformation related to the urethane C-O-C soft bond [38]. After crosslinking treatment in the oven, increased ab-sorption at this frequency is observed in the formulations with a higher lignin content (PU-1:3) compared to curing at room temperature, in which the maximum absorption is observed for the formulation with higher isocyanate content (PU-3:1). The fact that in the FTIR spectrum of OL, no absorbance is observed at this frequency, strongly indicates the successful formation of urethane bonds in the formulation PU-1:3 after successive crosslinking at 60 °C. This behavior indicates that isocyanate spontaneously tends to react with the hydroxyl groups of water present in the atmosphere. In the case of temperature-induced crosslinking, the vibrational stretching

is greater in the formulation with a greater amount of lignin (PU-1:3), indicating a more intense interaction between isocyanate and hydroxyl groups from lignin.

FTIR maps were produced of all three coating formulations applied on wood samples as well as the reference PU coating, respectively, based on the band intensity at 1720 cm^{-1} (Figure 5). The absorbance scale of the reference sample PU-R shows a very narrow range of 0.004 absorbance units, indicating very high homogeneity of the commercial PU coating. Confronting the absorbance scales of the different prepared PU formulations, higher heterogeneity compared to the commercial PU coating is evident. However, a trend to a more homogeneous coating is observed when the lignin content increases. The absorbance of the urethane linkage IR band varies less over the mapped area for the formulations PU-1:1 and PU-1:3. Even if the coatings containing more lignin show superficial defects such as cracks, the rather homogeneous distribution of urethane bonds indicates successful crosslinking of the lignin-based PU coatings and a promising base for the development of bio-based PU coating solutions.

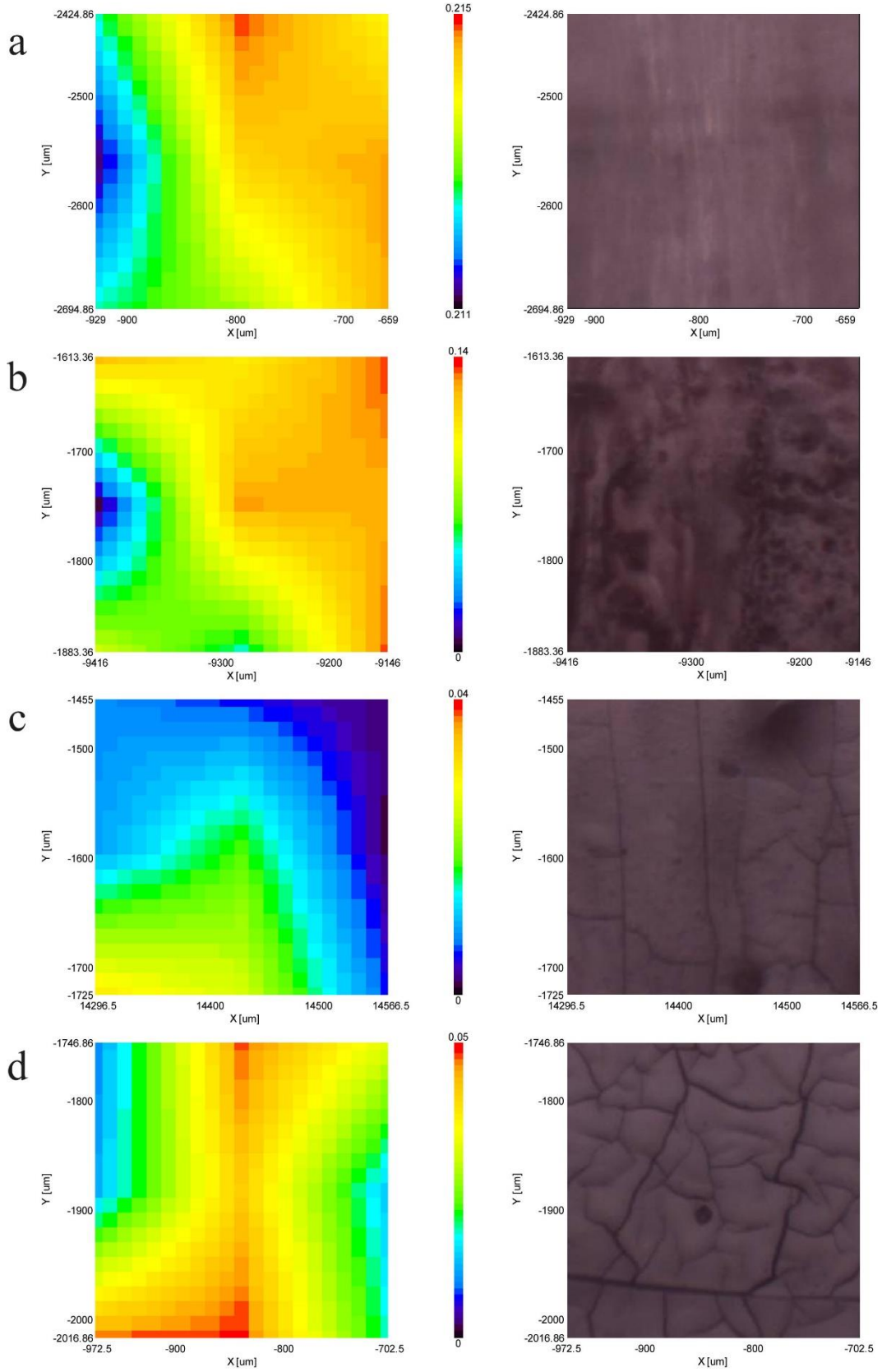

Figure 5. FTIR mapping images based on the absorbance band at 1720 cm^{-1} (left) and respective microscope pictures of the measurement areas (right). (a) WPU-R, (b) WPU-3:1, (c) WPU-1:1 and (d) WPU-1:3.

Pyrolysis-GC/MS

Figure 6 shows the pyrograms of the lignin sample OL and one PU formulation (PU-3:1) synthesized based on OL. The numbered peaks of the respective pyrolysis products are listed in Table 5. The S/G ratio of the utilized OL, which was isolated from beech wood, is much lower than that calculated for a beech lignin sample isolated using mild acidolysis [39]. However, the fact that the OL sample used here was isolated using a rather harsh Organosolv process that results in degradation of the lignin macromolecule could explain why the S/G ratios of OL differ from values determined for a mildly isolated lignin sample. For the sample PU-3:1, the S/G ratio could not be deter-mined correctly since the peaks of the pyrolysis products of PU overlapped with the respective peaks of major lignin pyrolysis products, and therefore the contribution of the respective compounds to the peak area was not conclusive. In the pyrogram of the PU sample, PU degradation products such as trimethylolpropane (PU-D1), isomers of toluene diisocyanate (PU-D2 and PU-D3) and 4-penten-2-ol (PU-D4) form the major peaks, while lignin pyrolysis products are detected at lower abundancies (Table 5). The strong excess of PU degradation products compared to lignin-derived compounds derives from the ratio of TDI:lignin of 3:1 in the analyzed sample (PU-3:1). Interestingly, the PU degradation products represent the main components of the commercial isocyanate Desmodur®L75 used in this study plus the compound PU-D4 deriving from further degradation of diethylenglycol. This degradation pattern cleaving the urethane bonds in the PU network is in concordance with thermal degradation mechanisms of polyurethanes reported by Jiao et al. [40] and indicates a straightforward polymerization reaction without side products' creation between the commercial isocyanate and the OL used as a polyol in the prepared PU formulations.

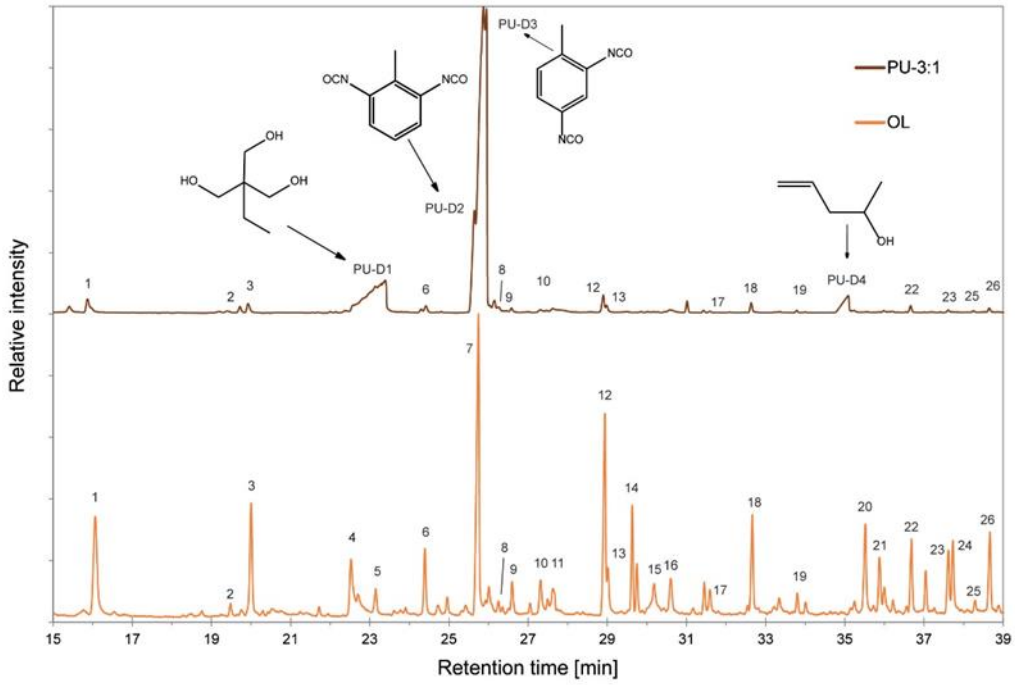

Figure 6. Pyrograms of the Organosolv lignin (OL) used and one of the pro-duced PU sample (PU-3:1).

Table 5. Retention times, relative abundances, assignment to guaiacyl-type (G) or syringyl-type (S) aromatic lignin subunits of pyrolysis products and respective S/G ratios of the Organosolv lignin (OL) used and one of the produced PU sample (PU-3:1).

#	Pyrolysis Product	RT (min)	PU-3:1 (%)	OL (%)
1	Guaiacol	16.07	1.3	6.7
2	5-Methylguaiacol	19.48	0.4	0.5
3	Creosol	20.01	0.7	4.6
4	5-Methoxyresinol	22.53	-	2.8
PU-D1	Trimethylolpropane	23.13	15.0	-
5	4-Ethylguaiacol	23.15	-	1.0
6	4-Vinylguaiacol	24.39	0.7	2.6
PU-D2	2.6-Diisocyanate toluene	25.65	9.1	-
7	Syringol	25.75	-	15.1
PU-D3	2,4-Diisocyanate toluene	25.95	63.3	-
8	Dihydroeugenol	26.25	-	0.4
9	Methylsyringol	26.60	0.2	1.1
10	Vanillin	27.31	0.1	1.6
11	Isoeugenol, cis	27.63	-	1.4
12	Vanillic acid	28.94	1.1	8.5
13	Isoeugenol, trans	29.01	0.4	1.6
14	Lauryl chloride	29.63	-	3.4
15	1-Dodecanol	29.75	-	1.6
16	Acetoguaiacone	30.18	-	0.9
17	Guaiacylacetone	31.59	0.1	0.9
18	3,5-Dimethoxyacetophenone	32.67	0.6	3.9
19	Methoxyeugenol	33.80	0.1	0.7
PU-D4	4-Penten-2-ol	35.08	2.7	-
20	Syringaldehyde	35.52	-	3.7
21	Myristyl chloride	35.89	-	2.7
22	Ferulic acid	36.68	0.4	2.8

23	Acetosyringone	37.61	0.1	2.6
24	Myristyl alcohol	37.73	-	2.7
25	Stearic acid	38.29	0.1	0.4
26	Homosyringic acid	38.67	0.3	3.2
	S/G ratio		-	1.0

Conclusions

In conclusion, with the increasing lignin content, the color change between un-coated and coated wood increased, tending to red-yellow darker tones. On the other hand, the commercial PU coating barely affected the color change. In addition, WPU-R is transparent, in strong contrast to the prepared lignin-based PU coatings, which made the wood surface opaque. For a higher lignin concentration, solid content, and consequently weight gain, increased as well, whereas WPU-R had a higher SC and weight gain supposedly because of different additives. Coating film profiles appeared more homogenous for the commercial coating than for the prepared formulations, even if an application by brush generally renders the film profile slightly irregular. Contact angles decreased with higher lignin contents and were always lower com-pared to standard PU coatings at the used lignin concentrations. However, confronting the determined contact angles with the ones observed with virgin wood, an increase in hydrophobicity of the wood surfaces was evident. The lignin concentration also affected the general appearance of the coatings, which presented many cracks for higher lignin contents. FTIR spectroscopy showed the chemical incorporation of lignin in the structure of the prepared polyurethanes, creating urethane bonds between the applied and the iso-cyanate and hydroxyl groups of lignin, especially at higher lignin contents. The use of an FTIR microscope for the construction of FTIR maps proved very useful in order to evaluate the homogeneity of the surfaces of PU coating films. Py-GC/MS of the prepared PU formulation further strongly indicated a successful incorporation of lignin in the polyurethane network, since no side-products were detected, and thermal degradation of the PU resulted in the original components of the commercial isocyanate on one side and usual lignin pyrolysis products on the other.

References

1. Tamantini, S.; Del Lungo, A.; Romagnoli, M.; Paletto, A.; Keller, M.; Bersier, J.; Zikeli, F. Basic Steps to Promote Biorefinery Value Chains in Forestry in Italy. Sustainability 2021, 13, 11731, https://doi.org/10.3390/su132111731

2. Nitzsche, R.; Gröngröft, A.; Köchermann, J.; Meisel, K.; Etzold, H.; Verges, M.; Leschinsky, M.; Bachmann, J.; Saake, B.; Torkler, S.; et al. Platform and fine chemicals from woody biomass: Demonstration and assessment of a novel biorefinery. Biomass Convers. Biorefinery 2020, 11, 2369–2385 –17, https://doi.org/10.1007/s13399-020-00769-z

3. De Angelis, M.; Romagnoli, M.; Vek, V.; Poljanšek, I.; Oven, P.; Thaler, N.; Lesar, B.; Kržišnik, D.; Humar, M. Chemical composition and resistance of Italian stone pine (Pinus pinea L.) wood against fungal decay and wetting. Ind. Crop. Prod. 2018, 117, 187–196, https://doi.org/10.1016/j.indcrop.2018.03.016

4. Füchtner, S.; Brock-Nannestad, T.; Smeds, A.; Fredriksson, M.; Pilgård, A.; Thygesen, L.G. Hydrophobic and Hydrophilic Ex-tractives in Norway Spruce and Kurile Larch and Their Role in Brown-Rot Degradation. Front. Plant Sci. 2020, 11, 1-20, https://doi.org/10.3389/fpls.2020.00855

5. Romagnoli, M.; Cavalli, D.; Pernarella, R.; Zanuttini, R.; Togni, M. Physical and mechanical characteristics of poor-quality wood after heat treatment. Iforest-Biogeosci. For. 2015, 8, 884–891, https://doi.org/10.3832/ifor1229-007

6. Khan, A.; Huang, K.; Sarwar, M.G.; Cheng, K.; Li, Z.; Tuhin, M.O.; Rabnawaz, M. Self-healing and self-cleaning clear coating. J. Colloid Interface Sci. 2020, 577, 311–318, https://doi.org/10.1016/j.jcis.2020.05.073

7. Jusic, J.; Tamantini, S.; Romagnoli, M.; Vinciguerra, V.; Di Mattia, E.; Zikeli, F.; Cavalera, M.; Scarascia Mugnozza, G. Im-proving sustainability in wood coating: Testing lignin and cellulose nanocrystals as additives to commercial acrylic wood coatings for bio-building. Iforest-Biogeosci. For. 2021, 14, 499–507, https://doi.org/10.3832/ifor3782-014

8. Thakur, V.K.; Thakur, M.K.; Raghavan, P.; Kessler, M.R. Progress in Green Polymer Composites from Lignin for Multifunctional Applications: A Review. ACS Sustain. Chem. Eng. 2014, 2, 1072–1092, https://doi.org/10.1021/sc500087z

9. Mattos, B.D.; Tardy, B.L.; Magalhães, W.L.E.; Rojas, O.J. Controlled release for crop and wood protection: Recent progress toward sustainable and safe nanostructured biocidal systems. J. Control. Release 2017, 262, 139–150, https://doi.org/10.1016/j.jconrel.2017.07.025

10. Papadopoulos, A.N.; Bikiaris, D.N.; Mitropoulos, A.C.; Kyzas, G.Z. Nanomaterials and Chemical Modifications for Enhanced Key Wood Properties: A Review. Nanomaterials 2019, 9, 607.

11. UNI EN 927-1:2013 Paints and Varnishes-Coating Materials and Coating Systems for Exterior Wood-Part 1: Classification and Selec-tion; ISO: Geneva, Switzerland, 2013.

12. Singh, T.; Singh, A.P. A review on natural products as wood protectant. Wood Science and TechnologyWood Sci. Tech-nol . 2011, 46, 851–870, https://doi.org/10.1007/s00226-011-0448-5

13. Teacă, C.A.; Rosu, D.; Mustaţă, F.; Rusu, T.; Roşu, L.; Irina, R.; Varganici, C.-D. Natural bio-based products for wood coating and protection against degradation: A Review. BioResources 2019, 14, 4873–4901, https://doi.org/10.15376/biores.14.2.Teaca

14. Bulian, F.; Graystone, J.A. Chapter 3-raw materials for wood coatings (1)-film formers (binders, resins and polymers). In Wood Coatings; Bulian, F., Graystone, J.A., Eds.; Elsevier: Amsterdam, The Netherlands, 2009; pp. 53–94, https://doi.org/10.1016/B978-0-444-52840-7.00003-5

15. Ahvazi, B.; Wojciechowicz, O.; Ton-That, T.-M.; Hawari, J. Preparation of Lignopolyols from Wheat Straw Soda Lignin. J. Agric. Food Chem. 2011, 59, 10505–10516, https://doi.org/10.1021/jf202452m

16. Aristri, M.A.; Lubis, M.A.R.; Yadav, S.M.; Antov, P.; Papadopoulos, A.N.; Pizzi, A.; Fatriasari, W.; Ismayati, M.; Iswanto, A.H. Recent Developments in Lignin- and Tannin-Based Non-Isocyanate Polyurethane Resins for Wood Adhesives—A Review. Appl. Sci. 2021, 11, 4242, https://doi.org/10.3390/app11094242

17. Jia, Z.; Lu, C.; Zhou, P.; Wang, L. Preparation and characterization of high boiling solvent lignin-based polyurethane film with lignin as the only hydroxyl group provider. RSC Adv. 2015, 5, 53949–53955, https://doi.org/10.1039/C5RA09477A

18. Wang, Y.-Y.; Cal, C.M.; Ragauskas, A.J. Recent advances in lignin-based polyurethanes. Tappi J. 2017, 16 , 203-207, https://doi.org/17/APR/17APR203.aspx

19. Stachak, P.; Łukaszewska, I.; Hebda, E.; Pielichowski, K. Recent Advances in Fabrication of Non-Isocyanate Polyure-thane-Based Composite Materials. Materials 2021, 14, 3497, https://doi.org/10.3390/ma14133497

20. Rokicki, G.; Parzuchowski, P.G.; Mazurek, M. Non-isocyanate polyurethanes: Synthesis, properties, and applications. Polym. Adv. Technol. 2015, 26, 707–761, https://doi.org/10.1002/pat.3522

21. Wei, D.; Zeng, J.; Yong, Q. High-Performance Bio-Based Polyurethane Antismudge Coatings Using Castor Oil-Based Hyper-branched Polyol as Superior Cross-Linkers. ACS Appl. Polym. Mater. 2021, 3, 3612–3622, https://doi.org/10.1021/acsapm.1c00503

22. Alinejad, M.; Henry, C.; Nikafshar, S.; Gondaliya, A.; Bagheri, S.; Chen, N.; Singh, S.K.; Hodge, D.B.; Nejad, M. Lignin-Based Polyurethanes: Opportunities for Bio-Based Foams, Elastomers, Coatings and Adhesives. Polymers 2019, 11, 1202, https://doi.org/10.3390/polym11071202

23. Balakshin, M.Y.; Capanema, E.A.; Sulaeva, I.; Schlee, P.; Huang, Z.; Feng, M.; Borghei, M.; Rojas, O.J.; Potthast, A.; Rosenau, T. New Opportunities in the Valorization of Technical Lignins. ChemSusChem 2021, 14, 1016–1036, https://doi.org/10.1002/cssc.202002553

24. Ralph, J.; Lapierre, C.; Boerjan, W. Lignin structure and its engineering. Curr. Opin. Biotechnol. 2019, 56, 240–249, https://doi.org/10.1016/j.copbio.2019.02.019

25. Gadhave, R.V.; S. Kasbe, P.; Mahanwar, P.A.; Gadekar, P.T. Synthesis and characterization of lignin-polyurethane based wood adhesive. Int. J. Adhes. Adhes. 2019, 95, 102427, https://doi.org/10.1016/j.ijadhadh.2019.102427

26. Zikeli, F.; Vinciguerra, V.; D'Annibale, A.; Capitani, D.; Romagnoli, M.; Scarascia Mugnozza, G. Preparation of Lignin Na-noparticles from Wood Waste for Wood Surface Treatment. Nanomaterials 2019, 9, 281, https://doi.org/10.3390/nano9020281

27. Pan, X.; Saddler, J.N. Effect of replacing polyol by organosolv and kraft lignin on the property and structure of rigid polyu-rethane foam. Biotechnol. Biofuels 2013, 6, 1–10, https://doi.org/10.1186/1754-6834-6-12

28. Faix, O.; Meier, D.; Fortmann, I. Thermal degradation products of wood: Gas chromatographic separation and mass spec-trometric characterization of monomeric lignin derived products. Holz Als Roh Werkst. 1990, 48, 281–285, https://doi.org/10.1007/bf02626519

29. Faix, O.; Meier, D.; Fortmann, I. Thermal degradation products of wood: A collection of electron-impact (EI) mass spectra of monomeric lignin derived products. Holz Als Roh- Und Werkst. 1990, 48, 351–354, https://doi.org/10.1007/bf02639897

30. UNI EN ISO/CIE 11664-4:2019 Colorimetry-Part 4: CIE 1976 L*a*b* Colour Space; ISO: Geneva, Switzerland, 2019.

31. UNI EN 927-6:2019 Paints and Varnishes-Coating Materials and Coating Systems for Exterior Wood-Part 6: Exposure of Wood Coatings to Artificial Weathering Using Fluorescent Uv Lamps and Water; ISO: Geneva, Switzerland, 2019.

32. Klein, S.E.; Rumpf, J.; Kusch, P.; Albach, R.; Rehahn, M.; Witzleben, S.; Schulze, M. Unmodified kraft lignin isolated at room temperature from aqueous solution for preparation of highly flexible transparent polyurethane coatings. RSC Adv. 2018, 8, 40765–40777, https://doi.org/10.1039/C8RA08579J

33. Griffini, G.; Passoni, V.; Suriano, R.; Levi, M.; Turri, S. Polyurethane Coatings Based on Chemically Unmodified Fractionated Lignin. ACS Sustain. Chem. Eng. 2015, 3, 1145–1154, https://doi.org/10.1021/acssuschemeng.5b00073

34. Lang, J.M.; Shrestha, U.M.; Dadmun, M. The Effect of Plant Source on the Properties of Lignin-Based Polyurethanes. Front. Energy Res. 2018, 6, 1-12, https://doi.org/10.3389/fenrg.2018.00004

35. Nasar, A.S.; Kalaimani, S. Synthesis and studies on forward and reverse reactions of phenol-blocked polyisocyanates: An in-sight into blocked isocyanates. RSC Adv. 2016, 6, 76802–76812, https://doi.org/10.1039/C6RA15643F

36. Chauhan, M.; Gupta, M.; Singh, B.; Singh, A.; Gupta, V. Effect of functionalized lignin on the properties of lignin–isocyanate prepolymer blends and composites. Eur. Polym. J. 2014, 52, 32–43, https://doi.org/10.1016/j.eurpolymj.2013.12.016

37. Faix, O. Classification of Lignins from Different Botanical Origins by FT-IR Spectroscopy. Holzforschung 1991, 45, 21–28, https://doi.org/10.1515/hfsg.1991.45.s1.21

38. Bandekar, J.; Klima, S. FT-IR spectroscopic studies of polyurethanes Part I. Bonding between urethane C-O-C groups and the NH Groups. J. Mol. Struct. 1991, 263, 45–57, https://doi.org/10.1016/0022-2860(91)80054-8

39. Zikeli, F.; Vinciguerra, V.; Taddei, A.R.; D'Annibale, A.; Romagnoli, M.; Scarascia Mugnozza, G. Isolation and characterization of lignin from beech wood and chestnut sawdust for the preparation of lignin nanoparticles (LNPs) from wood industry side-streams. Holzforschung 2018, 72, 961–972, https://doi.org/10.1515/hf-2017-0208

40. Jiao, L.; Xiao, H.; Wang, Q.; Sun, J. Thermal degradation characteristics of rigid polyurethane foam and the volatile products analysis with TG-FTIR-MS. Polym. Degrad. Stab. 2013, 98, 2687–2696, https://doi.org/10.1016/j.polymdegradstab.2013.09.032

CHAPTER 2: Extraction and Characterization of Acidolysis Lignin from Turkey Oak (*Quercus cerris* L.) and Eucalypt (*Eucalyptus camaldulensis* Dehnh.) Wood from Population Stands in Italy

Sara Bergamasco *, Florian Zikeli, Vittorio Vinciguerra, Anatoly Petrovich Sobolev, Luca Scarnati, Giorgio Tofani, Giuseppe Scarascia Mugnozza and Manuela Romagnoli *

Polymers **2023**, *15*(17), 3591; https://doi.org/10.3390/polym15173591

Abstract

Acidolysis lignins from the species *Quercus cerris* L. and *Eucalyptus camaldulensis* Dehnh. were iso-lated and characterized using high pressure size exclusion chromatography (HP-SEC), Fourier-transform (FTIR) infrared spectroscopy, analytical pyrolysis–gas chromatography–mass spectrometry (Py-GCMS), and two-dimensional heteronuclear single quantum coherence (2D HSQC) NMR spectroscopy. The acidolysis lignins from the two different species varied in chemical com-position and structural characteristics, with Q. cerris L. lignin having a higher S/G ratio and higher molar mass averages with a bimodal molar mass distribution. The different analytical techniques FTIR spectroscopy, Py-GCMS, and 2D NMR spectroscopy provided consistent results regarding the S/G ratio of the lignins from the two wood species. Based on the determined high S/G ratio of both oak and eucalypt lignin, the two wood sources could be promoted as substrates for efficient lignin isolation in modern forest biorefineries in order to develop innovative lignin-based value-added biorefinery products.

Keywords: acidolysis lignin; oak; eucalyptus; wood; HP-SEC; FTIR; Py-GCMS; 2D HSQC NMR spectroscopy; bioresources; short supply chain; bioeconomy

Introduction

The principle of a circular economy as a tool to establish a future green economy is of particular relevance when applied to the wood industry. Considering the forest-wood sector, the concept of cascading needs to be implemented as good practice, meaning that a processed wood product or wood processing residues are used at least once more as material or for energy generation [1]. Recently, Stafford et al. [2] highlighted the potential of forest biorefineries with their existing well developed infrastructure for the processing of huge amounts of biomass to develop new bioproduct value chains for product diversification, which could generate new revenues and improve their overall resilience. Furthermore, through the cascade use of wood in forest biorefineries, the global warming potential of these systems can be significantly reduced [3]. Forest biorefineries are characterized by a large portfolio of lignin and cellulose-based products, such as biocomposites, resins, platform chemicals, building blocks for fine chemicals or bioactive compounds utilizing wood residues and wastes from the forest, timber, and pulp, and paper industry [2,4]. Additionally, there is a large potential in the feedstock supply considering the huge abundance of sawdust from sawing processes [4,5] and great volumes of different waste streams containing lignin, hemicelluloses, and extractives generated in the pulp and paper industry [2,6]. Among the most important components, lignin attracted high interest in recent times as it can be used for the production of several biomaterials [7–9]. The main reason for this interest is the fact that this biopolymer contains a broad range and high contents of chemical functionalities such as hydroxyl, carbonyl, and carboxyl groups [8,10–13]. The presence of these reactive functional groups allows for its utilization in biobased polymers development, such as a substitute for fossil-based compounds in polyurethane systems, polyesters, and epoxy resins [14–16]. One of the biggest challenges regarding the utilization of lignin is the fact that its molecular structure, properties, and reactivity are influenced by the original feedstock (softwood, hardwood and grass biomass) as well as the extraction process used for its isolation [17,18]. For this reason, the study of the chemical structure and presence of functional groups of lignins isolated from different plant sources is crucial to deter-mine species-specific lignin properties and reactivity for possible eventual applications. The intention of this article is to valorize certain Italian local wood resources. The first one is Turkey oak (*Quercus cerris* L.), which is one of the most widespread deciduous oak species in Italy together with pubescent oak (*Q. pubescens* Willd) [19]. Turkey oak was used for railway sleepers and barrels in the past, but today it is mainly used as firewood. Wood chemistry studies regarding oak are not so frequent; some contributions are related to the interest for oak wood properties, for example in wine and spirit ageing [20]. The second short supply chain species investigated in this study is *Eucalyptus camaldulensis* Dehnh., which is present in many windbreaks in Italy. Eucalypt trees used for wind-breaking stripes in coastal agricultural areas protect crop cultivations from continuous stress

due to constant winds and eventual water loss in the soil. Eucalyptus spp. Is frequently planted because of its high adaptability to different climatic conditions, fast growth, and high-level wood properties, i.e., in Brazil, 77% of all newly planted trees were from eucalypt species [5]. In Italy, there are more than 70,000 ha of eucalypt plantations and the most common species is *E. camaldulensis*, which was first described in 1832 from the botanical garden *Hortus Camaldulensis* near Naples, Italy. Besides the protection from soil erosion, eucalypt trees were massively introduced for the production of pulpwood for the Italian pulp and paper industry in the first half of the 20th century [21,22]. Because of the reduced importance of paper mills in Italy nowadays and limitations for high-value applications of eucalypt wood due to excessive shrinking and eventual splitting during drying causing low yields [23], eucalypt wood is often used for energy purposes as its caloric value is in the range of other common firewoods used in Italy like oak and beech [24]. A detailed knowledge of lignin structure of both species represents the first step for a rational exploitation of respective wood chips and wood processing residues for value-added future lignin applications. A wide range of analytical techniques has been used for the elucidation of lignin structural characteristics and the methods applied in the presented work are among the most important and most frequently used ones, namely FTIR and NMR spectroscopy, analytical Py-GCMS, as well as SEC analysis [17,19,25–28].

Materials and Methods

Materials

The studied oak wood was derived from a disk of an adult tree of *Q. cerris* from the Roccarespampani Estate close to Tuscania (Viterbo province, Italy). The eucalypt wood was derived from windbreak trees of *E. camaldulensis* close to Tarquinia (Viterbo province, Italy). The wood was obtained during tree management activities in 2022. For lignin extraction, the following solvents were used: acetone Re pure, 1,4-dioxane, hydro-chloric acid 37%, dimethyl sulfoxide-d6 99.5% (Isotopic), and potassium bromide (KBr) were purchased from Carlo Erba Reagents (Cornaredo, Italy). Polystyrene sulfonate standards were purchased from PSS Polymer Standard Services (Mainz, Germany), Millex®-GV syringe filters (0.22 µm) in PVDF were purchased from Millipore Corporation (Belford, MA, USA). Sodium hydroxide was purchased from Merck Life Science S.r.l. (Milan, Italy).

Lignin Isolation

Acidolysis lignins (AL) from oak and eucalypt were isolated using a mild acidolysis method, which was described in detail in earlier works of the group [27,28] and is based on the protocol of Gellerstedt et al. [29]. Prior to extraction, oak and eucalypt wood was physically pretreated, reducing it to a particle size of 0.25 mm using a cutting mill (MF 10 basic, IKA Werke, Staufen im Breisgau,

Germany) and subsequently extracted with acetone-water (90:10, v/v) using a Soxhlet apparatus (24 g wood meal in 400 mL acetone-water).

The extracted wood meal was collected, oven-dried at 40 °C (FD 115, Binder GmbH, Tuttlingen, Germany), and weighed. The extractives dissolved in acetone-water were brought to dryness and weighed as well to determine the extractives content of the used oak and eucalypt wood. The extracted biomass (13.5 g) was cooked under re-flux using dioxane-water (400 mL) in a volumetric ratio of 82:18 in a 0.1 M HCl solution for two hours. At the end, the solution was filtered for removal of the acidolysis residue. The filtration residue was washed with a portion of 200 mL dioxane-water (82:18 vol%). In order to precipitate the dissolved lignin in the filtrate, dioxane was removed by rotary evaporation and replaced with water of equal volume fractions. Finally, the solution was filtered, and the collected lignin was further washed with acidified (pH 2) distilled water to remove sugar residues. Finally, the lignin was dried in a ventilated oven (J.P. Selecta, Barcelona, Spain) at 40 °C for 2 h and weighed to calculate the yield.

High Performance Size Exclusion Chromatography (HP-SEC)

The molecular weights of the extracted lignins were determined by HP-SEC. The analysis was performed using an Agilent 1100 HPLC system equipped with a temperated column compartment and a diode array detector using Agilent Chemstation (version B.03.02) for operation (Agilent Technologies Inc., Santa Clara, CA, USA). Molar mass analysis was performed using a PSS MCX column with 5 µm particle size and 1000 Å pore size (PSS Polymer Standard Services, Mainz, Germany) which was kept at 40 °C. The mobile phase was a 10 mM NaOH solution with addition of 20 mM NaNO3 as neutral salt. The flow rate was set to 0.5 mL/min and the UV signal at 280 nm was used for molar mass determination. For calibration, polystyrene sulfonate standards were used with the following molar masses at peak maximum: 65,400, 33,500, 15,800, 6430, 1670, 891, and 208 Da. Weight- and number-average molar masses were calculated using the GPC Add-on (version B.01.02) of Agilent Chemstation software.

Fourier Transform Infrared (FTIR) Spectroscopy

For FTIR analysis, potassium bromide (KBr) pellets containing 2 wt% of the respective lignin samples were prepared and measured against a background of pure KBr. Samples were prepared using a mini pellet press at 2 bar for 5 min (Specac Inc., Fort Washington, MD, USA). The FTIR spectra were acquired in absorbance mode with a resolution of 4 cm^{-1} and an average of 16 scans in a wavenumber range of 4000–800 cm^{-1} using a FTIR-4100 Fourier Transform Infrared spectrometer (Jasco Corp., Easton, MD, USA). The fingerprint region (1800–900 cm^{-1}) was studied for each

sample and the absorption bands were interpreted and assigned using reference literature reported in Table 3.

Pyrolysis–Gas Chromatography–Mass Spectrometry (Py–GCMS)

Samples of about 1.5 mg of the isolated AL from oak and eucalyptus wood were heated to 450 °C using a Pyrojector II (SCE Analytical Science, Trajan Scientific and Medical, Melbourne, Australia), connected to a GCMS-QP5050 instrument (Shimadzu Corporation, Kyoto, Japan). Helium was the carrier gas at a pressure of 100 kPa in the pyrolyzer and 70 kPa in the GC injector (280 °C, 1:20 split ratio). Furnace temperature was initially set at 45 °C for 4 min, then increased to 240 °C at a rate of 4 °C min^{-1}, and finally to 280 °C at a rate of 39 °C min^{-1}. The mass spectrometer was used in electron ionization (EI) mode at 70 eV and scans from m/z 35 to 500 were run in 0.7 s cycles. The pyrolysis products were identified by comparing their mass spectra with those of the NIST and Wiley libraries and those reported in literature as published in earlier works [26–28,30]. The peaks of interest were identified, the spectra were normalized to the most intense peak, and the respective peak areas were expressed as percentages.

Two-Dimensional (2D) HSQC NMR Spectroscopy

Two-dimensional ^{1}H-^{13}C heteronuclear single quantum coherence (2D HSQC) NMR spectra were recorded on a Bruker AVANCE 600 spectrometer operating at the proton frequency of 600.13 MHz with a z-gradient probe using 50 mg of the lignin samples in 700 µL DMSO-d6. The HSQC experiments were acquired using a time do-main of 1024 data points in the F2 dimension (1H) and 512 data points in the F1 dimension (13C). A ^{1}JC-H coupling constant of 145 Hz and spectral widths of 12 ppm and 220 ppm in the 1H- and 13C-dimensions, respectively, were used applying 128 scans with a recycle delay of 3 s. For a semi-quantitative analysis, the integrals of the C-H cross-peaks were determined and compared using MestReNova v6.0.2 software (Mestrelab Research S.L., Santiago de Compostela, Spain). Signal assignment was conduct-ed according to the literature [31–37]. The monomeric ratio of the AL fractions was estimated from the C_2-H_2 correlations from syringyl (S), guaiacyl (G), and p-hydroxyphenyl (H) lignin subunits as well as ferulic acid (FA) groups in the aromatic region of the HSQC spectra. The Cα-Hα correlations were used for the determination of the relative abundances of the different lignin inter-unit linkages as well as the ratio of stilbene structures.

Results and Discussion

Table 1 shows the respective extractives and AL yields for Turkey oak and eucalypt wood in relation to the mass of the starting material. The determined extractives content was three times higher in eucalypt wood compared to oak, while the AL isolation yields were comparable in the two different wood species. Comparing these yields with the Klason lignin contents of the two species reported in

literature, which can vary a lot depending on the source [38–42], it could be concluded that the acidolysis method, independent of the used wood species and its respective lignin con-tent, has a maximum extraction efficiency of about 7% relative to the dry wood mass and about 30% of the respective Klason lignin content.

Table 1. Extractives content and acidolysis lignin (AL) isolation yield as well as Klason lignin con-tents for oak (*Q. cerris*) and eucalypt (*E. camaldulensis*) wood reported in reference literature [38–42]

Wood Species	Extractives (%)	AL (%)	Klason Lignin (%)
Q. cerris	2.0	7.3	23.2–25.5
E. camaldulensis	6.1	7.2	21.4–27.7

Molar Mass Distribution (MMD)

Analysis through HP-SEC offers a clear insight concerning the molecular weight distribution of extracted lignins, which enriches knowledge in terms of reactivity and chemical-physical properties of lignin since they are partly determined by their MMD. As a result of the extraction process, lignins are depolymerized into smaller fractions, and so HPSEC analysis can provide an estimate of the delignification and of pulping rate of a certain extraction process [43]. Figure 1 shows the HP-SEC chromatograms (left) of the two isolated acidolysis lignins AL-OA and AL-EU and their respective molar mass distributions (MMDs) (Figure 1b). While AL-OA shows a bimodal MMD, the elugram of AL-EU exhibits a broad single peak. The maximum of the elution curve of AL-EU is found in between the two maxima of AL-OA and the overall MMD appears slimmer, which reflects in the calculated dispersity (Đ, Table 2). Thus, the calculated weight-average molar mass (Mw) of AL-OA is higher than the one of AL-EU while the number-average molar mass (Mn) is lower.

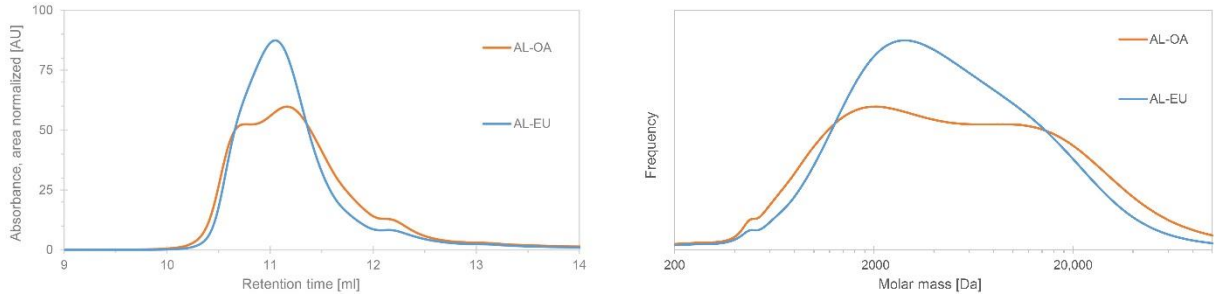

(**a**) (**b**)

Figure 1. HP-SEC chromatograms (a) and molar mass distributions (b) of the isolated acidolysis lignins from oak (AL-OA) and eucalypt (AL-EU).

Table 2. Weight-average (Mw) and number-average (Mn) molar mass, and dispersity (Đ) of the isolated acidolysis lignins from oak and eucalypt wood (AL-OA and AL-EU). Acidolysis lignins from beech wood (AL-B), chestnut sawdust (AL-Ch), iroko (AL-IR), and mixed iroko and Norway spruce sawdust (AL-IRNS) from earlier works are also reported.

LIGNIN SAMPLE	M_w (Da)	M_n (Da)	Đ
AL-OA	5170	1227	4.21
AL-EU	4841	1472	3.29
AL-B	4510	1032	4.37
AL-Ch	3583	1099	3.26
AL-IR	3270	1084	3.02
AL-IRNS	3895	1126	3.46

Interestingly, the determined molar mass averages of AL-OA and AL-EU were a little higher than the results obtained for ALs isolated from beech and chestnut as well as iroko and mixed iroko and Norway spruce sawdust using the same protocol, which were re-analyzed under the same HP-SEC conditions and using the same software for molar mass determination [27,28]. Comparing those ALs from six different wood species, AL from oak wood had the highest value for M_w but also a high dispersity (Đ), which was in the range of AL from beech wood. High molar mass averages indicate little cleavage of lignin inter-unit linkages during isolation, which was an objective of the used mild acidolysis protocol in order to obtain rather native lignin samples. Further, the very intense cross-peak of the Cα atom assigned to β-O-4′ linkages (Figure 4) and the corresponding high relative abundance of β-O-4′ bonds (Table 5) support the conclusion that little lignin depolymerization occurred during acidolysis. Considering the high M_w as well as M_n of AL-EU, resulting in a rather low dispersity, AL from eucalypt wood could be considered as the one with the highest molar mass out of the selection of the six ALs from different wood species. Molar mass value has an impact on lignin properties and its possible applications. For example, it was shown that lignin fractions with lower molecular weights, and as a consequence, exhibits stronger scavenging and antioxidant abilities with higher amounts of phenolic hydroxyl groups, making it a promising active ingredient in bio-medical engineering applications [44].

FTIR Spectroscopy

The FTIR spectra of AL-OA and AL-EU were of similar shape; specific differences of the IR bands intensities were observed. The chemical structures assigned to the respective characteristic IR absorbance bands in Figure 2 are listed in Table 3. The IR band 1 located at 1725–1719 cm^{-1} corresponds to the stretching vibration of carbonyl groups in unconjugated ketones, aldehydes, and esters in hemicelluloses. The low intensity of this IR band indicates a low contribution of hemicelluloses and thus a high purity of the prepared AL samples. Band 2 around 1611–1593 cm^{-1} was assigned to the aromatic skeletal vibration with contributions of carbonyl C=O stretching modes. There was a significant difference in IR band 2 between the AL samples of the two species with AL-

EU showing a wider absorbance band with a maximum shifted to a higher wavenumber, most probably deriving from additional C=O stretching modes indicating a higher content of Cα-oxidized structures in AL-EU. Therefore, a contribution to this signal could be the Cα-oxidized structures which are present in both lignin samples, as observed by 2D NMR analysis (Table 5). However, the relative contents of Cα-oxidized structures determined by 2D NMR spectroscopy were higher in AL-OA than in AL-EU, indicating further structures present in AL-EU, which cause the high absorbance in the region of IR band 2. Comparing the FTIR spectrum of AL-EU with the one of an AL isolated from iroko sawdust, which was apparently rich of contributions form extractives moieties [28], it could be speculated that there is also a considerable presence of extractives in the AL-EU isolated in this study. An additional explanation of the high IR absorbance at 1640–1610 cm^{-1} is given by Xiao et al. [34], who attribute this phenomenon to the presence of small molecular compounds like polyphenols, condensed tannins, or calcium oxalate crystals, which is the most common formed minerals in plants, inside the wood structure of eucalypt.

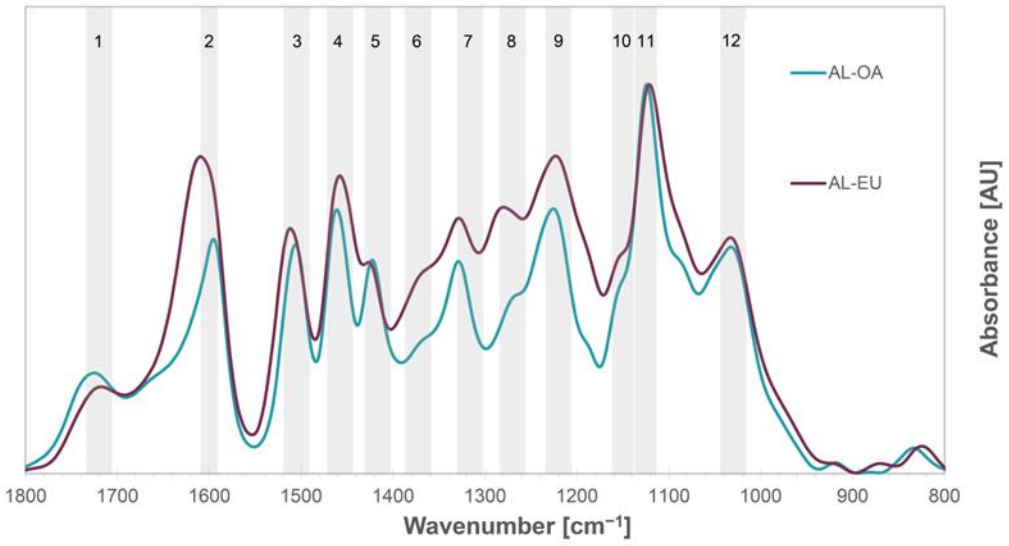

Figure 2. FTIR spectra of the isolated acidolysis lignins from oak (AL-OA) and eucalypt wood (AL-EU). The respective signal assignments of the IR band numbers are given in Table 3.

Table 3. IR bands and assigned chemical structures found in the lignin samples.

IR Band	Wavenumber (cm^{-1})		Assignment	Reference
	Oak	Eucalypt		
1	1725	1719	C=O stretch in unconjugated ketones, in carbonyl and ester group	[45,46]
2	1593	1611	Aromatic skeletal vibrations plus C=O stretching, C=C aromatic ring vibration (S > G), G condensed > G etherified	[45,47,48]
3	1505	1512	C=C aromatic ring vibration (G> S)	[49]
4	1461	1459	C-H deformation in methyl and methylene groups	[48]
5	1422	1425	C=C aromatic ring vibration and C-H in plane deformation	[45]
6	1367	1372	Aliphatic C-H stretching in CH3 (not in OCH_3) and phenolic O-H stretching vibration, C-H bending vibration in cellulose and hemicelluloses	[47,50]
7	1328	1327	Syringyl ring breathing with C-O stretching	[49]
8	1265	1282	Guaiacyl ring breathing, C=O stretching in lignin and C-O linkage in guaiacyl aromatic methoxyl groups	[49]
9	1224	1223	C-C plus C-O stretching and C=O stretching; G condensed > G etherified, syringyl and guaiacyl ring breathing	[51,52]
10	1148	1150	C-H stretching in aromatic ring (guaiacyl)	[49]
11	1125	1122	Aromatic skeletal and C-O stretching (typical for S units)	[48,50]
12	1031	1031	Aromatic C-H in-plane deformation in guaiacyl and C–O deformation in primary alcohol	[48,50]

The absorption bands at 1512–1505 cm^{-1} (IR band 3) and at 1425–1422 cm^{-1} (IR band 4) correspond to aromatic ring breathing modes. The IR band between 1372–1367 cm^{-1} (IR band 6) represents aliphatic C–H stretching in methyl but not in methoxyl groups and phenolic O–H stretching vibration, as well as C-H bending deformation for cellulose and hemicelluloses. The low intensity of this band indicates a low content of free phenolic OH groups, which coincides with rather high molar masses determined by HP-SEC (Table 2) as well as low carbohydrate impurities. The band at 1328–1327 cm^{-1} is characteristic for aromatic ring breathing of syringyl moieties, while the IR band around 1282–1265 cm^{-1} corresponds to guaiacyl ring breathing, with additional contributions of C=O structures. The absorbance band at 1224–1223 cm^{-1} (IR band 9), instead, reflects both syringyl and guaiacyl ring breathing. A strong absorption band at 1125–1122 cm^{-1} stands for aromatic skeletal C-H in-plane deformations and C-O stretching modes and represents the most prominent IR band in the spectra of both AL samples. In addition, the IR band 12 at 1031 cm^{-1} corresponds to aromatic C–H stretching in-plane deformation and C=O stretching modes in lignin and cellulose. According to Faix et al. [48], these specific IR band intensities can be used for the classification of lignins into G and different types of GS lignins depending on the ratio of G and S units, respectively. The higher the ratio of S units, the more dominant the maximum at 1125 cm^{-1} (IR band 11). Considering that IR

band 11 is the most prominent IR band in the spectra of both AL-OA and AL-EU lignins, it can be concluded that their respective S/G ratio is in favor of S units and both lignins could be characterized as lignins of type GS 4 according to Faix et al. [48]. The second requisite of this lignin type is that the intensity of IR band 4 is higher than the one of IR band 3, which is the case for both AL-OA and AL-EU. The bigger difference between A1462 (IR band 4) and A1505 (IR band 3) in the FTIR spectrum of AL-EU compared to the one of AL-OA in-dicates that the respective S/G ratio of AL-EU is higher than in AL-OA. The third characteristic is a higher intensity of IR band 7 than IR band 8 and that the intensity at 1268 cm^{-1} (IR band 8) is very low. This is the case for AL-OA but not for AL-EU, indicating that AL-OA is more dominated by S units than AL-EU and thus the S/G ratio of AL-OA should be higher than the one of AL-EU. Similar observations were reported also by Xiao et al. [34], who identified their isolated eucalypt lignins as typical GS lignins with rather high S units content based on the acquired FTIR spectra.

Analytical Py-GCMS

Analytical Py-GCMS is a method that allows to study the complex structure of lignin after thermal degradation of the polymer by destruction of certain chemical bonds, leading to the formation of a mixture of volatile aromatic compounds that are separated by GC and finally analyzed by MS. The pyrograms of AL-OA and AL-EU showed similar profiles, and pyrolysis products were identified (Figure 3, Table 4). Among the phenolic compounds, mainly compounds derived from guaiacol (G) and syringol (S) units were found. Usually the S/G ratio of hardwood lignins is expected to be over 1, due to the higher abundance of syringyl moieties in hardwoods in general. However, different studies observed a great variability in hardwoods S/G ratios with values < 1, such as in *Eucalyptus tereticornis* (0.7), *Acer macrophyllum* (0.51), or in *A. negundo* (0.4), as pointed out by Vinciguerra et al. [26]. Variations of the S/G ratio are also possible within the same species like for chestnut lignin where Vinciguerra et al. [26] determined values between 1.29 and 3.49, while in a later work an S/G ratio for chestnut AL of 0.56 was observed [27]. In the case of AL-EU, the highest abundance was observed for 4-vinylguaiacol, syringol, 4-methylsyringol, and 4-vinylsyringol and the respective S/G ratio for AL-EU was 2.11, corresponding with literature values for *Eucalyptus globulus* as well as *E. camaldulensis* lignins [42,53]. Regarding AL-OA, slightly different peak areas of the pyrolysis products were identified and the respective S/G ratio was 2.73, which is in good concordance with the S/G ratio determined for dioxane lignin by [20] using 2D HSQC NMR spectroscopy. In the case of AL-OA, the main pyrolysis products were 4-vinylguaiacol, syringol, 4-methylsyringol, 4-vinylsyringol, 4-propenylsyringol, and sinapaldehyde. There was one pyrolysis product, 4-oxy-allylsyringol, which was detected exclusively in the pyrogram of AL-OA. According to literature reports, hardwoods with a higher lignin S/G ratio can be processed with more efficiency, which brings

a higher lignin isolation yield due to stronger delignification during pulping [54]. Therefore, both *E. camaldulensis* and *Q. cerris* can be considered as preferred starting materials for an efficient lignin isolation, which is the base for the development of a cost-effective and sustainable lignin valorization route.

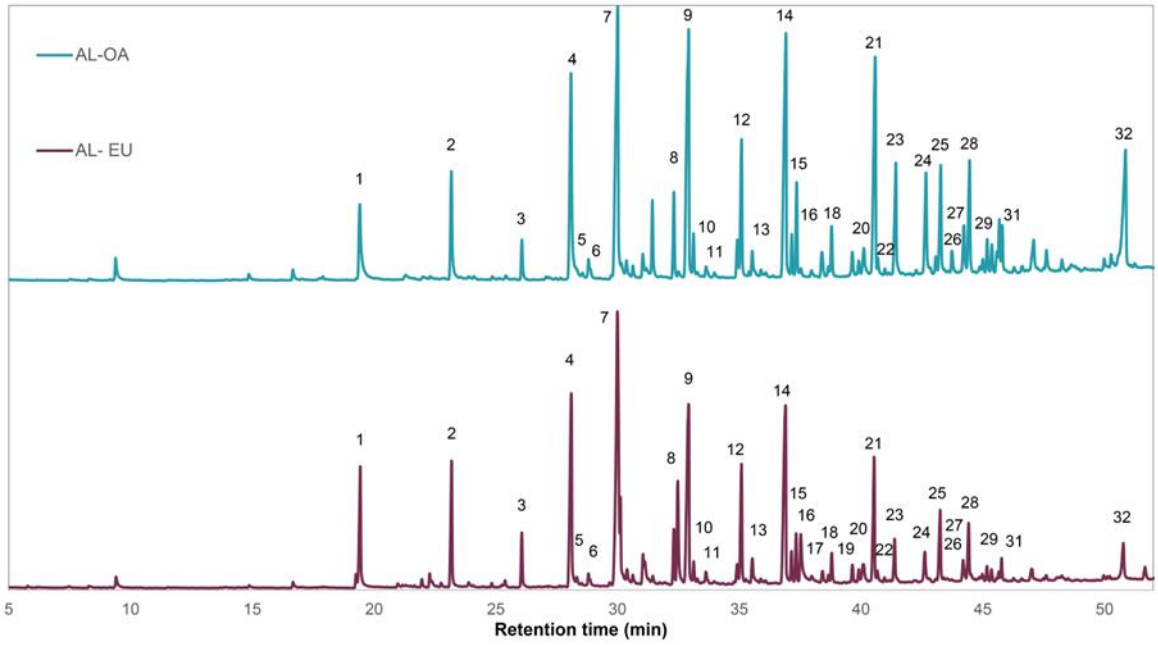

Figure 3. Pyrograms of the isolated acidolysis lignins from oak (AL-OA) and eucalypt wood (AL-EU). Peak numbers refer to the pyrolysis products listed in Table 4.

Table 4. Relative abundance of pyrolysis products of the isolated acidolysis lignins from oak (AL-OA) and eucalypt (AL-EU).

Peak Number	Pyrolysis Product	Origin	RT (min)	AL–OA	AL–EU
				Area (%)	Area (%)
1	Guaiacol	G	19.42	2.39	3.50
2	4-Methylguaiacol	G	23.17	2.43	3.30
3	4-Ethylguaiacol	G	26.09	0.80	1.34
4	4-Vinylguaiacol	G	28.09	6.24	7.08
5	Eugenol	G	28.85	0.34	0.28
6	4-Propylguaiacol	G	28.86	0.15	0.15
7	Syringol	S	29.99	9.47	13.06
8	Isoeugenol (trans)	G	32.30	1.61	1.35
9	4-Methylsyringol	S	32.91	8.00	7.84
10	Vanillin	G	33.11	0.77	0.57
11	Homovanillin	G	34.90	0.82	0.59
12	4-Ethylsyringol	S	35.08	2.85	3.46
13	Acetoguaiacol	G	35.52	0.70	0.91
14	4-Vinylsyringol	S	36.91	7.67	7.67
15	Guaiayl acetone	G	37.15	0.70	0.79
16	4-Allylsyringol	S	37.34	1.69	1.21
17	Propioguaiacone	G	37.90	0.17	0.44

18	Coniferyl alcohol (structure isomer)	G	38.39	0.69	0.41
19	4-Propenylsyringol (cis)	S	38.78	0.98	0.77
20	Levoglucosan	PS	40.11	0.97	1.00
21	4-Propenylsyringol (trans)	S	40.55	6.29	3.85
22	Dihydroconiferyl alcohol	G	40.67	0.44	0.40
23	Syringaldehyde	S	41.39	2.86	1.32
24	Homosyringaldehyde	S	42.66	2.50	1.05
25	Acetosyringone	S	43.26	2.43	2.20
26	Coniferyl alcohol (cis)	G	43.74	0.50	0.04
27	Coniferaldehyde	G	44.21	1.15	0.70
28	Syringyl acetone	S	44.43	2.51	1.66
29	Propiosyringone	S	54.17	0.60	0.37
30	4-Oxy-allylsyringol	S	45.57	0.41	---
31	Sinapyl alcohol (structure isomer)	S	45.66	0.98	0.25
32	Sinapaldehyde	S	50.81	5.36	1.43
	S/G Ratio			2.73	2.11

2D NMR Spectroscopy

Both oak and eucalypt ALs showed a monomeric composition almost exclusively of S and G units with minimal contributions of H units and FA groups (Table 5 and Figure 4). The respective structures are illustrated in Figure 5. Interestingly, the corresponding C2, C6, and Cβ cross-peaks (FA2, FA6, and FAβ) for FA were found, while the Cα cross-peak was not detected. Moreover, the NMR spectra show the presence of polysaccharides contamination (Xn and X'n). In AL-OA, S units were more abundant than in AL-EU, resulting in a higher S/G ratio. Both lignins were mainly connected through β-O-4' bonds, which accounted for around 75–82% when including also α-oxidized β-O-4' substructures. AL-OA showed about 10% more β-O-4' interunit linkages and fewer phenylcoumaran structures, which could come as a con-sequence of a higher S units ratio. Resinol (β-β') structures were more abundant than phenylcoumaran-type interunit linkages (β-5') in both lignins, most probably caused by the strong presence of S units which do not allow for phenylcoumaran-type interu-nit linkages. Further, benzylether (BE), open β-1′, stilbene (I) structures, and cinnamal-dehyde (CA) end groups were identified in the 2D NMR spectra of the two different lignins. The determined S/G ratio of the isolated oak AL was higher than the values reported by Lourenco et al. [31] for the lignin of cork oak xylem isolated after ball-milling using dioxane-water (2.31 vs. 1.2–1.6), but in good accordance with the one reported by Vivas et al. [20], as already mentioned above. On the other hand, the S/G ratio of eucalypt AL was close to the one from E. camaldulensis milled wood lignin (MWL) reported by Wang et al. [40] as well as in the range of the S/G ratios reported for E. camaldulensis by Kawamura et al. [42]. Other studies found considerably higher S/G between 2.7 and 3.45 for an enzymatically isolated lignin (SREL) from Eucalyptus urophylla × E. grandis [34]. However, it was also shown that the S/G ratio of an SREL preparation was considerably higher than the one of an

MWL from the same starting material [40]. Since the isolation protocol applied in this study involves the same sol-vent as used for MWL isolation, it can be expected that the isolated AL fraction also contains the MWL of the processed eucalypt wood and therefore the S/G ratio was found in the range of a eucalypt MWL, as mentioned above. The AL samples of the different wood species showed differences in their acylation degree of lignin sidechains. While for AL-EU no cross-peaks for Cγ acylated lignin sidechains were de-tected (A'γ), the respective signals were identified in the spectrum of AL-OA.

Table 5. Monomeric ratios, S/G ratios, and relative abundance of lignin inter-unit linkages of the Acidolysis lignins from oak (AL-OA) and eucalypt (AL-EU).

Lignin Sample	Monomers (%)									Interunit linkages (%)						
	S Units	Sox Units	G Units	Gox Units	H Units	SA	CA	FA	S/G Ratio	β-O-4′	α-oxid. β-O-4′	β-5′	β-β′	BE	Open β-1	Stilbenes
AL-OA	62	5	24	5	1	1	1	1	2.31	79	3	4	7	3	2	2
AL-EU	57	3	33	3	1	2	0	1	1.69	73	2	6	8	5	4	2

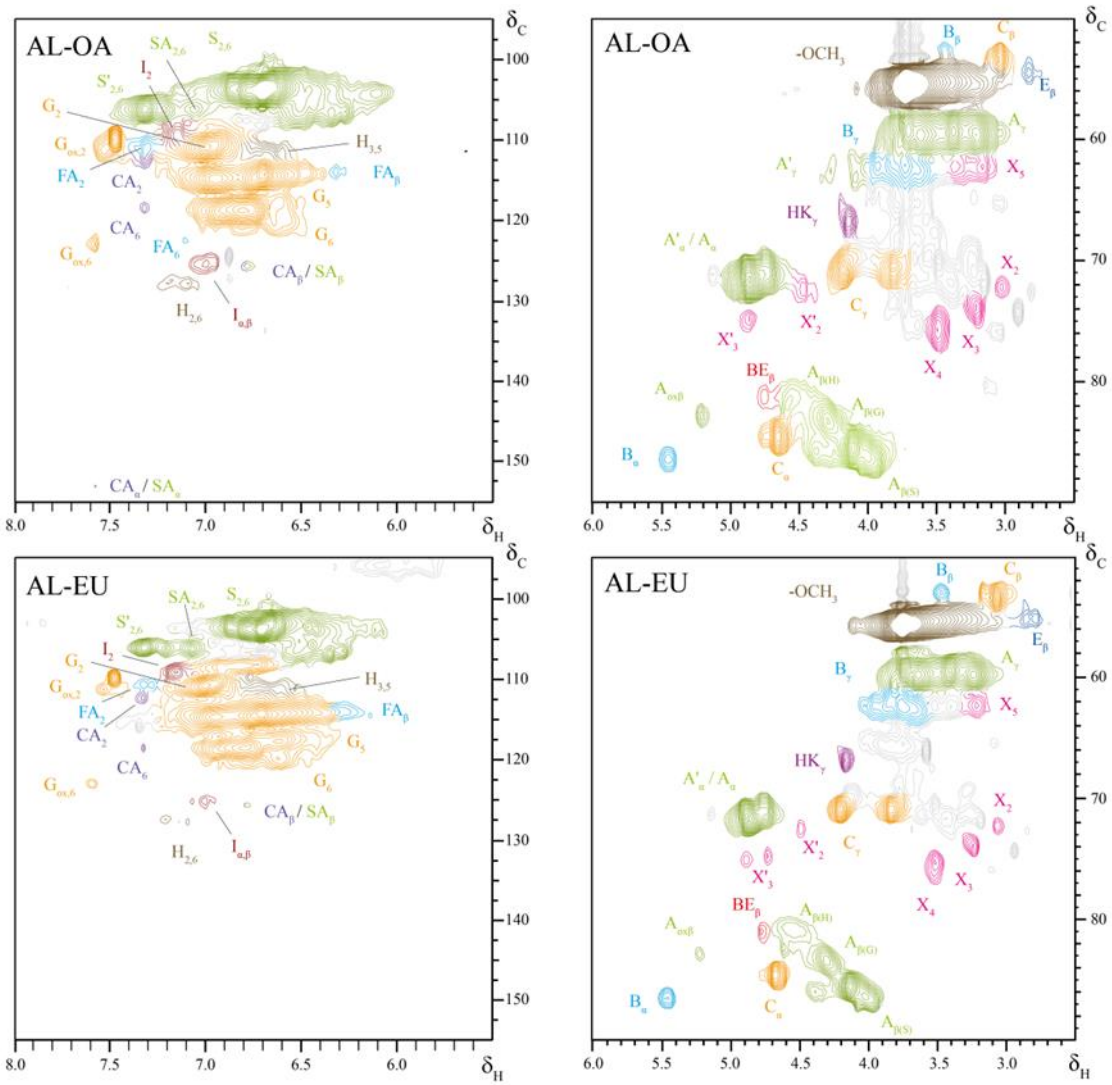

Figure 4. 2D HSQC NMR spectra of the acidolysis lignins isolated from oak and eucalypt wood (AL-OA, AL-EU). Left: aromatic regions. Right: oxygenated side-chain regions. For the corresponding chemical structures and respective NMR shifts, see Figure 5 and Table 6.

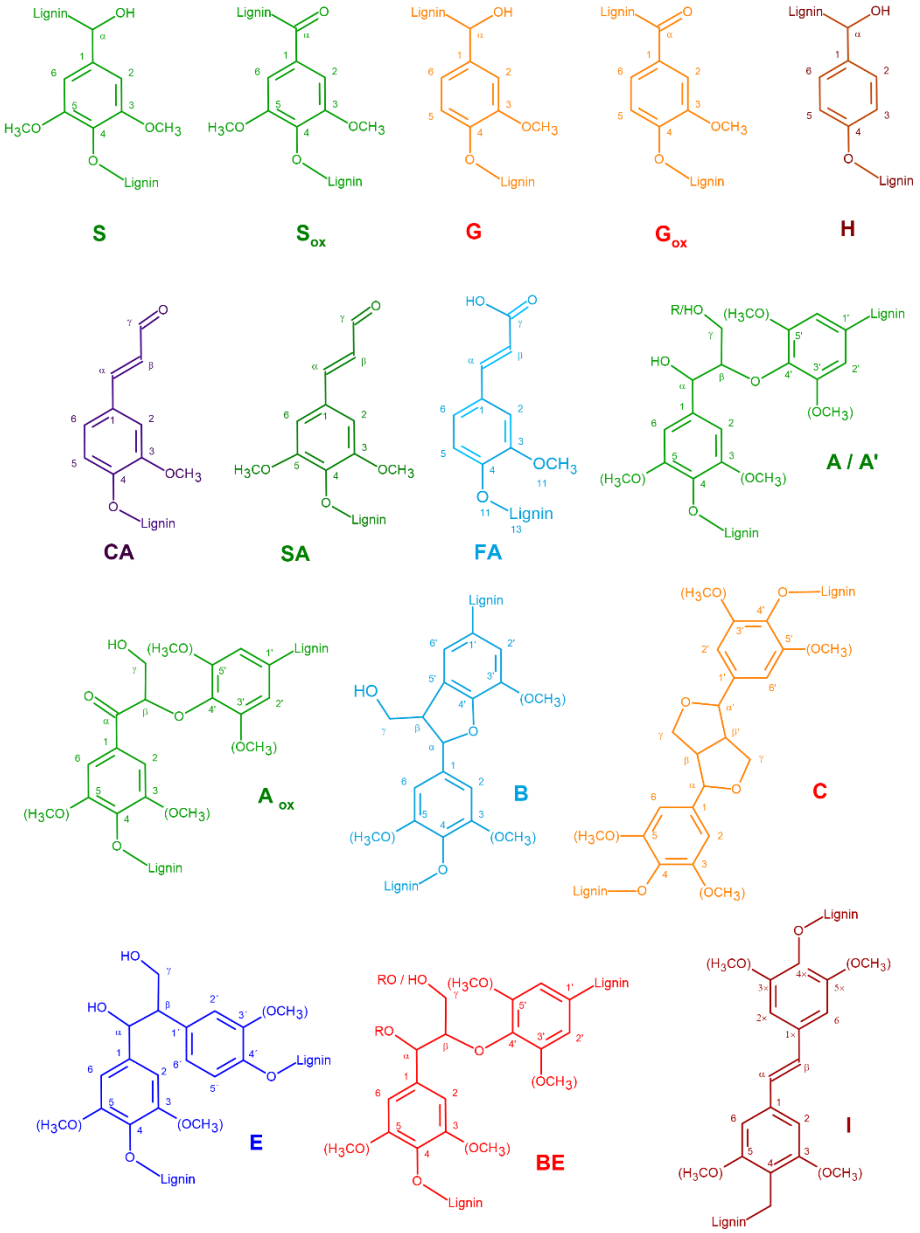

Figure 5. Lignin substructures identified in the respective 2D HSQC NMR spectra of oak and eucalypt acidolysis lignin. S … syringyl units, Sox … α-oxidized S units, G … guaiacyl units, Gox … α-oxidized G units, H … p-hydroxyphenyl units, CA … coniferaldehyde, SA … sina-paldehyde, FA … ferulic acid, A … β-O-4' linkages, A' … acylated β-O-4' linkages, Aox … α-oxidized β-O-4' linkages, B … β-5' phenylcoumaran bonds, C … β-β' resinol bonds, I … stilbene structures, BE … benzyl ether structures, E … open β-1′ structures.

Table 6. Signal assignments of the 13C−1H correlation peaks in the 2D HSQC NMR spectra of the isolated wheat straw lignin fractions, according to [31–37]. The labels correspond to the respective lignin substructures shown in Figure 4.ù

δC/δH (ppm)	Assignment (Label)
52.7/3.43	C_β-H_β in phenylcoumaran β-5′ substructures (**B**$_\beta$)
53.3/3.05	C_β-H_β in resinol substructures β-β' (**C**$_\beta$)
54.2/2.82	C_β-H_β in open β-1′ substructures (**E**$_\beta$)
59.6/3.05–3.93	C_γ-H_γ in γ-hydroxylated β-O-4′ substructures (**A**$_\gamma$)
62.1/3.17	C_5-H_5 in β-D-xylopyranoside (**X**$_5$)
62.5/3.76	C_γ-H_γ in phenylcoumaran β-5′ substructures (**B**$_\gamma$)
62.5/4.29	C_γ-H_γ in γ-acylated β-O-4′ substructures (**A**$_\gamma$′)
66.9/4.14	C_γ-H_γ in Hibbert's ketone (**HK**$_\gamma$)
70.8/3.80 + 4.15	C_γ-H_γ in resinol substructures β-β' (**C**$_\gamma$)
71.5/4.84	C_α-H_α in β-O-4′ substructures (**A**$_\alpha$) linked to a G unit
74.1/3.02	C_2-H_2 in β-D-xylopyranoside (**X**$_2$)
72.6/4.49	C_2-H_2 in 2-O-acetyl-β-D-xylopyranoside (**X′**$_2$)
74.7/3.23	C_3-H_3 in β-D-xylopyranoside (**X**$_3$)
75.5/4.86	C_3-H_3 in 3-O-acetyl-β-D-xylopyranoside (**X′**$_3$)
76.0/3.48	C_4-H_4 in β-D-xylopyranoside (**X**$_4$)
81.5/4.73	C_α-H_α in benzyl ether substructures (**BE**$_\alpha$)
81.6/4.53	C_β-H_β in β-O-4′ substructures (**A**$_{\beta(H)}$) linked to a H unit
83.1/5.20	C_β-H_β in α-oxidized (C_α=O) β-O-4′ substructures (**A**$_{o\alpha\beta}$)
83.4/4.28	C_β-H_β in β-O-4′ substructures (**A**$_{\beta(G)}$) linked to a G unit
85.0/4.67	C_α-H_α in resinol β-β' substructures (**C**$_\alpha$)
86.2/4.01	C_β-H_β in β-O-4′ substructures (**A**$_{\beta(S)}$) linked to a S unit
87.1/5.50	C_α-H_α in phenylcoumaran β-5′ substructures (**B**$_\alpha$)
103.4/6.64	$C_{2,6}$-$H_{2,6}$ in syringyl units (**S**$_{2,6}$)
106.2/7.06	$C_{2,6}$-$H_{2,6}$ in sinapaldehyde units (**SA**$_{2,6}$)
106.2/7.30	$C_{2,6}$-$H_{2,6}$ in α-oxidized (C_α=O) syringyl units (**S′**$_{2,6}$)
110.6/7.32	C_2-H_2 in ferulic acid (**FA**$_2$)
110.6/7.51	C_2-H_2 in oxidized guaiacyl units (**G′**$_2$)
110.8/6.97	C_2-H_2 in guaiacyl units (**G**$_2$)
111.8/6.66	$C_{3,5}$-$H_{3,5}$ in *p*-hydroxyphenyl units (**H**$_{3,5}$)
112.9/7.33	C_2-H_2 in coniferaldehyde (**CA**$_2$)
115.2/6.80	C_5-H_5 in guaiacyl units (**G**$_5$)
119.3/6.88	C_6-H_6 in guaiacyl units (**G**$_6$)
118.4/7.32	C_6-H_6 in coniferaldehyde (**CA**$_6$)
123.0/7.11	C_6-H_6 in ferulic acid (**FA**$_6$)
122.8/7.62	C_6-H_6 in oxidized guaiacyl units (**G′**$_6$)
125.6/7.01	$C_{\alpha,\beta}$-$H_{\alpha,\beta}$ in stilbene units (**I**$_{\alpha,\beta}$)
126.0/6.77	C_β-H_β in cinnamyl aldehyde end groups (**CA**$_\beta$)
128.1/7.14	$C_{2,6}$-$H_{2,6}$ in *p*-hydroxyphenyl units (**H**$_{2,6}$)
153.6/7.60	C_α-H_α in cinnamyl aldehyde end groups (**CA**$_\alpha$, **SA**$_\alpha$)

Conclusion

The structural and chemical differences between oak and eucalypt lignins from the same extraction process were highlighted. As the lignins from the two wood species showed rather different structures, the detected differences could be considered as intrinsic to their respective nature. In particular, different analysis techniques, such as FTIR spectroscopy, Py-GCMS, and NMR spectroscopy, delivered consistent results, confirming that AL-OA has a higher S/G ratio than AL-EU. As the isolated lignins of both species exhibit high S/G ratios, they qualify as preferred lignin extraction sources due to higher extraction efficiency based on their high abundance of S units. Two-dimensional NMR spectroscopy indicated a rather homogenous and linear lignin structure based on a high ratio of *β*-O-4' substructures, and FTIR spectroscopy indicated AL fractions with low carbohydrates impurities although 2D NMR revealed xylan contributions in the lignin macromolecule. Molar mass analysis showed rather small molecular weights of the isolated lignins, indicating their suitability for application as antioxidant or radical scavengers considering that these activities increase with lower molar mass. Knowledge of the chemical properties and the complex molecular structure of the species-specific lignins provides important information in order to valorize the wood resources studied in the presented work for the development of sustainable and competitive products in different value-added application fields. Further studies regarding purity and a quantification of functional groups contents (phenolic, aliphatic, and carboxylic hydroxyl groups) using 31P-NMR spectroscopy will provide useful data in order to define clearer future application fields of the isolated lignins.

References

1. Vis, M.; Mantau, U.; Allen, B. CASCADES: Study on the Optimised Cascading Use of Wood. 2016. Available online: https://data.europa.eu/doi/10.2873/827106 (accessed on 13 July 2023).

2. Stafford, W.; De Lange, W.; Nahman, A.; Chunilall, V.; Lekha, P.; Andrew, J.; Johakimu, J.; Sithole, B.; Trotter, D. Forestry biorefineries. Renew. Energy 2020, 154, 461–475. https://doi.org/10.1016/j.renene.2020.02.002

3. Navare, K.; Arts, W.; Faraca, G.; Van den Bossche, G.; Sels, B.; Van Acker, K. Environmental impact assessment of cascading use of wood in bio-fuels and bio-chemicals. Resour. Conserv. Recycl. 2022, 186, 106588. https://doi.org/10.1016/j.resconrec.2022.106588

4. Tamantini, S.; Del Lungo, A.; Romagnoli, M.; Paletto, A.; Keller, M.; Bersier, J.; Zikeli, F. Basic steps to promote biorefinery value chains in forestry in Italy. Sustainability 2021, 13, 11731. https://doi.org/10.3390/su132111731

5. Tavares, D.; Cavali, M.; Tanobe, V.d.O.A.; Torres, L.A.Z.; Rozendo, A.S.; Zandoná Filho, A.; Soccol, C.R.; Woiciechowski, A.L. Lignin from Residual Sawdust of Eucalyptus spp.—Isolation, Characterization, and Evaluation of the Antioxidant Properties. Biomass 2022, 2, 195–208. https://doi.org/10.3390/biomass2030013

6. Tofani, G.; Cornet, I.; Tavernier, S. Estimation of hydrogen peroxide effectivity during bleaching using the Kappa number. Chem. Pap. 2021, 75, 5749–5758. https://doi.org/10.1007/s11696-021-01756-y

7. Gan, M.J.; Niu, Y.Q.; Qu, X.J.; Zhou, C.H. Lignin to value-added chemicals and advanced materials: Extraction, degradation, and functionalization. Green Chem. 2022, 24, 7705–7750. https://doi.org/10.1039/D2GC00092J

8. Balakshin, M.Y.; Capanema, E.A.; Sulaeva, I.; Schlee, P.; Huang, Z.; Feng, M.; Borghei, M.; Rojas, O.J.; Potthast, A.; Rosenau, T. New opportunities in the valorization of technical lignins. ChemSusChem 2021, 14, 1016–1036. https://doi.org/10.1002/cssc.202002553

9. Tardy, B.L.; Lizundia, E.; Guizani, C.; Hakkarainen, M.; Sipponen, M.H. Prospects for the integration of lignin materials into the circular economy. Mater. Today 2023, 65, 122–132. https://doi.org/10.1016/j.mattod.2023.04.001

10. Kai, D.; Tan, M.J.; Chee, P.L.; Chua, Y.K.; Yap, Y.L.; Loh, X.J. Towards lignin-based functional materials in a sustainable world. Green Chem. 2016, 18, 1175–1200. https://doi.org/10.1039/C5GC02616D

11. Tian, D.; Hu, J.; Bao, J.; Chandra, R.P.; Saddler, J.N.; Lu, C. Lignin valorization: Lignin nanoparticles as high-value bio-additive for multifunctional nanocomposites. Biotechnol. Biofuels 2017, 10, 1–11. https://doi.org/10.1186/s13068-017-0876-z

12. Laurichesse, S.; Avérous, L. Chemical modification of lignins: Towards biobased polymers. Prog. Polym. Sci. 2014, 39, 1266–1290. https://doi.org/10.1016/j.progpolymsci.2013.11.004

13. Chung, H.; Washburn, N.R. Chemistry of lignin-based materials. Green Mater. 2013, 1, 137–160. https://doi.org/10.1680/gmat.12.00009

14. Bergamasco, S.; Tamantini, S.; Zikeli, F.; Vinciguerra, V.; Scarascia Mugnozza, G.; Romagnoli, M. Synthesis and characteriza-tions of eco-friendly organosolv lignin-based polyurethane coating films for the coating industry. Polymers 2022, 14, 416. https://doi.org/10.3390/polym14030416

15. Scarica, C.; Suriano, R.; Levi, M.; Turri, S.; Griffini, G. Lignin functionalized with succinic anhydride as building block for bi-obased thermosetting polyester coatings. ACS Sustain. Chem. Eng. 2018, 6, 3392–3401. https://doi.org/10.1021/acssuschemeng.7b03583

16. Hao, C.; Liu, T.; Zhang, S.; Brown, L.; Li, R.; Xin, J.; Zhong, T.; Jiang, L.; Zhang, J. A high-lignin-content, removable, and glycol-assisted repairable coating based on dynamic covalent bonds. ChemSusChem 2019, 12, 1049–1058. https://doi.org/10.1002/cssc.201802615

17. Tofani, G.; Cornet, I.; Tavernier, S. Multiple linear regression to predict the brightness of waste fibres mixtures before bleaching. Chem. Pap. 2022, 76, 4351–4365. https://doi.org/10.1007/s11696-022-02181-5

18. Bajwa, D.; Pourhashem, G.; Ullah, A.H.; Bajwa, S. A concise review of current lignin production, applications, products and their environmental impact. Ind. Crops Prod. 2019, 139, 111526. https://doi.org/10.1016/j.indcrop.2019.111526

19. Romagnoli, M.; Vinciguerra, V.; Silvestri, A. Heat treatment effect on lignin and carbohydrates in Corsican pine earlywood and latewood studied by PY–GC–MS technique. J. Wood Chem. Technol. 2018, 38, 57–70. https://doi.org/10.1080/02773813.2017.1372479

20. Vivas, N.; Nonier, M.-F.; Pianet, I.; de Gaulejac, N.V.; Fouquet, É. Structure of extracted lignins from oak heartwood (Quercus petraea Liebl., Q. Robur L.). Comptes Rendus Chim. 2006, 9, 1221–1233. https://doi.org/10.1016/j.crci.2006.02.005

21. Sabo, V.A.; Knezevic, P. Antimicrobial activity of Eucalyptus camaldulensis Dehn. plant extracts and essential oils: A review. Ind. Crops Prod. 2019, 132, 413–429. https://doi.org/10.1016/j.indcrop.2019.02.051

22. Deidda, A.; Buffa, F.; Linaldeddu, B.T.; Pinna, C.; Scanu, B.; Deiana, V.; Satta, A.; Franceschini, A.; Floris, I. Emerging pests and diseases threaten Eucalyptus camaldulensis plantations in Sardinia, Italy. Iforest-Biogeosciences For. 2016, 9, 883. https://doi.org/10.3832/ifor1805-009

23. Nocetti, M.; Pröller, M.; Brunetti, M.; Dowse, G.P.; Wessels, C.B. Investigating the potential of strength grading green Euca-lyptus grandis lumber using multi-sensor technology. BioResources 2017, 12, 9273–9286. https://doi.org/10.15376/biores.12.4.9273-9286

24. Palmieri, N.; Suardi, A.; Pari, L. Italian consumers' willingness to pay for eucalyptus firewood. Sustainability 2020, 12, 2629. https://doi.org/10.3390/su12072629

25. Lin, S.Y.; Dence, C.W. Methods in Lignin Chemistry; Springer Science & Business Media: Berlin/Heidelberg, Germany, 2012. https://doi.org/10.1007/978-3-642-74065-7

26. Vinciguerra, V.; Spina, S.; Luna, M.; Petrucci, G.; Romagnoli, M. Structural analysis of lignin in chestnut wood by pyrolysis-gas chromatography/mass spectrometry. J. Anal. Appl. Pyrolysis 2011, 92, 273–279. https://doi.org/10.1016/j.jaap.2011.06.009

27. Zikeli, F.; Vinciguerra, V.; Taddei, A.R.; D'Annibale, A.; Romagnoli, M.; Scarascia Mugnozza, G. Isolation and characterization of lignin from beech wood and chestnut sawdust for the preparation of lignin nanoparticles (LNPs) from wood industry side-streams. Holzforschung 2018, 72, 961–972. https://doi.org/10.1515/hf-2017-0208

28. Zikeli, F.; Vinciguerra, V.; D'Annibale, A.; Capitani, D.; Romagnoli, M.; Scarascia Mugnozza, G. Preparation of lignin nano-particles from wood waste for wood surface treatment. Nanomaterials 2019, 9, 281. https://doi.org/10.3390/nano9020281

29. Gellerstedt, G.; Pranda, J.; Lindfors, E.-L. Structural and molecular properties of residual birch kraft lignins. J. Wood Chem. Technol. 1994, 14, 467–482. https://doi.org/10.1080/02773819408003108

30. Faix, O.; Meier, D.; Fortmann, I. Thermal degradation products of wood. Gas chromatographic separation and mass spec-trometric characterization of monomeric lignin-derived products. Holz Als Roh-Und Werkst. 1990, 48, 281–285. https://doi.org/10.1007/BF02626519

31. Lourenco, A.; Rencoret, J.; Chemetova, C.; Gominho, J.; Gutierrez, A.; Del Rio, J.C.; Pereira, H. Lignin composition and structure differs between xylem, phloem and phellem in Quercus suber L. Front. Plant Sci. 2016, 7, 1612. https://doi.org/10.3389/fpls.2016.01612

32. Penín, L.; Lange, H.; Santos, V.; Crestini, C.; Parajó, J.C. Characterization of Eucalyptus nitens lignins obtained by biorefinery methods based on ionic liquids. Molecules 2020, 25, 425. https://doi.org/10.3390/molecules25020425

33. Marques António, V.; Rencoret, J.; Gutiérrez, A.; del Río José, C.; Pereira, H. Ferulates and lignin structural composition in cork. Holzforschung 2016, 70, 275–289, doi:10.1515/hf-2015-0014. Velez Marques, A.; Rencoret, J.; Gutiérrez, A.; del Río, J.C.; Pereira, H. Ferulates and lignin structural composition in cork. Holzforsch. Int. J. Biol. Chem. Phys. Technol. Wood 2016, 70, 275–289. https://doi.org/10.1515/hf-2015-0014

34. Xiao, M.-Z.; Chen, W.-J.; Hong, S.; Pang, B.; Cao, X.-F.; Wang, Y.-Y.; Yuan, T.-Q.; Sun, R.-C. Structural characterization of lignin in heartwood, sapwood, and bark of eucalyptus. Int. J. Biol. Macromol. 2019, 138, 519–527. https://doi.org/10.1016/j.ijbiomac.2019.07.137

35. Li, H.-Y.; Wang, C.-Z.; Chen, X.; Cao, X.-F.; Sun, S.-N.; Sun, R.-C. Structural elucidation of Eucalyptus lignin and its dynamic changes in the cell walls during an integrated process of ionic liquids and successive alkali treatments. Bioresour. Technol. 2016, 222, 175–181. https://doi.org/10.1016/j.biortech.2016.09.111

36. Rico, A.; Rencoret, J.; Del Río, J.C.; Martínez, A.T.; Gutiérrez, A. In-depth 2D NMR study of lignin modification during pre-treatment of Eucalyptus wood with laccase and mediators. BioEnergy Res. 2015, 8, 211–230. https://doi.org/10.1007/s12155-014-9505-x

37. Ralph, S.; Ralph, J.; Landucci, L. NMR Database of Lignin and Cell Wall Model Compounds. 2009. Available online: https://www.glbrc.org/databases_and_software/nmrdatabase/ (accessed on 15 July 20 22).

38. Bajraktari, A.; Nunes, L.; Knapic, S.; Pimenta, R.; Pinto, T.; Duarte, S.; Miranda, I.; Pereira, H. Chemical characterization, hardness and termite resistance of Quercus cerris heartwood from Kosovo. Maderas. Cienc. Y Tecnol. 2018, 20, 305–314. https://doi.org/10.4067/S0718-221X2018005003101

39. Todaro, L.; Dichicco, P.; Moretti, N.; D'Auria, M. Effect of combined steam and heat treatments on extractives and lignin in sapwood and heartwood of Turkey oak (Quercus cerris L.) wood. BioResources 2013, 8, 1718–1730. https://doi.org/10.15376/biores.8.2.1718-1730

40. Wang, H.-M.; Wang, B.; Wen, J.-L.; Yuan, T.-Q.; Sun, R.-C. Structural characteristics of lignin macromolecules from different Eucalyptus species. ACS Sustain. Chem. Eng. 2017, 5, 11618–11627. https://doi.org/10.1021/acssuschemeng.7b02970

41. Vieira, T.A.S.; Arriel, T.G.; Zanuncio, A.J.V.; Carvalho, A.G.; Branco-Vieira, M.; Carabineiro, S.A.C.; Trugilho, P.F. Determi-nation of the chemical composition of Eucalyptus spp. for cellulosic pulp production. Forests 2021, 12, 1649. https://doi.org/10.3390/f12121649

42. Kawamura, I.; Bland, D. The Lignins of Eucalyptus Wood from Tropical and Temperate Zones. Holzforschung 1967, 21, 65-74, https://doi.org/10.1515/hfsg.1967.21.3.65. Available online: https://www.degruyter.com/document/doi/10.1515/hfsg.1967.21.3.65/html (accessed on)

43. Baumberger, S.; Abaecherli, A.; Fasching, M.; Gellerstedt, G.; Gosselink, R.; Hortling, B.; Li, J.; Saake, B.; de Jong, E. Molar mass determination of lignins by size-exclusion chromatography: Towards standardisation of the method. Holzforschung 2007, 61, 459-468, https://doi.org/10.1515/HF.2007.074. Available online: https://www.degruyter.com/document/doi/10.1515/HF.2007.074/html (accessed on).

44. Zheng, L.; Lu, G.; Pei, W.; Yan, W.; Li, Y.; Zhang, L.; Huang, C.; Jiang, Q. Understanding the relationship between the structural properties of lignin and their biological activities. Int. J. Biol. Macromol. 2021, 190, 291–300. https://doi.org/10.1016/j.ijbiomac.2021.08.168

45. Awal, A.; Sain, M. Spectroscopic studies and evaluation of thermorheological properties of softwood and hardwood lignin. J. Appl. Polym. Sci. 2011, 122, 956–963. https://doi.org/10.1002/app.34211

46. Rana, R.; Langenfeld-Heyser, R.; Finkeldey, R.; Polle, A. FTIR spectroscopy, chemical and histochemical characterisation of wood and lignin of five tropical timber wood species of the family of Dipterocarpaceae. Wood Sci. Technol. 2010, 44, 225–242. https://doi.org/10.1007/s00226-009-0281-2

47. Yan, C.; Yin, M.; Zhang, N.; Jin, Q.; Fang, Z.; Lin, Y.; Cai, Y. Stone cell distribution and lignin structure in various pear varieties. Sci. Hortic. 2014, 174, 142–150. https://doi.org/10.1016/j.scienta.2014.05.018

48. Faix, O. Classification of lignins from different botanical origins by FT-IR spectroscopy. Holzforschung 1991, 45, 21-28, https://doi.org/10.1515/hfsg.1991.45.s1.21. Available online: https://www.degruyter.com/document/doi/10.1515/hfsg.1991.45.s1.21/html (accessed on).

49. Reyes-Rivera, J.; Terrazas, T. Lignin analysis by HPLC and FTIR. Xylem Methods Protoc. 2017 , 1544, 193–211. https://doi.org/10.1007/978-1-4939-6722-3_14

50. Pandey, K.; Pitman, A. FTIR studies of the changes in wood chemistry following decay by brown-rot and white-rot fungi. Int. Biodeterior. Biodegrad. 2003, 52, 151–160. https://doi.org/10.1016/S0964-8305(03)00052-0

51. Dörrstein, J.; Scholz, R.; Schwarz, D.; Schieder, D.; Sieber, V.; Walther, F.; Zollfrank, C. Dataset on the structural characteri-zation of organosolv lignin obtained from ensiled Poaceae grass and load-dependent molecular weight changes during ther-moplastic processing. Data Brief 2018, 17, 647–652. https://doi.org/10.1016/j.dib.2018.01.060

52. Moghaddam, L.; Rencoret, J.; Maliger, V.R.; Rackemann, D.W.; Harrison, M.D.; Gutierrez, A.; del Río, J.C.; Doherty, W.O. Structural characteristics of bagasse furfural residue and its lignin component. An NMR, Py-GC/MS, and FTIR study. ACS Sustain. Chem. Eng. 2017, 5, 4846–4855. https://doi.org/10.1021/acssuschemeng.7b00274

53. Rodrigues, J.; Meier, D.; Faix, O.; Pereira, H. Determination of tree to tree variation in syringyl/guaiacyl ratio of Eucalyptus globulus wood lignin by analytical pyrolysis. J. Anal. Appl. Pyrolysis 1999, 48, 121–128. https://doi.org/10.1021/acssuschemeng.7b00274. https://doi.org/10.1016/S0165-2370(98)00134-X

54. Happs, R.M.; Addison, B.; Doeppke, C.; Donohoe, B.S.; Davis, M.F.; Harman-Ware, A.E. Comparison of methodologies used to determine aromatic lignin unit ratios in lignocellulosic biomass. Biotechnol. Biofuels 2021, 14, 1–16. https://doi.org/10.1186/s13068-021-01897-y

CHAPTER 3: Fractionation of Eucalyptus and Oak Wood through 1-Ethyl-3-Methylimidazolium Acetate: Recovery and Characterization of Lignin

Abstract

Ionic liquids (IL) represent a sustainable alternative to traditional organic solvents used for lignin extraction from lignocellulosic biomass. In this ongoing study, we aim to illustrate how 1-ethyl-3-methylimidazolium acetate [C2mim]OAc successfully fractionated wood from the tree species *E. camaldulensis* and *Q. cerris*, allowing for the recovery of their respective lignins. These polymers were characterized through chemical analysis to fully understand their structure following the IL treatment. In particular, an investigation using size exclusion chromatography (HP-SEC) was conducted to determine the molecular weight distribution of the lignins. Additionally, Fourier-transform infrared spectroscopy FTIR spectra were acquired to identify signals and abundances of major functional groups. Finally, analytical Pyrolysis-Gas Chromatography Mass Spectrometry (Py-GCMS) provided information on the composition of volatile compounds of the respective lignins after pyrolytic degradation. The information obtained from these chemical characterizations was compared with data from lignins extracted from the same wood samples but using the acidolysis method (as reported in the previous chapter). This comparison offers a better understanding of how the extraction method influences the structure of the recovered lignins. In particular, in the case of eucalyptus lignin extracted with ionic liquid (ILL-EU), it exhibits many characteristics in common with eucalyptus lignin extracted using the acidolysis method (AL-EU). In the case of oak, the lignin extracted with ionic liquid (ILL-OA) shows a different structure compared to its counterpart extracted using the acidolysis method (AL-OA). The obtained results warrant further investigation into the mechanism related to biomass fractionation using ionic liquids.

Keywords: eucalyptus, oak, ionic liquid, HP-SEC; FTIR; Py-GCMS, biorefinery, bioresources

Introduction

The growing concern about environmental incompatibility of the use of fossil fuels has led to continuous research into alternatives [1]. It is now well known that, upon combustion, fossil fuels release a multitude of pollutants into the atmosphere, such as nitrogen and sulfur oxides, ammonia, carbon monoxide and dioxide, particulate matter, and volatile organic compounds [2-4]. The dispersion of these pollutants into the atmosphere contributes to a series of observed phenomena related to climate change, in addition to causing harmful effects on living beings' health. Among the alternative and sustainable pathways to break free from fossil fuel dependence, the concept of biorefineries is becoming increasingly attractive. Alongside this concept is the development and refinement of valid and sustainable processes for the better utilization and valorization of lignocellulosic biomass [5]. Lignin has traditionally been treated as waste, but in recent years, its potential as a raw material has drawn attention. It is an amorphous aromatic polymer, consisting of three different repetitive units: phenylpropanoid monomers such as p-coumaryl alcohol, coniferyl alcohol, and sinapyl alcohol, corresponding respectively to the building blocks of p-hydroxyphenyl, guaiacyl, and syringyl units [6]. Lignin is a highly abundant and renewable material in nature, rich in functional groups, and versatile in many applications due to its well-known antioxidant and antibacterial [7], UV protection properties [8], and its application as a structural analogue to fossil-derived materials, such as in the production of polyurethane-based coatings [9], adhesives [10], and as a carrier system for active principles and essential oils [11]. However, its extremely recalcitrant nature is well-known due to its complex structure, which provides resistance to degradation. In fact, lignin plays the role of structural protection in plant cell walls. To overcome lignin's recalcitrance, various strategies have been developed, including traditional physical and mechanical pretreatments, chemical methods such as acidolysis, hydrogenolysis, and oxidative methods, as well as enzymatic/biological approaches to improve its availability [12]. In the frame of biorefineries, it is not only important to engage new renewable raw materials, but also to develop novel sustainable methods for biomass processing. Among the various experimental scenarios being explored, ionic liquids are attracting particular interest for their use in the pretreatment of lignocellulosic biomass. Defined as green solvents due to their environmental friendliness, they are liquid salts consisting of a cation-anion pair with modifiable properties depending on the selected ionic pair, allowing for modulation of various properties such as solvent properties, hydrophilicity, and polarity according to specific needs. Additionally, ionic liquids share common features such as low volatility, non-flammability, non-toxicity, and the possibility of recycling and reuse. Ionic liquids have proven to be effective, either alone or in combination with other treatments, in the deconstruction and fractionation of plant biomass from various sources such as corn straw [13], wheat straw [14], rice straw [15],

switchgrass [16], and woody biomass from various species [17]. In general, ionic liquids have the ability to dissolve lignocellulosic biomass, disrupting non-covalent interactions between cellulose and lignin [18] and ester bonds between hemicellulose sugars and lignin [19], separating them into different fractions and allowing for recovery. Both aprotic and protic ionic liquids have shown their ability to dissolve hardwood biomass via similar mechanisms but different performances. [20]. Among them, 1-ethyl-3-methylimidazolium acetate has proven to be one of the best for this type of treatment [21], considered even a benchmark system [22]. The purpose of this study is to treat eucalyptus and oak woody biomass with 1-ethyl-3-methylimidazolium acetate to isolate and recover lignins from both species. The study on the chemical characterization of the extracted polymers was conducted following the same approach used in the previous study, where lignin recovery from eucalyptus and oak woody biomass was performed using the acidolysis method [23]. This allows for a comparison and evaluation of the differences in lignins, attributable solely to the extraction method.

Materials and Method

Materials

The studied oak wood was derived from a disk of an adult tree of *Q. cerris* from the Roccarespampani Estate close to Tuscania (Viterbo province, Italy). The eucalypt wood was derived from windbreak trees of *E. camaldulensis* close to Tarquinia (Viterbo province, Italy). The wood was obtained during tree management activities in 2022. For lignin extraction, the following solvents were used: 1-ethyl-3-methylimidazolium acetate [C2mim]OAc was purchased from Proionic (Raaba-Grambach, Austria), acetone Re pure, sulfuric acid 96% and potassium bromide (KBr) were purchased from Carlo Erba Reagents (Cornaredo, Italy). Polystyrene sulfonate standards were purchased from PSS Polymer Standard Services (Mainz, Germany), Millex®-GV syringe filters (0.22 µm) in PVDF were purchased from Milli-pore Corporation (Belford, MA, USA). Sodium hydroxide was purchased from Merck Life Science S.r.l. (Milan, Italy).

Lignin isolation

Ionic liquid lignin (ILL) from eucalyptus and oak was isolated using the ionic liquid 1-ethyl-3-methylimidazolium acetate based on the protocol described by Sun et al. [21]. Prior to the treatment for lignin isolation and recovery, the woody biomass was initially ground with a blade mill until reaching particles of a size of 0.25 mm (MF 10 basic, IKA Werke, Staufen im Breisgau, Germany). Subsequently, the ground biomass underwent chemical pretreatment to remove extractives using a mixture of acetone-water (90:10, v/v) in a Soxhlet apparatus. The biomass was recovered and oven-dried at 40 °C (FD 115, Binder GmbH, Tuttlingen, Germany). 3 g of biomass was treated with 60 ml of 1-ethyl-3-methylimidazolium acetate. The solution was placed under magnetic stirring for 16 hours

at a controlled temperature of 110 °C. After this period, 200 ml of a mixture of water-acetone (50:50 vol%) was added to the solution, and the solution was kept under magnetic stirring for 1 hour at room temperature. At the end, the solution was filtered with filter paper to remove the cellulosic residue. At this point, acetone was removed from the filtered solution using a rotary evaporator. Finally, the lignin was recovered through filtration, and the precipitate was washed with acidified water at pH 2 to remove residual sugars.

Lignin characterization

ILL-EU and ILL-OA are characterized to obtain information regarding the distribution of molecular weights through HP-SEC, spectroscopic investigations using (FTIR) spectroscopy and Py-GCMS are performed. The methods reported in the previous chapter [23] are faithfully reproduced.

Results and discussion

In Table 1, the yields of lignin extracted from the sawdust of wood from the two examined species are reported and compared. Furthermore, the lignin yields are compared, with the same starting biomass, by changing the treatment used for its recovery. From these data, it is observed that in the case of lignin extracted from eucalyptus wood, the percentage decreases from 7.2 to 4.7%, while in the case of oak, this decrease is even more pronounced, dropping from 7.3 to 2.1%.

Table 1: Comparison of yields of lignins extracted from oak and eucalyptus wood using acidolysis (AL) and ionic liquid (ILL) treatments

Wood Species	AL (%) [a]	ILL (%)
Q. cerris	7.3	2.1
E. camaldulensis	7.2	4.7

[a]: Referred from previous study

Molar mass Distribution (MMD)

The analysis conducted via HPLC-SEC reveals that the extraction using an ionic liquid influences the fractionation of lignin. In Figure 1, the HP-SEC elution curves are compared between the two extractions for each lignin species.

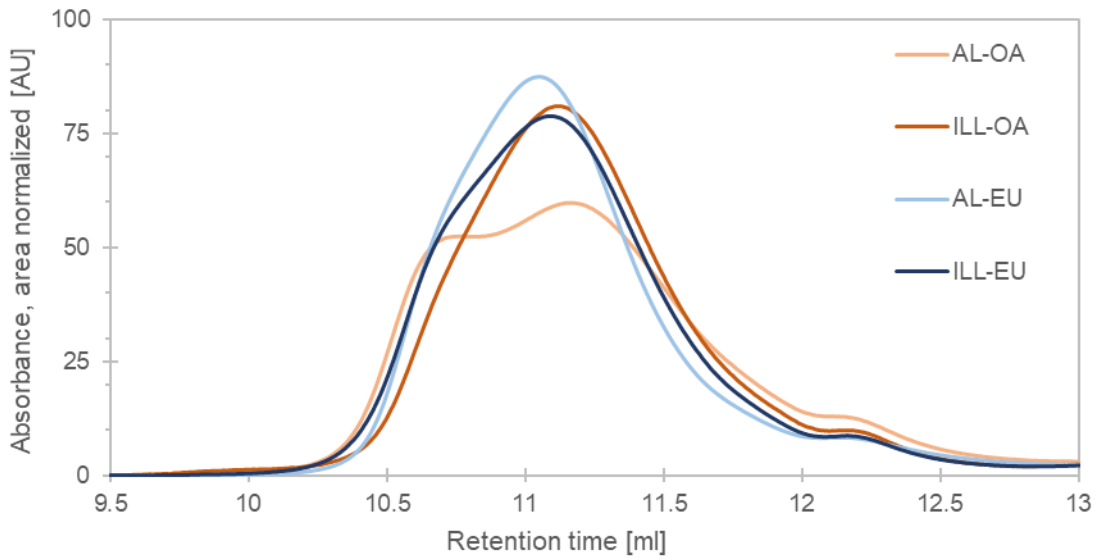

Figure 1: HP-SEC elution curves of the different isolated lignins using [C2mim]OAc (ILL-EU and ILL-OA) and acidolysis (AL-EU and AL-OA)

From a comparison of the values reported in Table 2, it is observed that, in the case of eucalyptus, ILL-EU and AL-EU have similar values. In this case, eucalyptus wood does not seem to be affected by the different treatments used for lignin extraction. A different scenario applies to ILL-OA, where a decrease in the weight-average molecular weight of lignin is observed while the values for the number-average molecular weight are nearly similar, contributing to a reduction in dispersity of the molar mass distribution of ILL-OA. This suggests a stronger fragmentation of lignin following the ILL treatment [24] [25] and the creation of a lower number of condensed molecules during lignin depolymerisation. This is also supported by the respective HP-SEC elugrams where the high-molar mass peak of AL-OA is missing in the elution curve of ILL-OA (Figure 1). In summary, the results suggest that the ionic liquid treatment has a different impact on the extracted lignin from different lignocellulosic sources, highlighting the need to carefully assess extraction conditions to obtain products with desired characteristics.

Table 2: Weight-average (Mw) and number-average (Mn) molar mass, and dispersity (Đ) of the isolated acidolysis lignins from oak and eucalypt wood (ILL-OA and ILL-EU)

Lignin sample	Mw (Da)	Mn (Da)	Đ
ILL-OA	3997	1328	3.01
ILL-EU	4927	1453	3.39
AL-OA [a]	5170	1227	4.21
AL-EU [a]	4841	1472	3.29

[a]: Referred from previous study

Py-GCMS

Twenty-six volatile compounds were identified and the pyrograms are reported in Figure 2 for both ILL lignins, with the difference that only in ILL-OA, propioguaiacone was observed, while in ILL-EU, the presence of 4-propylguaiacol was noted. For this determination, as in the previous analysis, the experimental parameters were kept constant to allow an accurate comparison between extraction techniques. An immediate aspect that emerges is the absence of some volatile compounds, which instead were found in the analyses of lignins extracted by acidolysis; the compounds in question are: homovanillin, homosyringaldehyde, coniferaldehyde and 4-oxy-allylsyringol. As highlighted in the table, levoglucosan was detected among the pyrolysis products. In the case of acidolysis treatment, the presence of this single carbohydrate-derived compound was also observed, but its yield is lower in the ionic liquid treatment.

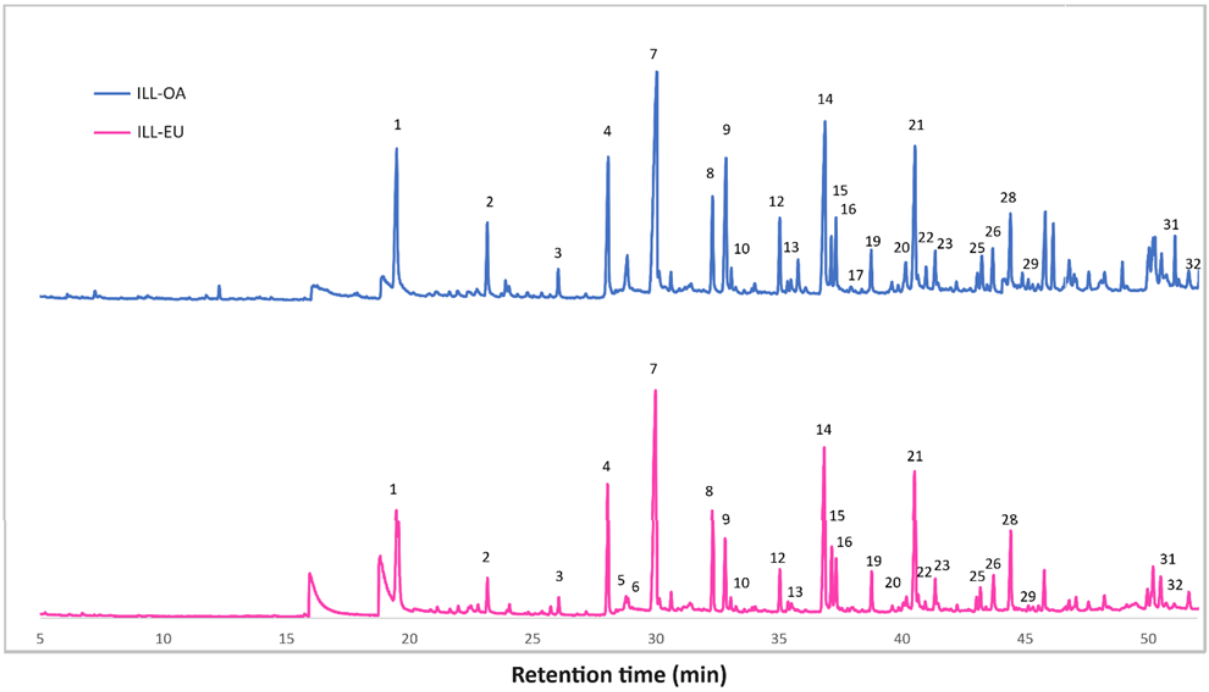

Figure 2. Pyrograms of the isolated lignins from oak (ILL-OA) and eucalypt wood (ILL-EU) after ionic liquid treatment.

Table 3. Relative abundance of pyrolysis products from ILL-OA and ILL-EU.

Peak number	Pyrolysis Product	Origin	RT (min)	ILL – OA	ILL - EU
				Area (%)	Area (%)
1	Guaiacol	G	19.42	5.7	4.02
2	4-Methylguaiacol	G	23.17	1.69	0.86
3	4-Ethylguaiacol	G	26.09	0.6	0.46
4	4-Vinylguaiacol	G	28.09	4.09	3.74
5	Eugenol	G	28.85	1.44	0.53
6	4-Propylguaiacol	G	28.86	-	0.31
7	Syringol	S	29.99	9.58	10.41
8	Isoeugenol (trans)	G	32.30	2.26	2.61

9	4-Methylsyringol	S	32.91	3.72	2.09
10	Vanillin	G	33.11	0.5	0.39
11	Homovanillin	G	34.90	-	-
12	4-Ethylsyringol	S	35.08	1.44	1.06
13	Acetoguaiacol	G	35.52	0.34	0.4
14	4-Vinylsyringol	S	36.91	5.6	6.22
15	Guaiacyl acetone	G	37.15	1.2	1.68
16	4-Allylsyringol	S	37.34	1.72	1.59
17	Propioguaiacone	G	37.90	0.25	-
18	Coniferyl alcohol (structure isomer)	G	38.39	-	-
19	4-Propenylsyringol (cis)	S	38.78	0.93	0.96
20	Levoglucosan	PS	40.11	0.97	0.32
21	4-Propenylsyringol (trans)	S	40.55	4.08	4.96
22	Dihydroconiferyl alcohol	G	40.67	0.36	0.48
23	Syringaldehyde	S	41.39	0.79	0.83
24	Homosyringaldehyde	S	42.66	-	-
25	Acetosyringone	S	43.26	0.85	0.71
26	Coniferyl alcohol (cis)	G	43.74	1.32	1.24
27	Coniferaldehyde	G	44.21	-	-
28	Syringyl acetone	S	44.43	2.01	2.64
29	Propiosyringone	S	45.17	0.27	0.14
30	4-Oxy-allylsyringol	S	45.57	-	-
31	Sinapyl alcohol (structure isomer)	S	45.66	0.68	1.11
32	Sinapaldehyde	S	50.81	0.92	0.24
	S/G Ratio			**1.65**	**1.97**

–: not detected.

From the analysis performed on ILL-OA, the formation of the volatile compounds 4-propylguaiacol, homovanillin, coniferyl alcohol (structural isomer), homosyringaldehyde, coniferaldehyde, and 4-oxy-allylsyringol is not observed. Similarly, in the case of ILL-EU, except for 4-propylguaiacol, the same volatile compounds mentioned for ILL-OA are not observed. Another relevant observation concerns the yield of volatile compounds. For lignins extracted with ionic liquid, there is a decrease in the number of pyrolysis products. However, a higher yield is observed for those volatile compounds of guaiacolic origin. Table 4 provides data for a more detailed comparison.

Table 4. Comparison of some pyrolysis products between oak (OA) and eucalypt (EU) lignins extracted using the acidolysis (AL) and ionic liquid (ILL) methods.

	Origin	**AL – OA[a]**	**ILL-OA**	**AL– EU[a]**	**ILL - EU**
Pyrolysis Product		**Area (%)**	**Area (%)**	**Area (%)**	**Area (%)**
Guaiacol	G	2.39	5.7	3.50	4.02
Eugenol	G	0.34	1.44	0.28	0.53
Isoeugenol (trans)	G	1.61	2.26	1.35	2.61

Guaiacyl acetone	G	0.7	1.2	0.79	1.68
Propioguaiacone	G	0.17	0.25	0.44	-
Syringyl acetone	S	2.51	2.01	1.66	2.64

–: not detected.

[a]: Referred from previous study [23]

Except for propioguaiacone in AL-EU and syringyl acetone in AL-OA (the only S-type), whose values are slightly higher compared to their respective lignins extracted with ionic liquid, for all other compounds belonging to G-type lignin, higher yields are observed in the ILLs. All of this leads to a change in the S/G ratio estimation between different treatments for the same species. In particular, in the case of eucalyptus, the S/G ratio decreases slightly from a value of 2.11 for AL-EU to a value of 1.97 for ILL-EU. Meanwhile, in the case of oak, the value decreases significantly, from 2.73 for AL-OA to a value of 1.65 for ILL-OA. Based on the obtained data, it is possible to hypothesize that the biomass treatment with [C2mim]OAc results in a higher extraction of G-type lignin compared to S-type, causing a reduction in the S/G ratio, with a more pronounced effect on oak lignin compared to eucalyptus lignin. This result is consistent with studies conducted by Kim et al. [24] where poplar lignins extracted with ionic liquid [C2mim]OAc were compared with the respective milled wood lignin. Using the DFRC method, which determines the frequency of arylglycerol-β-aryl ether (β-O-4') bonds, it was observed that G-type lignin was more easily extracted than S-type. Additionally, in Varanasi et al. [26], the effect of treatment on the final composition of the extracted lignin was reported, which is influenced both by the selected temperature and the treatment duration.

FTIR spectroscopy

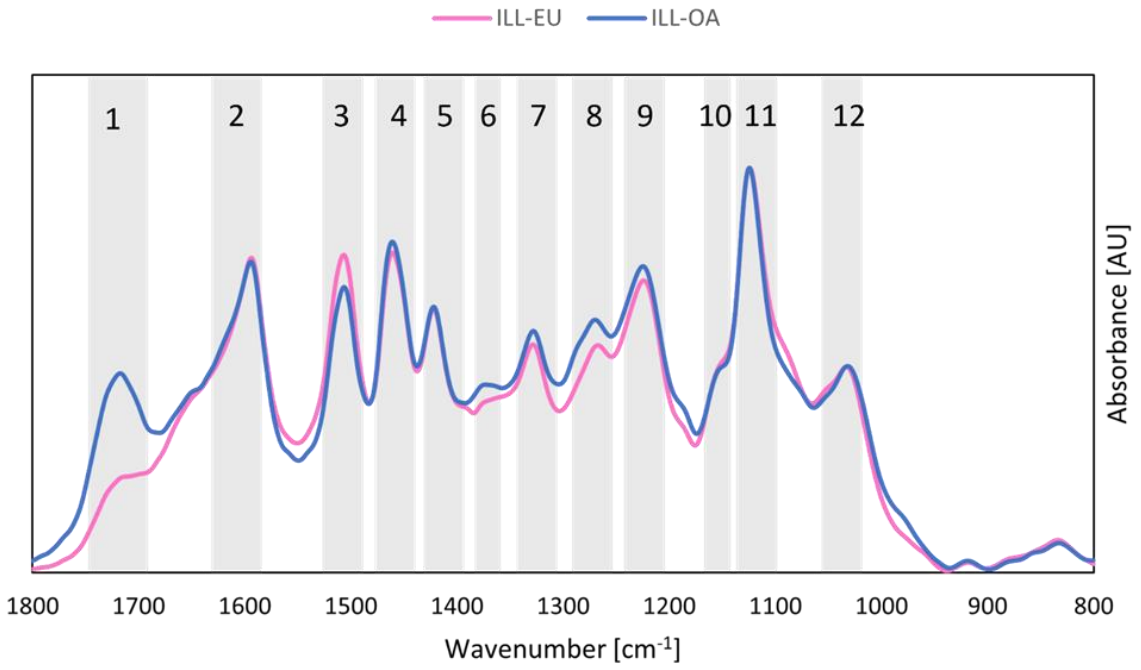

Figure 3. FTIR spectra of the isolated lignins from oak (ILL-OA) and eucalypt wood (ILL-EU) after ionic liquid treatment.

The FTIR spectra of ILL-EU and ILL-OA are depicted in Figure 3. The profiles appear similar, and like for the lignins described in chapter 2 (12 absorption bands were identified. The interpretation of the bands is described and presented in Table 3 (Chapter 2) from the preceding chapter and in Bergamasco et al. [23]. Some differences are observed compared to the acquired spectra of AL-EU and AL-OA. Similarly, as discussed in the previous section concerning the analysis of volatile components via Py-GCMS, the intensities of the IR bands can be analyzed and used for the classification of GS lignins based on the ratio between the intensities of the bands specific for G and S units, thus estimating their ratio. As observed for AL-EU and AL-OA lignins, lignins extracted via ionic liquid show a higher intensity corresponding to band 11, indicating a predominance of S units in the chemical structure. By comparing the intensity of bands 4 and 3, which are more intense in the case of ILL-EU compared to ILL-OA, it can be deduced that the S/G ratio is higher in the case of ILL-EU than ILL-OA. Finally, the intensities of bands 7 and 8 provide information about the abundance of S units (IR band 7) and G units (IR band 8), respectively. In the case of ILL-EU, the ratio between these bands indicates a predominance of S units over G units, confirming the data obtained by Py-GCMS. A different scenario is observed for ILL-OA, where, unlike the previous case, the intensity of band 8 is greater than the intensity of band 7. This indicates a significant guaiacolic component in the ILL-OA lignin, influencing the estimated S/G ratio and contributing to the decrease in the obtained value. As previously observed in Py-GCMS, the ionic liquid treatment of oak lignin leads to a decrease in the S/G ratio, from 2.73 for AL-OA to 1.65 for ILL-OA. In the case of eucalyptus, the decrease in the absolute value is not as pronounced, with AL-EU recording a value of 2.11, while ILL-EU shows a ratio of 1.97. A strong absorption is observed for band 1 at 1725 cm^{-1} corresponding to the stretching vibration of a non-conjugated carbonyl group. In this area, absorptions differ significantly between ILL-EU and ILL-OA. In ILL-EU, there is a low signal intensity, consistent with the trends in AL-EU and AL-OA. In the case of IIL-OA, the signal intensity is much more pronounced, indicating the presence of this type of structure. However, these structures cannot be attributed to the presence of sugars, as the only observable sugar following Py-CG-MS analysis is levoglucosan, with a relatively low abundance. Additionally, this signal is not attributed to the deformation of the C=O group related to the ionic liquid acetate, as literature suggests that the C=O stretching of acetate absorbs in other regions of the IR spectrum: specifically, the asymmetric deformation occurs at 1559 cm^{-1}, while the symmetric deformation is observed at 1324 cm^{-1} [27]. The increased intensity of this band could be due to the breakage of β-O-4' bonds, leading to the formation of non-conjugated β-ketones, called Hibbert ketones [22,28]. [29]. This justifies the increase in the

intensity of band 1, the higher intensity of band 8 compared to band 7, and the abundance of guaiacolic fractions in Py-GCMS. Additionally, for band 6, a higher intensity is observed in ILL-OA compared to ILL-EU, related to the stretching of aromatic OH groups, as a consequence of the cleavage of β-O-4' bonds, supported by the lower molar mass determined by HP-SEC.

2D HSQC (^{1}H-^{13}C) NMR spectroscopy

The comparison of structural characteristics determined by two-dimensional NMR spectroscopy of eucalypt and oak lignin isolated using the mild acidolysis method (AL-EU, AL-OA) and the ionic liquid method (ILL-EU, ILL-OA), respectively, revealed several differences. For both ILL-EU and ILL-OA, a significantly higher relative abundance of S units was determined leading to higher S/G ratios (Table 5 and 6). These findings are in different from Py-GCMS and FTIR spectroscopy results reported above. However, a further investigation of this discrepancy between analytical methods need further detailed studies, which are also outside the frame of this thesis work. Regarding the monomers, higher relative abundances of sinapaldehyde (SA), coniferyl aldehyde (CA), and ferulic acid (FA), as well as cross-peaks from p-benzoic acid (pBA) and benzoic acid esters (BA) were detected in the spectrum of ILL-EU in contrast to AL-EU. Similarly, also in the spectrum of ILL-OA cross-peaks for pBA and BA were detected in low abundance. This higher presence of non-conventional lignin subunits indicates that the isolation process using ionic liquid follows different lignin fractionation and fragmentation mechanisms leading to pBA and BA units as specific lignin degradation products using the ionic liquid method.

The sidechain area of the HSQC spectra of the two lignin preparations (Figure 4 and 5) reveals the absence of γ-acylation in AL-EU while the respective cross-peak (A'γ) is evident in the spectrum of ILL-EU. In ILL-EU further a higher relative ratio of β-O-4' linkages, no α-oxidized β-O-4' structures, less benzyl ether (BE) bonds, and no stilbene linkage types were detected. The higher content of β-O-4'linkages and the absence of α-oxidized β-O-4' structures in ILL-EU present further indications for different biomass degradation reactions when using ionic liquid. This is further supported by the presence of native spirodienone (SD) linkages and the absence of stilbene (I) structures in ILL-EU, which are known to be created by severe processing conditions through i.e. lignin recondensation reactions. In ILL-OA instead, a lower relative abundance of β-O-4'structures were determined, indicating a higher fragmentation of oak lignin when using the ionic liquid method compared to acidolysis. A higher fragmentation of ILL-OA compared to AL-OA was already indicated by the HPSEC elution curves of the two lignins. A lower ratio of stilbene structures in ILL-OA indicates that during lignin fragmentation using the ionic liquid less lignin recondensation occurred compared to AL-OA. The lower abundance of BE structures in ILL-EU and ILL-OA indicated that lignin-carbohydrate complexes (LCCs) in the form of benzyl ethers were cleaved during isolation giving a

purer lignin preparation with less carbohydrate residues. The lower abundance of xylan cross-peaks (X2, X3, X4, X2', and X3') further indicates less carbohydrate impurities in ILL-EU as well as in ILL-OA.

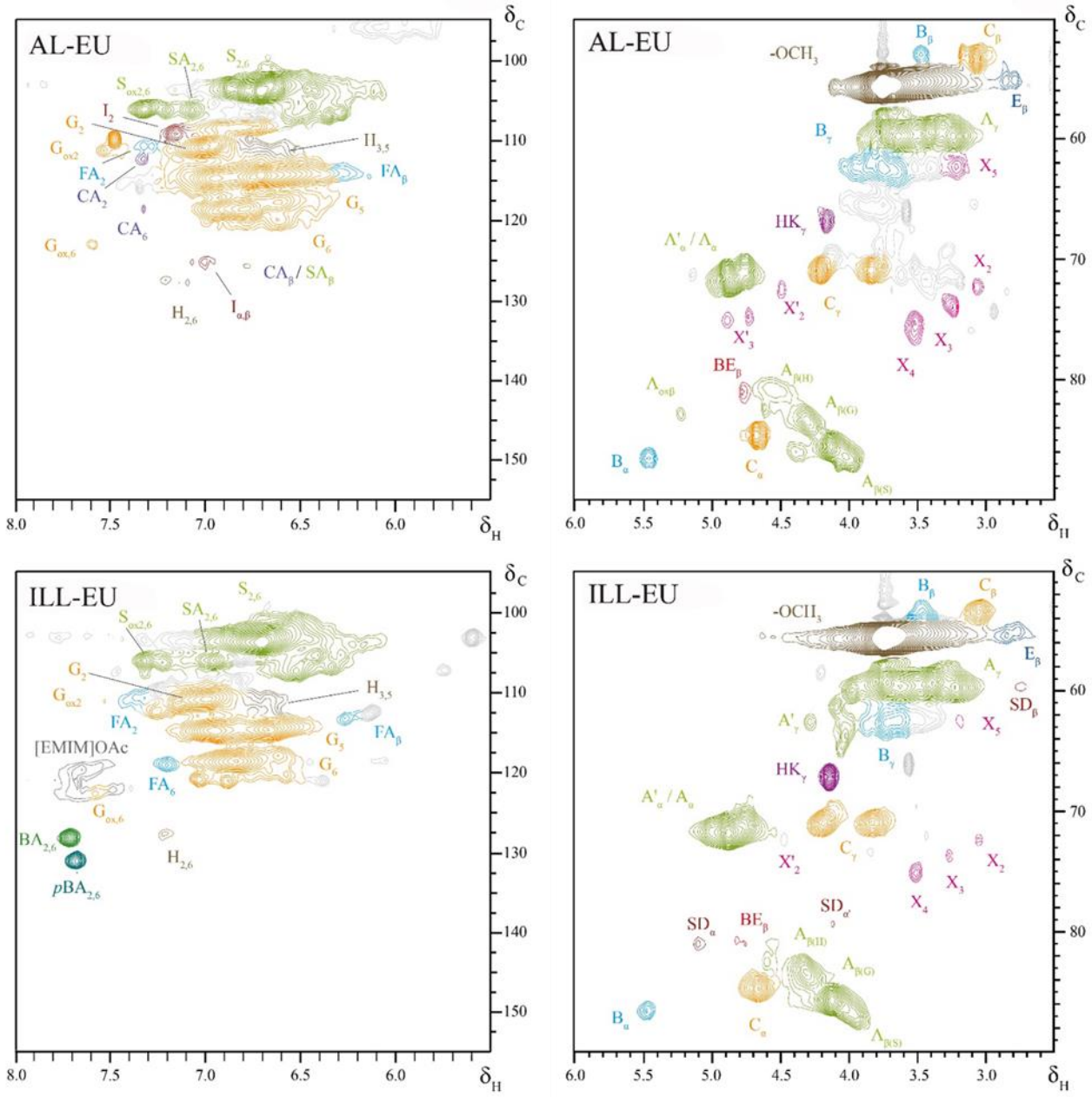

Figure 4: 2D HSQC NMR spectra of AL-EU (above) and ILL-EU (below).

Table 5: Monomeric ratios, S/G ratios, and relative abundance of lignin inter-unit linkages of the Acidolysis lignins (AL-EU) and Ionic liquid (ILL-EU) from eucalypt wood

Lignin Sample	Monomers (%)											Interunit linkages (%)						
	S Units	Sox Units	G Units	Gox Units	H Units	SA	CA	FA	*p*BA	BA	S/G Ratio	*β*-O-4′	*α*-oxid. *β*-O-4′	*β*-5′	*β*-*β*′	BE	Open *β*-1′	Stilbenes
AL-EU	57	3	33	3	1	2	0	1	0	0	1.69	73	2	6	8	5	4	2
ILL-EU	69	3	32	1	0	3	1	3	1	2	2.15	79	0	4	7	2	5	0

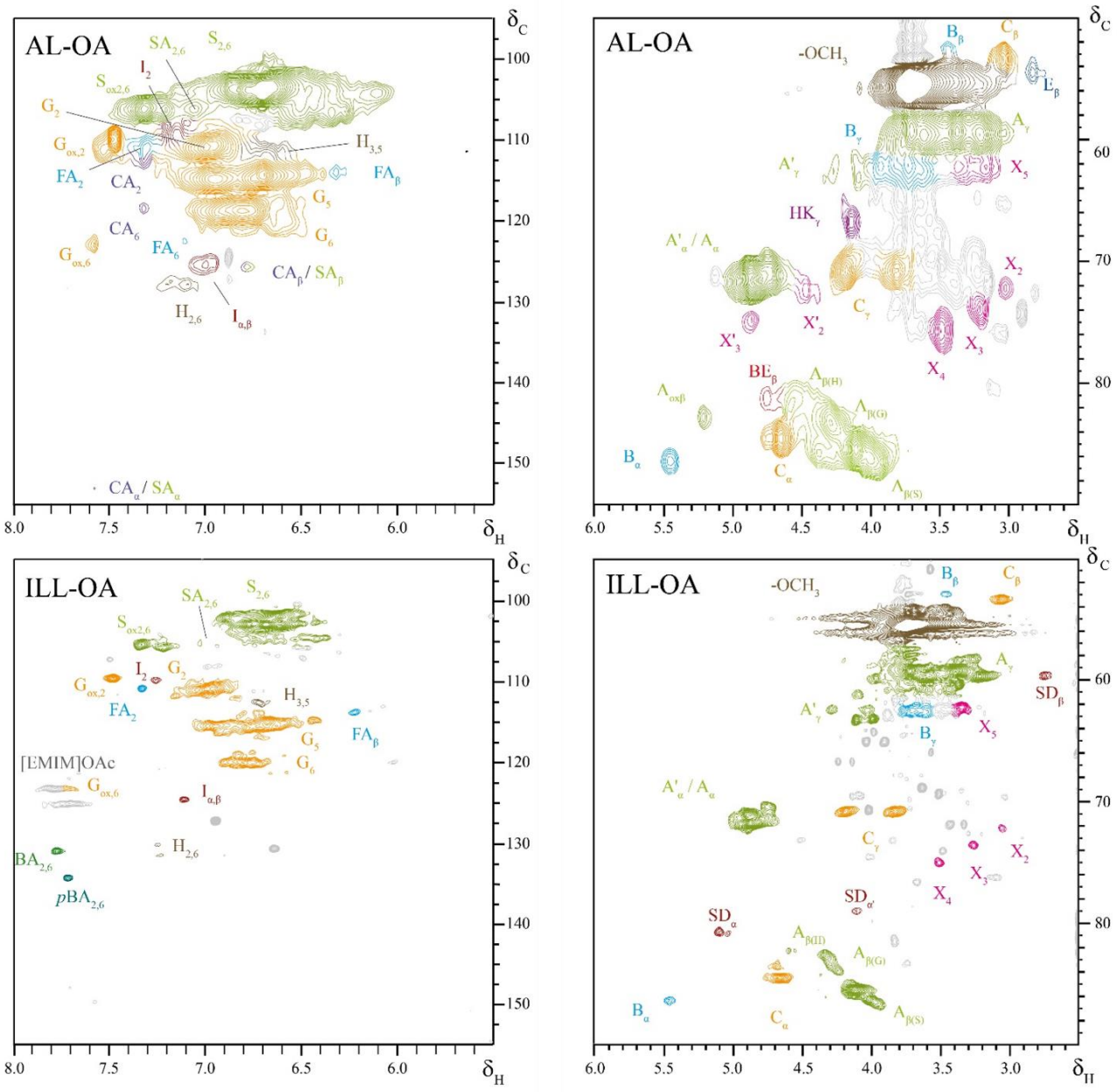

Figure 5: 2D HSQC NMR spectra of AL-OA (above) and ILL-OA (below).

Table 6: Monomeric ratios, S/G ratios, and relative abundance of lignin inter-unit linkages of the Acidolysis lignins (AL-OA) and Ionic liquid (ILL-OA) from oak wood

Lignin Sample	Monomers (%)											Interunit linkages (%)						
	S Units	Sox Units	G Units	Gox Units	H Units	SA	CA	FA	*p*BA	BA	S/G Ratio	*β*-O-4′	*α*-oxid. *β*-O-4′	*β*-5′	*β*-*β*′	BE	Open *β*-1′	Stilbenes
AL-OA	62	5	24	5	1	1	1	1	0	0	2.13	79	3	4	7	3	2	2
ILL-OA	66	4	22	4	1	1	1	1	0	1	2.70	77	0	3	7	1	7	1

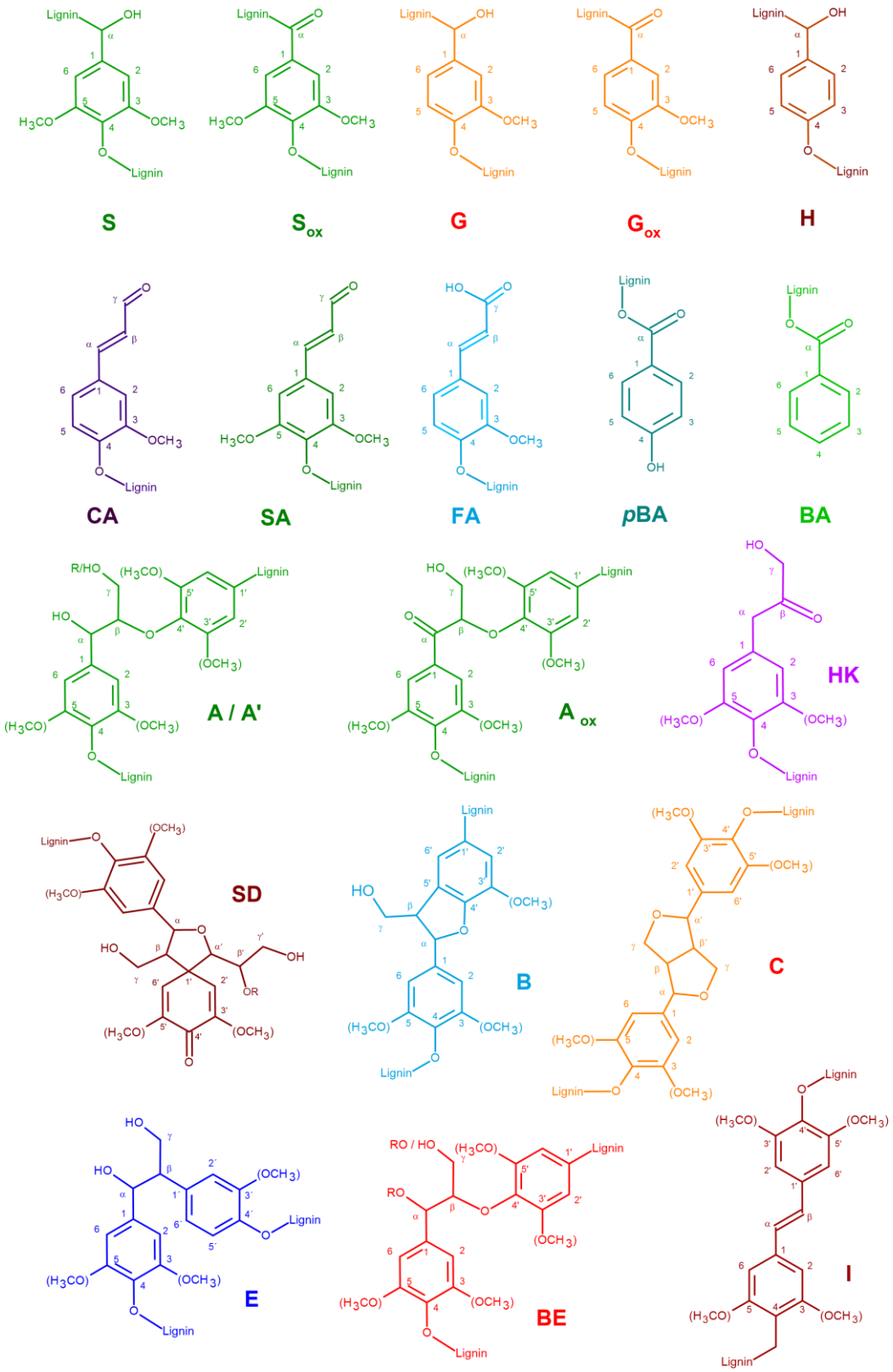

Figure 6. Lignin substructures identified in the respective 2D HSQC NMR spectra of oak and eucalypt acidolysis lignin. S ... syringyl units, Sox ... α-oxidized S units, G ... guaiacyl units, Gox ... α-oxidized G units, H ... p-hydroxyphenyl units, CA . . . coniferaldehyde, SA . . . sinapaldehyde, FA . . . ferulic acid, A . . . β-O-4' linkages, A' ... acylated β-O-4' linkages, Aox ... α-oxidized β-O-4' linkages, B ... β-5' phenylcoumaran bonds, C ... β-β' resinol bonds, I ... stilbene structures, BE ... benzyl ether structures, E ... open β-1' structures.

Conclusion

The data presented in this chapter is part of a broader study regarding the development of a sustainable method for recovering lignin from waste biomass. From these initial investigations, it is observed that the extracted lignin not only reflects the applied treatment but also varies depending on the species of origin. In the case of eucalyptus, except for a lower weight yield of ILL-EU compared to AL-EU, there are no significant differences in the molecular weight distribution, FTIR spectra profiles, and pyrolysis products identified by Py-GCMS. This indicates that eucalyptus lignin, from a chemical perspective, is not significantly affected by the used treatment, maintaining its structural characteristics unchanged. A different scenario is observed for oak lignin; here, a much more pronounced decrease in extraction yield is noted compared to eucalyptus. Following analyses using Py-GCMS, it is evident that ILL-OA shows a higher abundance of volatile compounds of G origin compared to what is observed for AL-OA. One possible explanation for the result, also confirmed by the FTIR analysis, concerns the formation of Hibbert ketones after the cleavage of β-O-4' bonds, to which oak lignin appears to be more sensitive than eucalyptus lignin. Further investigations are still ongoing to clarify the observed results.

References

1. Kaygusuz, K. Renewable energy: Power for a sustainable future. Energy exploration & exploitation 2001, 19, 603-626, https://doi.org/10.1260/0144598011492723

2. Malhotra, M.; Aulakh, I.K.; Gupta, M.; Monika, M. Meteorological parameters effects on pollutants in the air. In Proceedings of the AIP Conference Proceedings, 2023

3. Maciejczyk, P.; Chen, L.-C.; Thurston, G. The role of fossil fuel combustion metals in PM2. 5 air pollution health associations. Atmosphere 2021, 12, 1086, https://doi.org/10.3390/atmos12091086 .

4. Chmielewski, A.G. Environmental effects of fossil fuel combustion; 1999; pp. 56-74

5. Chaudhary, G.; Chaudhary, N.; Saini, S.; Gupta, Y.; Vivekanand, V.; Panghal, A. Assessment of pretreatment strategies for valorization of lignocellulosic biomass: path forwarding towards lignocellulosic biorefinery. Waste and Biomass Valorization 2023, 1-36, https://doi.org/10.1007/s12649-023-02219-z

6. Ralph, J.; Lapierre, C.; Boerjan, W. Lignin structure and its engineering. Current opinion in biotechnology 2019, 56, 240-249, https://doi.org/10.1016/j.copbio.2019.02.019

7. Lourençon, T.V.; de Lima, G.G.; Ribeiro, C.S.; Hansel, F.A.; Maciel, G.M.; da Silva, K.; Winnischofer, S.M.; de Muniz, G.I.; Magalhães, W.L. Antioxidant, antibacterial and antitumoural activities of kraft lignin from hardwood fractionated by acid precipitation. International Journal of Biological Macromolecules 2021, 166, 1535-1542, https://doi.org/10.1016/j.ijbiomac.2020.11.033

8. Sadeghifar, H.; Ragauskas, A. Lignin as a UV light blocker—a review. Polymers 2020, 12, 1134, https://doi.org/10.3390/polym12051134

9. Bergamasco, S.; Tamantini, S.; Zikeli, F.; Vinciguerra, V.; Scarascia Mugnozza, G.; Romagnoli, M. Synthesis and Characterizations of Eco-Friendly Organosolv Lignin-Based Polyurethane Coating Films for the Coating Industry. Polymers 2022, 14, 416, https://doi.org/10.3390/polym14030416 .

10. Li, R.J.; Gutierrez, J.; Chung, Y.-L.; Frank, C.W.; Billington, S.L.; Sattely, E.S. A lignin-epoxy resin derived from biomass as an alternative to formaldehyde-based wood adhesives. Green chemistry 2018, 20, 1459-1466, https://doi.org/10.1039/C7GC03026F

11. Zikeli, F.; Vettraino, A.M.; Biscontri, M.; Bergamasco, S.; Palocci, C.; Humar, M.; Romagnoli, M. Lignin Nanoparticles with Entrapped Thymus spp. Essential Oils for the Control of Wood-Rot Fungi. Polymers 2023, 15, 2713, https://doi.org/10.3390/polym15122713

12. Ragauskas, A.J.; Beckham, G.T.; Biddy, M.J.; Chandra, R.; Chen, F.; Davis, M.F.; Davison, B.H.; Dixon, R.A.; Gilna, P.; Keller, M. Lignin valorization: improving lignin processing in the biorefinery. science 2014, 344, 1246843, http://dx.doi.org/10.1126/science.1246843

13. Liu, Z.; Li, L.; Liu, C.; Xu, A. Pretreatment of corn straw using the alkaline solution of ionic liquids. Bioresource technology 2018, 260, 417-420, https://doi.org/10.1016/j.biortech.2018.03.117

14. da Costa Lopes, A.M.; João, K.G.; Rubik, D.F.; Bogel-Łukasik, E.; Duarte, L.C.; Andreaus, J.; Bogel-Łukasik, R. Pre-treatment of lignocellulosic biomass using ionic liquids: wheat straw fractionation. Bioresource technology 2013, 142, 198-208, https://doi.org/10.1016/j.biortech.2013.05.032

15. Hou, X.D.; Smith, T.J.; Li, N.; Zong, M.H. Novel renewable ionic liquids as highly effective solvents for pretreatment of rice straw biomass by selective removal of lignin. Biotechnology and bioengineering 2012, 109, 2484-2493, https://doi.org/10.1002/bit.24522

16. Li, C.; Knierim, B.; Manisseri, C.; Arora, R.; Scheller, H.V.; Auer, M.; Vogel, K.P.; Simmons, B.A.; Singh, S. Comparison of dilute acid and ionic liquid pretreatment of switchgrass: biomass recalcitrance, delignification and enzymatic saccharification. Bioresource technology 2010, 101, 4900-4906, https://doi.org/10.1016/j.biortech.2009.10.066

17. Brandt, A.; Gräsvik, J.; Hallett, J.P.; Welton, T. Deconstruction of lignocellulosic biomass with ionic liquids. Green chemistry 2013, 15, 550-583, https://doi.org/10.1039/C2GC36364J

18. Bernardo, J.R.; Gírio, F.M.; Łukasik, R.M. The effect of the chemical character of ionic liquids on biomass pre-treatment and posterior enzymatic hydrolysis. Molecules 2019, 24, 808, https://doi.org/10.3390/molecules24040808

19. Ralph, J.; Grabber, J.H.; Hatfield, R.D. Lignin-ferulate cross-links in grasses: active incorporation of ferulate polysaccharide esters into ryegrass lignins. Carbohydrate research 1995, 275, 167-178, https://doi.org/10.1016/0008-6215(95)00237-N

20. Hossain, M.M.; Rawal, A.; Aldous, L. Aprotic vs protic ionic liquids for lignocellulosic biomass pretreatment: anion effects, enzymatic hydrolysis, solid-state NMR, distillation, and recycle. ACS Sustainable Chemistry & Engineering 2019, 7, 11928-11936, https://doi.org/10.1021/acssuschemeng.8b05987

21. Sun, N.; Rahman, M.; Qin, Y.; Maxim, M.L.; Rodríguez, H.; Rogers, R.D. Complete dissolution and partial delignification of wood in the ionic liquid 1-ethyl-3-methylimidazolium acetate. Green Chemistry 2009, 11, 646-655, https://doi.org/10.1039/B822702K

22. Dutta, T.; Isern, N.G.; Sun, J.; Wang, E.; Hull, S.; Cort, J.R.; Simmons, B.A.; Singh, S. Survey of lignin-structure changes and depolymerization during ionic liquid pretreatment. ACS Sustainable Chemistry & Engineering 2017, 5, 10116-10127, https://doi.org/10.1021/acssuschemeng.7b02123

23. Bergamasco, S.; Zikeli, F.; Vinciguerra, V.; Sobolev, A.P.; Scarnati, L.; Tofani, G.; Scarascia Mugnozza, G.; Romagnoli, M. Extraction and Characterization of Acidolysis Lignin from Turkey Oak (Quercus cerris L.) and Eucalypt (Eucalyptus camaldulensis Dehnh.) Wood from Population Stands in Italy. Polymers 2023, 15, 3591, https://doi.org/10.3390/polym15173591

24. Kim, J.-Y.; Shin, E.-J.; Eom, I.-Y.; Won, K.; Kim, Y.H.; Choi, D.; Choi, I.-G.; Choi, J.W. Structural features of lignin macromolecules extracted with ionic liquid from poplar wood. Bioresource technology 2011, 102, 9020-9025, https://doi.org/10.1016/j.biortech.2011.07.081

25. Tan, S.S.; MacFarlane, D.R.; Upfal, J.; Edye, L.A.; Doherty, W.O.; Patti, A.F.; Pringle, J.M.; Scott, J.L. Extraction of lignin from lignocellulose at atmospheric pressure using alkylbenzenesulfonate ionic liquid. Green Chemistry 2009, 11, 339-345, https://doi.org/10.1039/B815310H

26. Varanasi, P.; Singh, P.; Arora, R.; Adams, P.D.; Auer, M.; Simmons, B.A.; Singh, S. Understanding changes in lignin of Panicum virgatum and Eucalyptus globulus as a function of ionic liquid pretreatment. Bioresource technology 2012, 126, 156-161, http://dx.doi.org/10.1016/j.biortech.2012.08.070

27. Aiello, A.; Hoffman, J.R.; Kotula, A.P.; Flagg, L.Q.; Li, R.; Woodcock, J.W. Trace Water Effects on Crystalline 1-Ethyl-3-methylimidazolium Acetate. The Journal of Physical Chemistry B 2023, https://doi.org/10.1021/acs.jpcb.3c02735

28. Wang, H.; Liu, Z.; Hui, L.; Ma, L.; Zheng, X.; Li, J.; Zhang, Y. Understanding the structural changes of lignin in poplar following steam explosion pretreatment. Holzforschung 2020, 74, 275-285, https://doi.org/10.1515/hf-2019-0087

29. Miles-Barrett, D.M.; Neal, A.R.; Hand, C.; Montgomery, J.R.; Panovic, I.; Ojo, O.S.; Lancefield, C.S.; Cordes, D.B.; Slawin, A.M.; Lebl, T. The synthesis and analysis of lignin-bound Hibbert ketone structures in technical lignins. Organic & biomolecular chemistry 2016, 14, 10023-10030, https://doi.org/10.1039/C6OB01915C

CHAPTER 4: Electrospun PCL filtration membranes enhanced with an electrosprayed lignin coating to control wettability and antibacterial properties

Sara Bergamasco, Noemi Fiaschini, Luis Alexander Hein, Marco Brecciaroli, Roberta Vitali, Manuela Romagnoli * and Antonio Rinaldi *

Polymers **2024**, *16*(5), 674; https://doi.org/10.3390/polym16050674

Abstract

This study reports on the two-step manufacturing process of a filtration media obtained by electrospinning a paper filter with a polycaprolactone (PCL) non vower layer, which in turn was subsequently coated with pure lignin via electrospraying. The manufacturing of pure lignin coatings by solution electrospraying represents a novel development that requires a fine control of the underlying electrodynamic processing. The effect of increasing deposition time on the lignin coating was investigated for electrospray time from 2.5 min to 120 min. Microstructural and physical characterization included SEM analysis, permeability tests by Gurley densometer, ATR-FTIR analysis, and contact angle measurements vs. both water and oil. From a functional viewpoint, such a natural coating exhibited an amphiphilic behavior that enabled modulating the hydrophilic/hydrophobic nature of the underlying PCL non-woven substrate. For example, the intrinsic hydrophobic behavior of bare PCL electrospun fibers is reduced, with a marked decrease already for a thin coating of less than 50 nm. Instead, the wettability of PCL vs. apolar liquids was altered, producing an initial increase of the oil contact angles (OCA) for short deposition times of a few minutes, followed by a steady decrease in OCA for thicker lignin coatings. To highlight the effect of the lignin type on the results two grades from oak (AL-OA) of the *Quercus cerris* L. species and eucalyptus (AL-EU) of the *Eucalyptus camaldulensis* Dehnh species are compared. Furthermore, the lignin coating possessed antibacterial properties, which were investigated against Staphylococcus aureus, with AL-EU showing superior antibacterial activity compared to oak lignin, increasing with lignin density. The findings are relevant for applications of this abundant biopolymer not only for filtration, but also in biotechnology, health, packaging and circular economy applications in general, where the reuse of such natural byproducts brings also a fundamental demanufacturing advantage.

Keywords: Electrospinning, electrospraying, lignin, oak, eucalypt, PCL, FTIR, SEM, morphology, wettability, antibacterial test

Introduction

Water filtration using separation membranes is one of the methods employed for wastewater treatment, where such membranes act as a physical barrier, allowing the passage of water molecules while sieving molecules, microorganisms, and dissolved substances larger than a given cutoff [1]. Polymeric membranes produced by electrospinning have shown significant potential for water filtration applications, garnering substantial interest over time due to their ability to create highly customizable materials with controlled porosity [2]. In fact, electrospinning is an advanced manufacturing method of great interest in the filtration industry as it enables the production of either self-standing fibrous non-woven membranes or just coatings characterized by high porosity, open-pore microstructure, and a large surface area [3]. The interconnected percolating pores within a fibrous electrospun layer are capable of enhancing filtration capacity [4] and can be easily tailored in pore size and overall void fraction to modulate the filtration performance to achieve selective removal of target contaminants, such as particulates [5], heavy metals [6], oils and organic compounds [7], and microbial agents like bacteria and viruses [8]. Electrospinning is recognized as a very versa-tile technique for processing various polymers to create nanofiber-based membranes and coatings, but it can also be used in electrospray mode to produce emulsions or coatings made of particles made of micronized polymer [9].

Several technological polymers are deployed in the electrospinning of filtering media. For example, polyacrylonitrile (PAN) is used for its excellent chemical, mechanical, and thermal properties [10]. This polymer is often used in synergy with other materials; e.g., Perekh et al. [11] produced electrospun PAN membranes incorporating silver nanoparticles to provide clean and drinkable water for underdeveloped countries. Polyvinylidene fluoride (PVDF) is another example of an interesting material with characteristics attractive for direct osmosis applications in seawater desalination [12]. Polysulfone (PSU) is also commonly used in this field, both alone and in combination with other materials [13]. For instance, PSU membranes coated with a layer of magnetite nanoparticles enabled the removal of model viruses (i.e., bacteriophage MS2) [14], whereas adding a nanocoating of silver nanoparticles endowed PSU electrospun membranes with antibacterial properties [15]. Yet, in the mainstream transition to a circular economy, the development of a new class of more sustainable electrospinning materials is becoming a key research objective.

In recent years, membranes made of poly(ε-caprolactone) (PCL) have been investigated as a relatively environmentally friendly option for water treatment applications [16]. Despite being a synthetic polymer, PCL possesses desirable properties such as biodegradability and biocompatibility [17]. These attributes are crucial for water treatment, as biodegradability allows for the degradation of PCL into products such as capronic acid, succinic acid, valeric acid, and butyric acid [18]. by the action of

micro-organisms, making them environmentally friendly and suitable for disposal without causing harm to the environment [19]. From the viewpoint of circular economy, this makes PCL a potential candidate to implement the demanufacturing of exhaust mem-branes and help address the end-of-life problems of current products. Biocompatibility is another important pre-requisite for safe exploitation, ensuring that the material is non-toxic to both humans and the environment [20]. Furthermore, PCL is easily work-able, offers excellent flexibility when combined with other polymers to modify its properties, and exhibits good solubility in a wide range of organic solvents commonly used in electrospinning processes [21].

In the field of water filtration, reportedly, PCL was deployed for the fabrication of composite electrospun membranes with high performance when used in combination with cellulose nanofibrils (CNF) [22]. In that case, the CNF enhanced the mechanical properties of the composite fibers and helped improve the filtration quality in terms of turbidity, conductivity, and the removal of metallic contaminants. This approach to membrane design is interesting as it yields a system that pairs a filtration performance tailorable by a functional additive (i.e., CNF in this example) to the intrinsic demanufacturing proneness of the PCL matrix. In another example, nanofibrous membranes made of chitosan and PCL delivered a composite architecture inheriting the antimicrobial properties of chitosan in combination with the advantageous characteristics of PCL [23]. In another example, hybrid nanocomposite membranes of PCL/TiO2 were investigated for the treatment of wastewater from the dairy industry, showing that such membranes could combine the hydrophobic properties and chlorine resistance of PCL with the antibacterial and anti-fouling properties associated with the hydrophilicity of titanium dioxide [24]. Finally, our group also investigated several compo-site electrospun systems based on PCL, such as the PCL/Ag endowed with a Ag nano-coating of PCL fibers via magnetron sputtering [25]. In conclusion, the design and manufacturing of advanced composite membranes obtained via electrospinning do represent a timely and rewarding exploration area.

In this paper, we investigate the combination of PCL with lignin, a new bio-material that is attractive and is currently receiving significant attention. Lignin is, in fact, the second most abundant natural polymer in nature [26] and represents a renewable and sustainable resource that can be harvested from several feedstocks of the wood industry. Lignin finds diverse applications across various industrial fields, including the coating industry for its UV protection capabilities [27], the synthesis of therapeutic hydrogels [28] for their antibacterial properties and biocompatibility, and as a precursor for high-value-added product manufacturing [29]. Additionally, the abundance of functional groups makes lignin suitable for the production of flocculants, adsorbents, and dispersants [30]. All these properties make lignins a worthy candidate to explore for water treatment applications.

Hereafter, we present a new 3-layered composite membrane consisting of a back-ing of filtering media, covered with a thick PCL layer inspired from our prior study [25], and here functionalized by an innovative biocoating made of lignin via an electrospinning process driven in electrospray mode. We recall that electrospinning and electrospraying coexist on the same technological platform and just represent two regimes of the same electrohydrodynamic technique, leading to two different outcomes depending on the polymer solution being processed. Electrospinning and electrospraying represent cutting-edge methodologies for producing nanofibers and particles with controlled dimensions down to the nanoscale, using electric fields on the or-der of kilovolts per centimeter. These processes offer broad versatility in structure de-sign, enabling manipulation of key parameters [31] to achieve the desired morphology. These parameters can be classified into factors related to the solution [32], operational parameters like applied electric field [33] and working distance [34,35], and environ-mental factors such as temperature and relative humidity. In this article, we do not aim to delve into the theoretical chemical-physics aspects underlying these phenomena, as they are not the focus of the presented work. However, we aim to provide some basic information on the main practical differences between the employed techniques. As widely recognized, the nanofiber formation process involves a series of complex phenomena [36], ranging from the initial formation of a straight jet from the solution, with the development of the Taylor cone, to the solidification of the polymeric material during its flight towards the collection substrate. The jet's expulsion is influenced by various forces, including surface tension, viscoelastic force, repulsive forces, air drag force, and gravity [37]. Furthermore, the driving force responsible for fiber generation is provided by the electrical potential difference between the injector and the collector.

In synergy with these aspects, the intrinsic properties of the polymeric solution play a crucial role. For example, each solution has a critical concentration value above which fiber formation is initiated, while lower concentrations allow for the production of monodisperse particles [38]. The polymer molecular weight, closely related to the solution concentration value, determines the formation of fibers or dispersed particles. Based on the choice of the polymer's molecular weight and the concentration of the solution, another important parameter arises, namely the final viscosity of the electro-spun solution. In cases of low molecular weights and low-concentration solutions, as well as in the case reported here, a homogeneous spray of the dispersed polymer is achieved, while increasing viscosity pushes the process towards fiber production, as illustrated by McKee et al. [39], who describe the correlation between solution rheology and the formation of electrospun fibers. Finally, electrical conductivity [40] can interact with gravity and electrical forces, contributing to the formation of conical jets. Careful management of these parameters and solution properties is essential for achieving the desired results.

As there are many lignin grades, two different types of lignin are investigated and benchmarked here, namely acidolysis lignin (AL) from oak wood (AL-OA) and from eucalyptus wood (AL-EU) [41]. Morphological, physical, and antibacterial studies were conducted on prototypical membranes, varying not only the type of lignin but also altering the electrospraying deposition time, with five different time points selected to monitor the evolution of the composite membrane properties and microstructure vs. deposition time. The main goal is to show that pure lignin can be processed by electrospraying to obtain a functional coating with thickness from the nanometer scale to the micrometer scale, but the scope of our research also covers aspects related to the possibility of varying the amount of deposited lignin (i.e., thickness or areal density of the coating) to modulate the functional properties. The latter aspect is relevant to adjusting the final filtration product to the specific requirements of a given engineering application.

Materials and Methods

Materials

PCL Capa 6800D from Perstorp (UK Limited, Warrington, UK), Acidolysis lignin from eucalypt (E. camaldulensis) and oak (Q. cerris) species, N,N-Dimethylformamide (DMF) from Supelco, Merck KGaA (Darmstadt, Germany), Chloroform ($CHCl_3$) stabilized with 2-methyl-2-butene, provided from VWR chemicals (Radnor, PA, USA), Qualitative filter paper 600 from VWR International (Radnor, PA, USA), Ethanol absolute from Merck KGaA (Darmstadt, Germany), deionized water, 1 Primary Wound Dressing© (1PWD) (CE 0344)—Phytoceuticals, Zurich, Switzerland). *Staphylococcus aureus* (ATCC 29213) and *Escherichia coli* (ATCC 25922) were used, respectively, as representatives for Gram-positive and Gram-negative pathogens.

Preparation of solutions and fabrication of membranes through two steps electrospinning

Step 1: Supported PCL membranes were electrospun on a selected paper filter media (600, VWR International, Radnor, PA, USA) to produce a microfiltration membrane using industrial electrospinning equipment (Fluidnatek® LE100, Bioinicia, Paterna, Spain) at Nanofaber srl, equipped with a large stationary planar collector and an environmental control unit, enabling to keep temperature at 25 °C and relative humidity (RH) at 40% throughout manufacturing. The electrospinning of PCL was performed according to the recipe of a commercially available product, the PCL-NBARE ™ series (Nanofaber srl, Rome, Italy), for the solution electrospinning of PCL granules in a mixture solvent of DMF and chloroform [25]. The filtration paper covered with bare PCL represented the reference system throughout the study, referred to as “PCL” or “uncoated PCL” hereafter.

Step 2: For electrospraying the coating of lignin, two 5% (*w,w*) solutions of oak (AL-OA) and eucalypt lignin (AL-EU) in DMF were prepared. These two solutions were prepared using a thermostated bath at 60 °C and were magnetically stirred for two hours. The lignin solutions were subsequently allowed to stabilize at room temperature for two days before being processed through electrospinning. The fabrication of the final composite membranes was performed according to protocols by Nanofaber s.r.l., by adding to Step 1 a second processing step of electrospray of a surface coating of AL-EU or AL-OA onto the PCL layer. The two steps were performed sequentially in situ using said industrial electrospinning equipment. Several coated membranes of 19 × 24 cm^2 in size were prepared for different sets of parameters, as listed in Table 1.

Table 1. Main process parameters for 2-step electrospinning/electrospraying coating of PCL and AL. Process temperature and RH kept at 25°C and 40% respectively for all steps and samples.

Electrospinning/ Electrospraying	Deposition time (min)	FR (ml/h)	Distance (mm)	V (KV)	Substrate
Step1 : **PCL**	60	6	150	20	Paper filter
Step 2: **Lignin**	2.5/5/10/60/120	0.75	130	25/-30	PCL

Morphology, Mechanical Testing and Roughness of the Membranes

The morphological study of the membranes was conducted using a field emission gun scanning electron microscope (SEM) (Leo 1530, ZEISS, Jena, Germany) working at a low extraction voltage of 3.00 kV to avoid charging. Samples were analyzed without applying a conductive Au nanocoating. To measure the thickness of the membranes (Th), cross-sectional sections were placed between two silicon wafers. Three measure-ment points were taken for each cross-sectional section. In these measurements, a Zeiss AXIO Zoom.V16 microscope (ZEISS, Jena, Germany) was used, and images were pro-cessed using Zen Blue Version 3.4.91 software. In addition to image-based analysis, an experimental assessment of membrane porosity was conducted using the displacement volume technique using absolute ethanol.

The mechanical properties of the filter paper and of the PCL layers alone were evaluated by tensile tests, similarly to prior work [15]. A macro-tensile loading frame (MICROTEST 200 N, DEBEN, Suffolk, UK) equipped with a 200 N load cell was used to test rectangular strips cut out of samples. The Young modulus (E) and the ultimate tensile strength (UTS) of each material were measured from their stress vs. strain curve, respectively, as the slope in the linear response region and as the maximum ten-sile stress reached before either the rupture or the onset of the softening phase.

The roughness value Ra (Arithmetic Average Roughness) for each sample was evaluated using NPS confocal scanning (NP1 probe, HIROX, Tokyo, Japan), a method-ology compliant with ISO 21920 [60].

Porosity and permeability Determination

The porosity of the membranes was measured using the liquid penetration method, a.k.a. liquid displacement method [42,43]. Ethanol (Merck, Germany) was chosen as penetrating liquid because it could permeate through the porous membrane while having lower density ($\rho_{EtOH} \cong 0.790$ g/ml) than the polymers under consideration. The percent porosity ($\varepsilon_{\%}$) was computed from Equation (1)

$$\varepsilon_{\%} = (m3 - m4 - m1)/(m2 - m4) \times 100 \quad (1)$$

by determining the weights m1, m2, m3, and m4 by a scale (ORMA, BCA120, UK) at a temperature of 20°C. For a given membrane specimen, m1 represents the "as-dry" weight, m2 represents the weight of a "control" graduated bottle filled with ethanol up to a specified "control volume", and m3 is the weight of the same bottle after the membrane specimen is inserted and immersed in the ethanol, with the displaced excess volume of ETOH carefully removed using a pipette to restore the control volume. Finally, m4 reflects the weight of the bottle containing the residual ethanol after the wet membrane is extracted.

The assessment of air permeability for the electrospun membranes was conducted using a Gurley densometer (model 4320, Troy, NY, USA). In this test, the time (t) in seconds required for a volume (V) of air equal to 100 cm^3 to pass through a surface (A) with a fixed area of 1.58 cm^2 was measured. Equation (2) renders the permeability value (P) for each sample in "cm/s" [44].

$$P = \frac{V}{A\,x\,t} \quad (2)$$

Wettability tests of membranes

The wettability tests of the membranes were conducted by measuring the contact angle using a Leica Wild M3Z (part of Hexagon, Stockholm, Sweden) stereomicro-scope. Images were captured using a Moticam 2000. For the contact angle analysis, two representative liquids were used: deionized water (WCA) to represent the hydrophilic part and "1PWD" (1 Primary Wound Dressing©) to represent the lipophilic part (OCA). The measurement of the contact angle between the membrane and a droplet of the liquid was performed 10 s after depositing 10 µL of the liquid onto the membrane surface.

ATR-FTIR analysis

For the ATR-FTIR (Attenuated Total Reflection Fourier-Transform Infrared) analysis of the samples, a Nicolet iS50 spectrometer, connected to the iD70 ATR accessory (Thermo Fisher Scientific, Waltham, MA, USA) was used. The crystal used for this ATR analysis was a monolithic diamond crystal. The spectra were recorded in absorbance mode with a resolution of 4 cm-1. Each sample was scanned 16 times in the wavelength range from 4000 to 400 cm^{-1}.

Antimicrobial test

Circular PCL disks with a diameter of 15 mm, created through the die-cutting process, were placed in 24-multiwell plates for Staphylococcus aureus (*S. aureus*) and Escherichia coli (*E. coli*) biological tests. S. aureus and E. coli stock cultures kept at −80 °C in 10% (w/v) glycerol (Merk Life Science S.r.l., Milan, Italy) were inoculated, respectively, into 3 mL of Nutrient broth (Biolife Italiana, Milan, Italy) and of Luria Bertani (LB) broth (Merck Life Science S.r.l., Milan, Italy). Both bacterial cultures were incubated at 37 °C O/N with constant shaking at 180 rpm before their use in experiments. The day of the test, the S. aureus bacterial concentration was diluted and grown until OD600 was 0.02, about 1.1×10^6 colony forming units/mL (CFU/mL); in-stead, the E. coli bacterial concentration was diluted and grown until OD600 was 0.028, about 5.0×10^6 colony forming units/mL (CFU/mL). Subsequently, the bacteria were introduced into a 24-well multiwell plate, where they were exposed to either uncoated PCL samples (blank disks) or Lignin-coated samples. The incubation took place at 37 °C under continuous agitation at 50 rpm. Two types of experiments were performed. In the first experiment, a control with *S. aureus* alone was also inserted, and the samples were incubated with the microbial population. The survival rate was deter-mined at 1.5 h and 3 h using the count plate method and the calculation of CFUs to determine the cytocitic action of the samples. In the second experiment, at times t = 1 ½, 3, and 4.5 h, 10 µL of each sample were diluted in phosphate-buffered saline (PBS) (Euroclone, Milan, Italy) (serial dilution from 10^{-1} to 10^{-8}) and 100 µL of each dilution were distributed on Nutrient agar dishes (15 g L^{-1} agar) (Panreac Química SLU, Barcelona, Spain) for *S. aureus* strain and on Luria Bertani agar (15 g L^{-1} agar) dishes for *E. coli* strain. All dishes were incubated for 18 h at 37 °C. Following the incubation period, colonies that had reached a size discernible bare-eye were enumerated, and the concentration corresponding to the counted colonies was determined. The antibacterial experiments were replicated twice for consistency and reliability of the results. The acquired data were expressed as the mean ± SEM. Prism 7 software was utilized to perform Student's *t-test*. Significant differences were highlighted for two significance levels as * $p < 0.05$ or ** $p < 0.01$.

Results and discussion

Self-standing membranes consisting of filtering paper and an electrospun PCL layer was used as the control and as basis for subsequent treatments obtained by per-forming a second coating step with lignin. At the end of all manufacturing processes, 11 membranes were produced (Figure 1) and, for each of the two lignins grade, five coatings were produced at five different deposition time, as summarized in the Table 2.

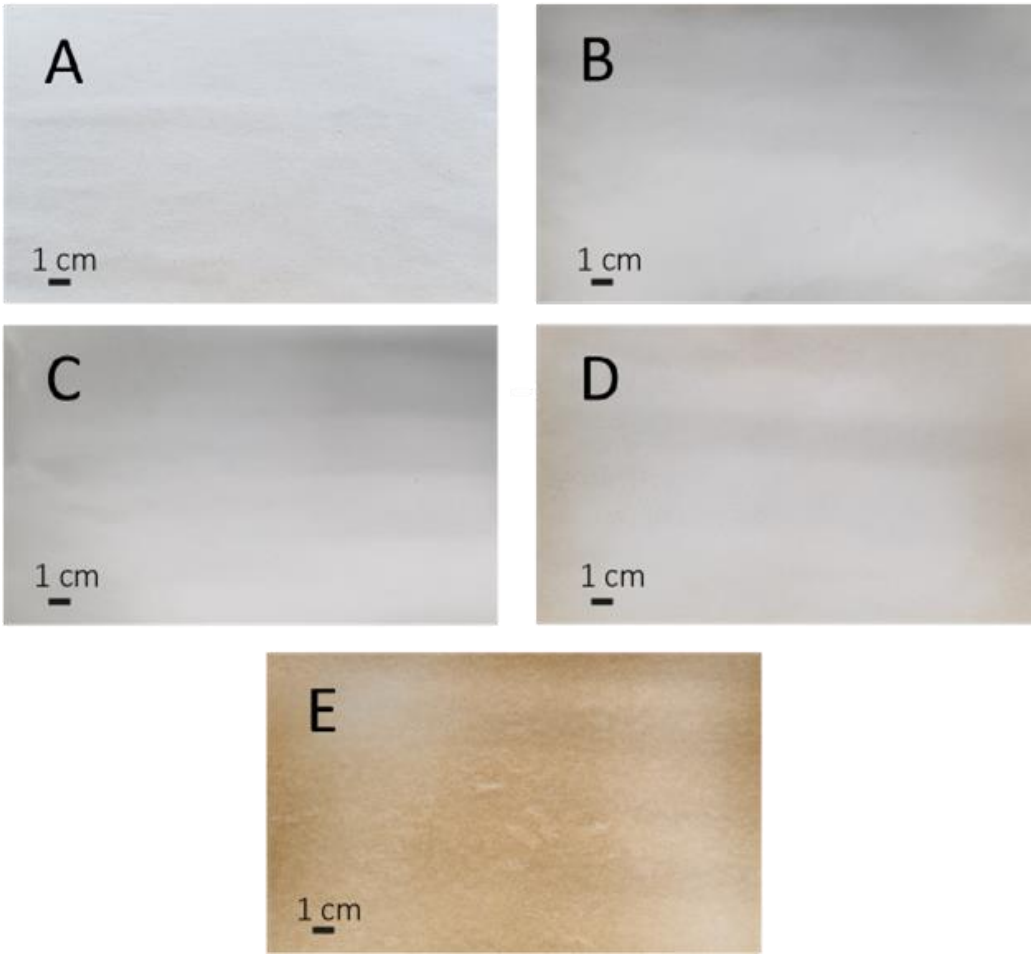

Figure 1. Pictures of PCL membrane and membranes coated with lignin at different times: (A) PCL, (B) AL-2.5, (C) AL-5, (D) AL-10, (E) AL-60

Table 2. Treatments from the 2-step electrospinning and corresponding label in this study, AL-EU and AL-OA corresponding to lignin from Eucalypt and Oak respectively.

Treatment	Label	Definition
1	PCL	basic membrane with PCL coating (step 1 only)
2	AL-EU-2.5	PCL coated for 2.5 minutes with AL-EU
3	AL-EU-5	PCL coated for 5 minutes with AL-EU
4	AL-EU-10	PCL coated for 10 minutes with AL-EU
5	AL-EU-60	PCL coated for 60 minutes with AL-EU
6	AL-EU-120	PCL coated for 120 minutes with AL-EU
7	AL-OA-2.5	PCL coated for 2.5 minutes with AL-OA
8	AL-OA-5	PCL coated for 5 minutes with AL-OA
9	AL-OA-10	PCL coated for 10 minutes with AL-OA
10	AL-OA-60	PCL coated for 60 minutes with AL-OA
11	AL-OA-120	PCL coated for 120minutes with AL-OA

Microstructure, Mechanical Properties and Roughness of Membranes

The investigation of our multilayer samples started with the microstructural analysis of surface texture (of the electrospun material) and thickness. The SEM images in Figure 2 portray the architecture of the PCL non-woven fibers along with the distribution of lignin sprayed on top of them, which appears

more pronounced with deposition time. Up to 60 min, the mesh structure of PCL fibers is still clearly visible, but for a deposition time of 120 min, the lignin coating becomes conformal and completely shields the underlying fibrous structure. Interestingly, although deposition time is proportional to the spatial density of lignin particles, the size distribution of said particles is seemingly invariant and estimated to be approximately 320 ± 130 nm (mean ± SD) for both lignin grades and for any deposition time. In contrast, the diameter distribution of the randomly oriented PCL fibers was about 240 ± 150 nm (Figure 2F), indicating that PCL fibers and lignin particles have a similar characteristic length scale.

Figure 3 shows the optical microscope images of PCL membranes coated for 10 minutes with AL-OA (A) and PCL coated for 120 minutes with AL-OA (B).

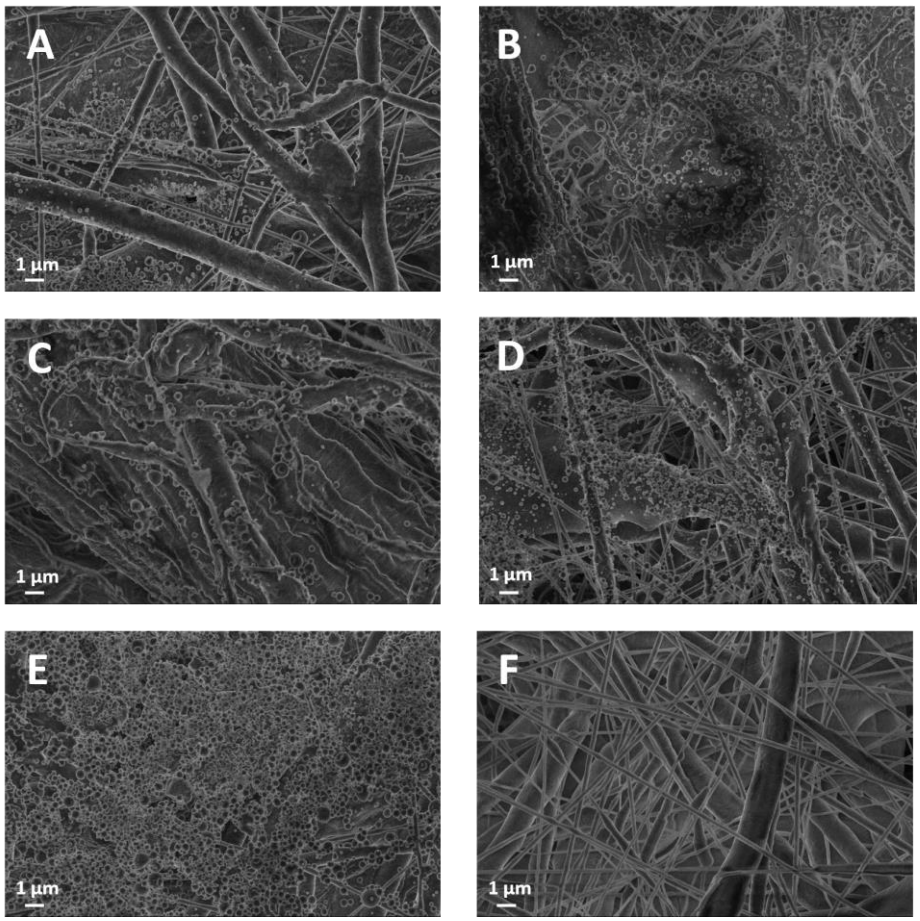

Figure 2. Scanning Electron Microscope (SEM) results: (a) AL-EU-2.5, (B) AL-EU-5, (C) AL-EU-10, (D) AL-EU-60, (E) AL-EU-120, (F) PCL

Regarding thickness measurements (*Th*), the average and SD for each sample are summarized in Table 3 (data net of the nominal filter paper support thickness equal to 110 µm for all cases), but do not offer an immediate interpretation for the observed trends. PCL/AL samples for coating times of 2.5 and 5 min, both with oak and eucalyptus lignin, exhibit thickness values similar to each other.

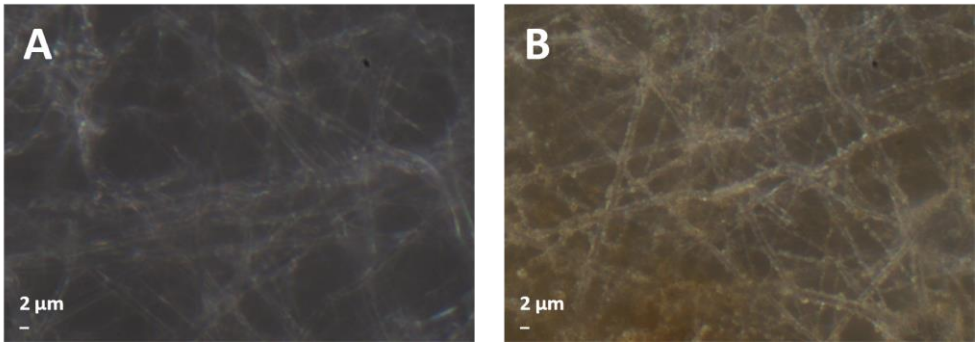

Figure 3. Optical microscope images: (A) PCL coated for 10 minutes with AL-OA, (B) PCL coated for 120 minutes with AL-OA (roughness analysis in supplementary information)

Table 3. Comparison of the thickness of electrospun layers (net of paper filter)

Deposition time of lignin (min)	Thickness ± SD (µm)	
	Eucalypt	Oak
AL-2.5 (+PCL)	52.95 ± 2.90	58.08 ± 11.70
AL-5 (+PCL)	61.23 ± 5.07	61.85 ± 8.87
AL-10 (+PCL)	49.70 ± 7.04	65.28 ± 2.05
AL-60 (+PCL)	42.75 ± 9.59	38.55 ± 9.23
AL-120 (+PCL)	43.77 ± 8.46	49 ± 5.02

However, everything else being equal, for a 10-min deposition time (AL-10), the thickness of the PCL membrane with eucalyptus lignin (49.75 µm) is lower compared to oak lignin (65.28 µm). This difference can be attributed to the intrinsic nature of the extracted lignins, with eucalyptus lignin being richer in lipophilic extractives. Before the acidolysis chemical treatment for lignin recovery, the woody biomasses were in fact pretreated with an acetone/water mixture to remove wood extractives, as reported by Bergamasco et al. [41]. While this chemical treatment enabled the removal of all wood extractives from both species, it is not selective with respect to lipophilic com-ponents. It is known that for the recovery of these hydrophobic components, the use of solvents such as dichloromethane [45] or n-hexane [46] is preferable. Then, we can assume that hydrophobic components are still present in a minimal percentage and that AL-EU contains more of them because lipophilic extractives were detected in the FTIR analysis previously reported [41]. These lipophilic components, as supported by the SEM image at the 60-min lignin deposition time (Figure 4B), seem to contribute to the formation of clusters of AL-EU nanoparticles, unlike the PCL-coated AL-OA sample (Figure 4A), where the nanoparticles are well separated. These oily clusters could interact with the PCL membrane, which demonstrated a hydrophobic nature following the analysis of the contact angle reported later herein, somehow permeating and intercalating between the PCL fibers and thus reducing the overall thickness of the obtained membrane.

As deposition time increases, this asymmetry between OA and EU disappears, and both AL-120 samples display a mild decrease in thickness as a direct consequence of the extended AL coating time.

In Table 4, the estimated values of the AL coating thickness achieved for different amounts of lignin deposited per cm2 of membrane are presented. To back-calculate the areal density (in grams of lignin per cm^2), we considered the concentration of the initial solution, the volume of solution required for the coating, and the nominal mem-brane surface area (19 × 24 cm^2). Since the volume of lignin deposited from electro-spinning is known and the reported lignin density is about 1.4 g/cm^3 [47], the thickness values in Table 4 are obtained. While these are approximate numbers, the AL-coating for shorted deposition times (2.5 and 5 min) is indeed nanocoating with a thickness around or below 50 nm and an area density of 30–60 g/m^2.

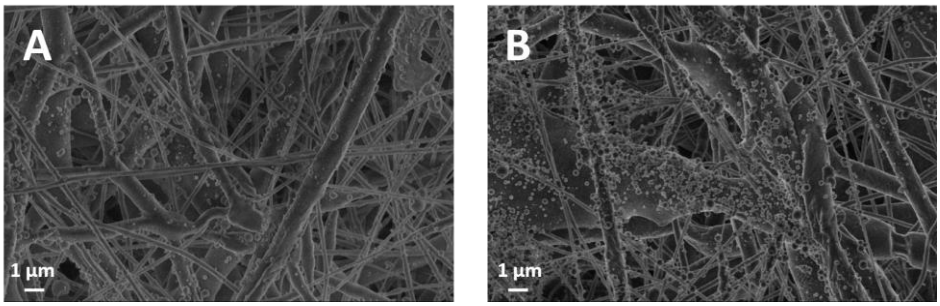

Figure 4. SEM micrographs of AL-OA-60 (A) and AL-EU-60 (B) indicating that lignin nanoparticles tend to coalescence more markedly in the case of eucalyptus lignin than for oak lignin.

Table 4. Surface density (per g/cm2) and thickness of the lignin coating deposited onto the PCL membranes.

ID sample	Time deposition of lignin (min)	Quantity of lignin / area PCL membrane (mg/cm^2)	Thickness of lignin (nm)
AL- 2.5	2.5	0.003	24.47
AL- 5	5	0.006	48.95
AL- 10	10	0.014	97.90
AL- 60	60	0.082	587.41
AL- 120	120	0.165	1174.81

From a structural viewpoint, the mechanical integrity of the entire filter relies entirely on the filter paper. In fact, neglecting the thin lignin layer, the filter paper is thicker and has higher performance (E = 18.8 MPa and UTS = 26.4 MPa) than PCL (E = 0.15 MPa and UTS = 1.9 MPa), such that the contribution of PCL to the load-bearing capability of the whole filter system under uniaxial tensile stress is estimated to be less than 1%, as computed from the ratio $\boldsymbol{E_{PCL} \cdot Th_{PCL}/(E_{PCL} \cdot Th_{PCL} + E_{PAPER} \cdot Th_{PAPER})}$.

Figure 5 illustrates the trend of the average roughness (Ra) as a function of the increasing coating time of lignin. A decrease in the average roughness (Ra) is generally observed with an increase in the

coating time. In particular, it is observed that for coating times up to 5 min, the average value of Ra tends to remain almost constant, close to 1.2 µm for both lignin grades used. After 10 min of coating, in the case of EU, the roughness decreases to 1.16 µm, while in the case of OA, a slight increase to 1.27 µm is measured. For long lignin coating times, the roughness value decreases and converges to 0.95 µm for both EU and OA after 60 min. After 120 min, in the case of EU, the roughness decreases slightly to 0.92 µm, while in the case of OA, the decrease in roughness is greater, dropping to 0.687 µm.

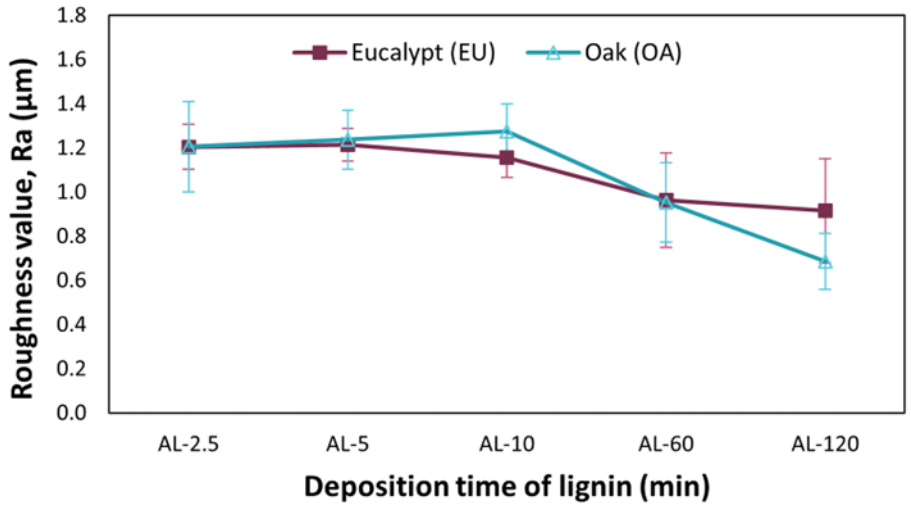

Figure 5. Trends in roughness Ra (Arithmetic Average Roughness) as a function of coating time with different lignins.

Porosity and air permeability analysis

The analysis of the overall porosity of the coated membranes was conducted using the volume displacement method and the average values obtained from three measurements for each membrane are presented in Table 5. As seen in the Figure 6, the porosity of the PCL coated membrane without lignin nanocoating was found to be 72.22%, a value consistent with what is reported in the literature, where such mem-branes typically exhibit porosity ranging between 60% and 90% [48]. The membranes containing lignin on the surface did not show significant deviations in porosity, which is to be expected because the lignin coating is much smaller than the PCL layer, as per reported in Table 5.

Table 5. Porosity (%) result for each sample

ID Sample	Porosity ± SD (%)
PCL	72.22 ± 6.98
AL-EU-2.5	67.96 ± 9.40
AL-EU-5	62.55 ± 2.89
AL-EU-10	68.88 ± 3.59

AL-EU-60	74.40 ± 4.78
AL-EU-120	67.09 ± 2.00
AL-OA-2.5	64.42 ± 4.96
AL-OA-5	68.13 ± 6.23
AL-OA-10	72.77 ± 5.90
AL-OA-60	77.27 ± 1.26
AL-OA-120	69.94 ± 6.56

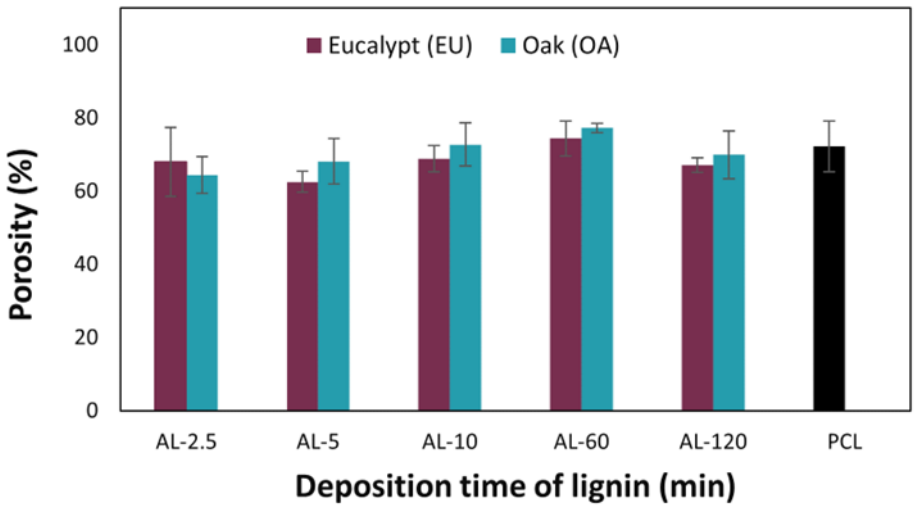

Figure 6. Trends in porosity of the layered membrane for each lignin grade and for different deposition times.

While the influence of the spray-coating step on porosity is negligible for all five deposition times under consideration, data indicates that for increasing deposition times (ref. AL-120 minutes in Figure 2 and AL-60 in Figure 4) the lignin nanoparticles tend to overlap and accumulate, filling in some of the pores underneath, in PCL layer. The relationship between the decrease in porosity and the formation of a conformal surface coating, confirmed by SEM for both AL-EU and AL-OA at 120 min, provides a rationale for the decrease in porosity for longer deposition time of lignin vs. the reference PCL membrane. This is in agreement with literature and, for example, Ahmadpour et al. [49] reported a surface modification of a membrane composed of polyether imide (PEI) by a fine spray of material, leading to a reduction in porosity of a filtration membrane.

In addition to porosity, permeability tests offer technological data that is relevant to the understanding of the linkage between microstructure and performance. The study conducted using the Gurley densometer revealed a significant reduction in air permeability of the membranes following the coating with lignin spray compared to sole PCL (Table 6 and Figure 7). For short coating times, the membranes exhibited permeability values significantly lower than average, especially when eucalyptus lignin was used, with permeability values of 0.57 at AL-2.5 and 0.49 cm/s at AL-5. This phenomenon could not be attributed to the intrinsic structure of the PCL membranes themselves

before the coating with eucalyptus lignin. These membranes appear to already possess a structure that offered greater resistance to permeation compared to the control. However, sweeping for increasing deposition time, from AL-10 to AL-120, the permeation data show remarkable similarity between the two lignins under study. Interestingly, in the case of AL-10 and AL-60 times, these membranes exhibit similar behavior in terms of permeability despite the significant difference in coating times. The SEM (Figures 2,4) indicated that in general the sprayed lignin particles tend to accumulate mainly on the surface of the PCL fibers, leaving the pores that make up the mesh structure of the membranes apparently unobstructed. However, as already mentioned, this is no longer the case for AL-120 membranes, where the situation is significantly different, and SEM shows lignin particles completely covering the membrane surface and masking the fibrous PCL microstructure underneath. The formation of such a homogeneous and dense coating at the microscopic level is reflected by the permeability values for eucalyptus (0.55 cm/s, AL-EU-120) and oak (0.58 cm/s, AL-OA-120) lignin coatings, which are significantly lower than reference membrane (0.91 cm/s).

Table 6. Air permeability test results by Gurley densometer

ID Sample	Permeability ± SD (cm/s)
Filter paper	1.20±0.17
PCL	0.91±0.08
AL-EU-2.5	0.57±0.06
AL-EU-5	0.49±0.03
AL-EU-10	0.68±0.05
AL-EU-60	0.68±0.05
AL-EU-120	0.55±0.01
AL-OA-2.5	0.71±0.05
AL-OA-5	0.64±0.07
AL-OA-10	0.64±0.03
AL-OA-60	0.67±0.02
AL-OA-120	0.58±0.02

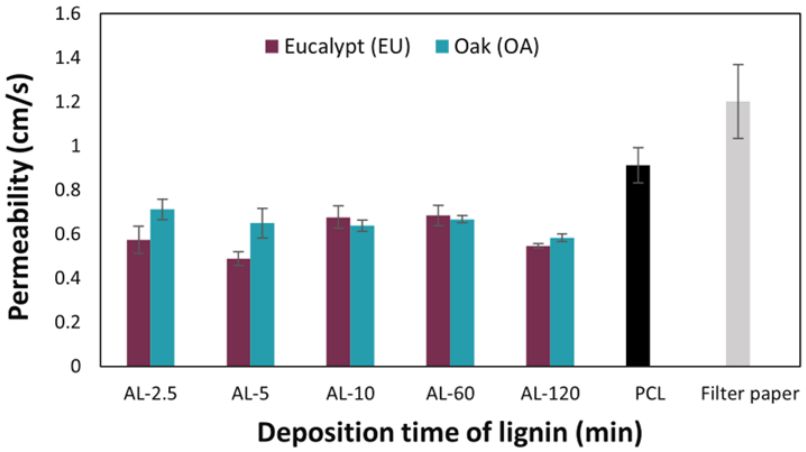

Figure 7. Comparison of permeability results (cm/s).

Contact angle

To assess the hydrophilic/ hydrophobic nature of PCL membranes uncoated and coated with lignin at different deposition times wettability tests were performed both for polar (i.e. water) and apolar (i.e. a 1PWD oil—1 Primary Wound Dressing© oil). The results in Table 7 demonstrate that the lignin coating leads to significant modification of the typically hydrophobic character of PCL membrane [25]. Water wettability tests on both AL-EU (Figure 8A) and AL-OA (Figure 8B) coatings decrease the water contact angle (WCA) compared to bare PCL membranes for electrospraying deposition times of 2.5, 5, and 10 min. For deposition times of 60 and 120 min, the effect is even more drastic and could not be measured with our method (i.e., 0° values in Table 7) because the water droplet completely disappeared, being quickly absorbed into the membrane within the set time (10 s) of the test and revealing a transition to full hydrophilicity of the surface. This behaviour can be attributed to the abundance of polar hydroxyl and carboxylic groups present in the structure of the lignin nanoparticles [50–52]. This result is of particular technological interest as it is possible to modulate the hydrophilicity of PCL membranes by a small lignin amount, i.e., short deposition times. In turn, the possibility of delivering a substantial increase in hydrophilicity for rather short coating times is crucial for the deployment of a new "green" coating technology in high-throughput manufacturing, such as in the filtration industry and textile applications.

Table 7. Comparison of the result measurements of water contact angle (WCA) and oil contact angle (OCA)

ID Sample	WCA(SD) (°)	OCA(SD) (°)
PCL	131.93 ± 3.34	19.15 ± 2.68
AL-EU-2.5	94.96 ± 22.95	25.09 ± 1.05
AL-EU-5	116.07 ± 12.76	22.27 ± 2.52
AL-EU-10	116.70 ± 8.13	17.81 ± 1.66
AL-EU-60	*	16.67 ± 3.18

AL-EU-120	*	18.11 ± 2.48
AL-OA-2.5	117.13 ± 7.22	21.28 ± 3.24
AL-OA-5	117.03 ± 3.87	17.89 ± 6.99
AL-OA-10	115 ± 6.45	14.56 ± 2.69
AL-OA-60	*	*
AL-OA-120	*	*

*: Measurement cannot be carried out due to complete sample absorption.

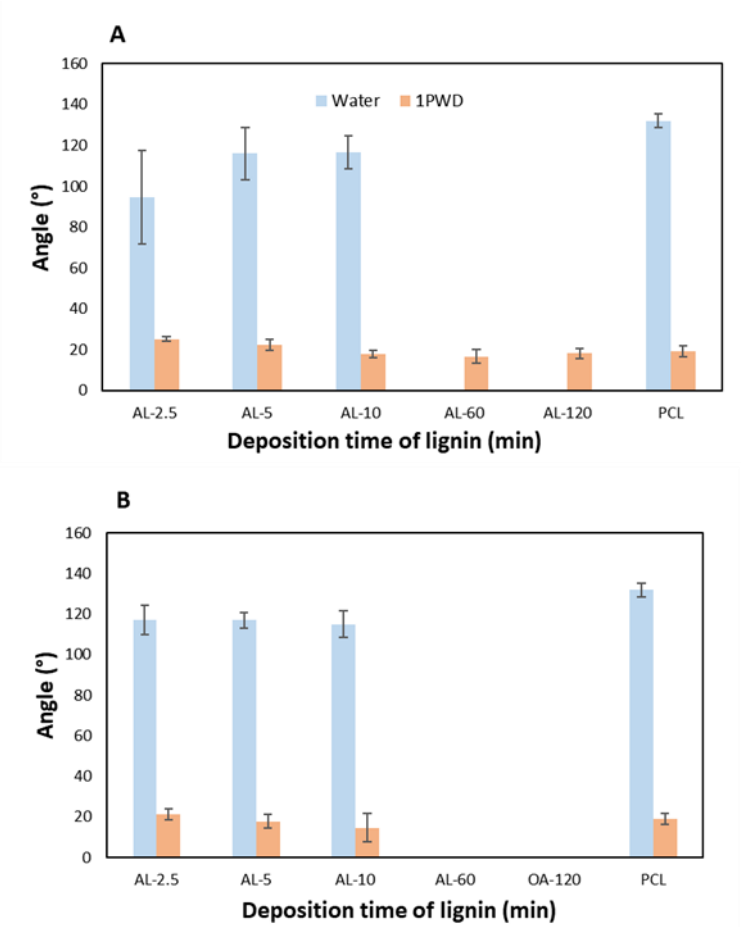

Figure 8. Contact angle histograms of AL-EU (A) and AL-OA (B) measured using water and 1PWD (1 Primary Wound Dressing©).

The scenario from oil wettability tests is quite different, since the PCL layer is very affine to oil and exhibits contact angle values much lower than water (19° vs. 131°). By dispensing droplets of 1PWD (1 Primary Wound Dressing©), a liquid oil markedly hydrophobic, the oil contact angle measurements (OCA) did not significantly differentiate from the PCL control, with a few notable exceptions. In the case of AL-EU-2.5 and AL-OA-2.5 coatings, an increase in OCA was observed. More importantly, for oak lignin, in the cases of AL-OA-60 and AL-OA-120, it was not possible to measure the con-tact angle due to the complete absorption of the 1PWD droplet within the set time. Conversely, the corresponding measurements for eucalyptus at 60 and 120 min appeared to be in trend without dropping to 0°. The reason for such a difference is un-clear, although a possible

explanation can be found in the different chemical structure of lignin. As highlighted by Py-GCMS analyses conducted on these polymers and re-ported in a previous study [41], those results revealed that in the case of AL-OA, the ratio of syringyl to guaiacyl units in lignin (S/G) is 2.73, which is higher compared to the value of 2.11 obtained from AL-EU. This indicates that in oak lignin, there is a greater quantity of syringyl units and, consequently, a higher presence of methoxy groups. Such a condition could promote an increase in the hydrophobicity of lignin, thereby resulting in a greater affinity with the oily medium used in the OCA analysis.

ATR-FTIR results

Spectral profiles were obtained by ATR-FTIR analysis for both lignin grades de-posited on PCL. Only the data for AL-EU are plotted in Figure 9, whereas the dataset for AL-OA is omitted because it is practically indistinguishable from the AL-EU. The FTIR spectra of PCL membranes coated with lignin were compared to the spectra of the uncoated PCL membrane. In Figure 9, the distinct stretching and bending signals of PCL are identifiable in all spectra, i.e., within Band 1 (at 1726 cm^{-1}) there is a stretching vibration of the –C=O group. Additionally, asymmetric and symmetric stretching vibrations of C–O–C can be observed at 1242 cm^{-1} (band 4) and 1186 cm^{-1} (band 5), stretching vibrations of C–O and C–C groups in the crystalline and amorphous phases at 1295 cm^{-1} (band 3) and 1167 cm^{-1} (band 6), and deformation vibrations of the $–CH_2$ groups at 1370 cm^{-1} (band 2) [53]. Instead, no significant signal related to lignin could be observed, with no change in either intensity or area of the absorption peaks at any lignin deposition between 2.5 and 10 min, thus suggesting that the coating is too thin for this analysis.

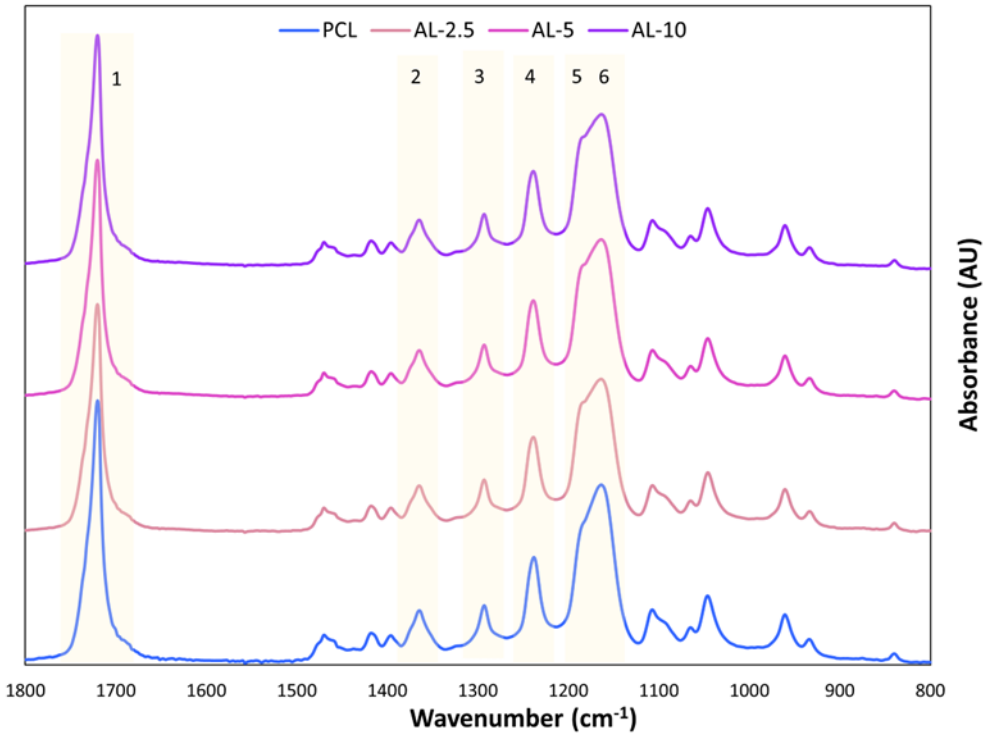

Figure 9. ATR-FTIR spectra comparison of the membrane PCL, AL-2.5, AL-5, and AL-10. PCL-specific peaks assignment: stretching vibration of the –C=O group (band 1), deformation vibrations of the –CH2 groups (band 2), stretching vibrations of C–O and C–C groups in the crystalline phase (band 3), asymmetric stretching vibrations of C–O–C (band 4), symmetric stretching vibrations of C–O–C (band 5), and stretching vibrations of C–O and C–C groups in the amorphous phase (band 6).

On the other hand, FTIR analysis of membranes coated with EU-60 and EU-120 in Figure 10 highlighted a clear effect of the lignin. The spectra indeed showed a decrease in the absorption intensity of characteristic PCL peaks, accompanied by the appear-ance of lignin-specific bands such as L1, L2, and L3. These bands are indicative of aro-matic skeletal vibrations: C=O stretching, C=C aromatic ring vibration (S > G), and C=C aromatic ring vibration (G > S). In the case of bands from L4 to L7, a decrease in signal intensity is observed with increasing coating deposition time. This suggests that the extended deposition time of lignin coating may weaken the characteristic PCL signals in this region, favoring instead the specific vibrations of lig-nin. These deformation bands represent aliphatic C−H stretching vibrations in CH_3 (L4), guaiacyl ring breathing (L5), C− C, C−O, and C=O stretching in condensed G units (L6), CH elongation in the G ring (L7), and the typical S ring CO stretching (L8) [41].

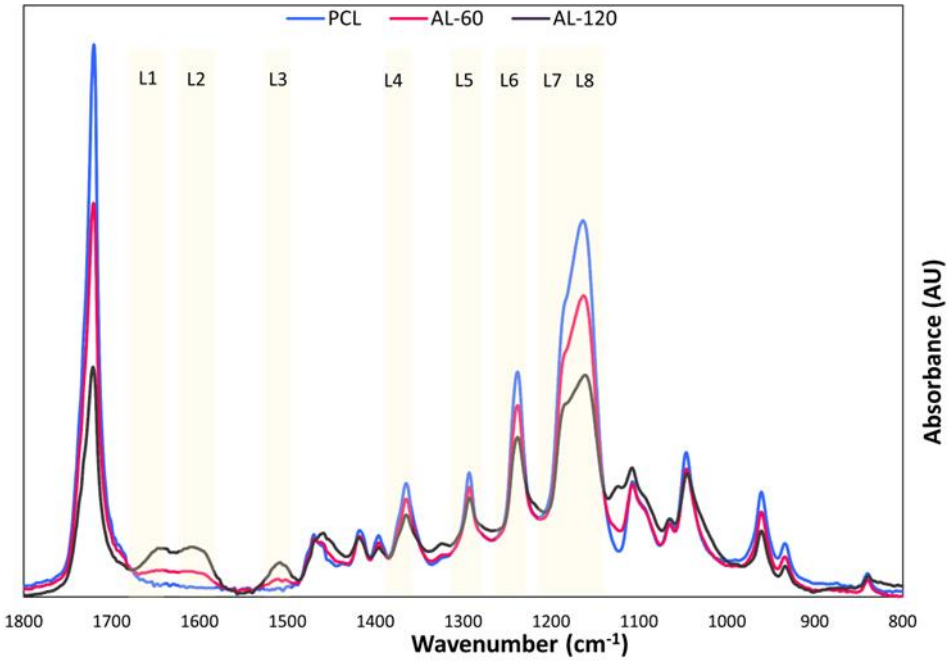

Figure 10. ATR-FTIR spectra comparison of the membrane PCL, AL-60, and AL-120. Lignin-specific peaks assignment: aromatic skeletal vibrations C=O stretching (band L1), C=C aromatic ring vibration (S>G) (band L2), C=C aromatic ring vibration (G>S) (band L3), aliphatic C-H stretching vibrations in CH3 (band L4), guaiacyl ring breathing (band L5), C−C, C−O, and C=O stretching in condensed G units (band L6), CH elongation in the G ring (band L7), and the typical S ring CO stretching (band L8).

Antimicrobial activity

While the main focus of this work is on manufacturing aspects, a biological assessment was designed and performed to assess the antibacterial activity due to the lignin coating, limiting the scope to a representative Gram-positive bacterial strain, i.e., *S. aureus*, and a representative Gram-negative bacterial strain, i.e., E. coli. The antibacterial investigation was conducted against Gram-positive and Gram-negative bacteria, although lignins were found to be more effective against Gram-positive bacteria than against Gram-negative bacteria such as *Klebsiella* sp. [54].

Our biological study is divided into two parts. At first, we compared three experimental conditions, for three time points (i.e., 0, 1.5, and 3 h), namely: bare PCL, AL-OA-10, and AL-EU-10. The results are shown in Figure 11. Such a biological assay was conducted to gain preliminary insight about the antibacterial performance; this was evaluated against the selected bacterial strain as representative for Gram-positive. As expected, the *S. aureus* culture in the absence of any material (positive control) kept growing steadily up to 3 h, rising from the initial concentration of 5×10^6 CFU/mL up to 3.2×10^7 CFU/mL. Instead, the blank PCL sample induced a weak reduction in bacterial growth. Between the two lignin-coated membranes, only AL-EU-10 showed a sizable antibacterial response, with a concentration of 1.3×10^7 CFU/mL at T2 (Figure 11 – Table 8) and a moderate, yet sustained,

antimicrobial action throughout the time interval T1-T2 of 1.5 h. This represents a promising and encouraging result, recalling that the AL-EU-10 sample has a lignin density of just 0.014 mg/cm^2 (ref. Table 4).

Table 8. Biological experiment 1—Data are reported as mean values in the table and as mean value ± SEM from two independent experiments, each in triplicate, in the graph.

Time (h)	*S. aureus* CFU/mL (Means)			
	S. aureus	PCL	AL-EU-10	AL-OA-10
T0	5×10^6	4.6×10^6	4.6×10^6	4.6×10^6
T1	9.3×10^6	9.1×10^6	5.4×10^6	1.2×10^7
T2	3.2×10^7	1.7×10^7	1.3×10^7	2.5×10^7

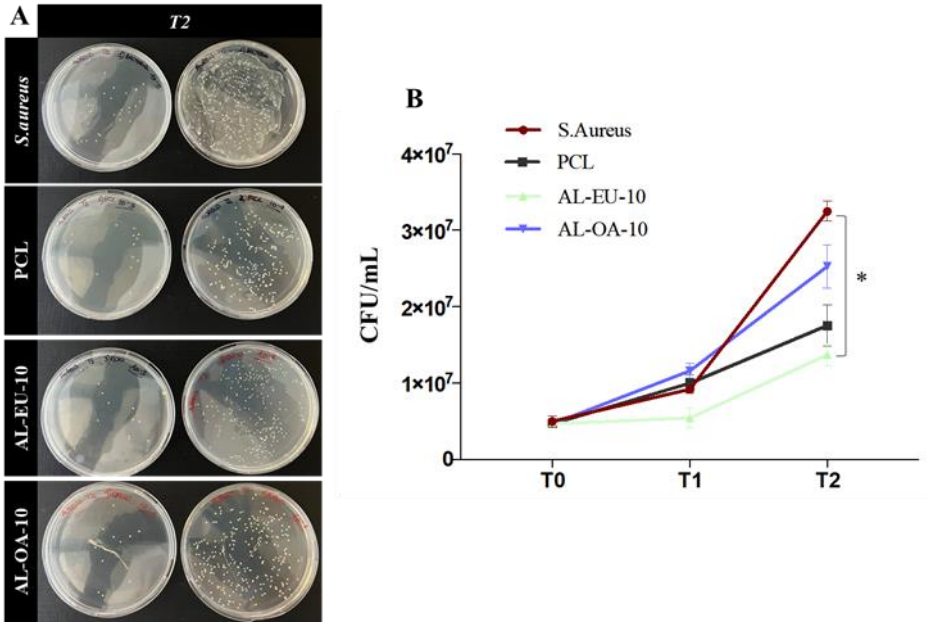

Figure 11. Biological experiment 1—Petri dishes obtained from S. aureus culture without any mat (control) and cultures with blank PCL and PCL-Lignin mats at two different serial dilutions (10^{-5} and 10^{-4}) and last sampled time (3 h); (B) Bacterial population (CFU/mL) measured for control, PCL, and coated samples at different time points: 0 (T0), 1.5 (T1), and 3 (T2) hours (* $p < 0.05$).

After determining the precise species of the lignin to be utilized, to expand on this baseline, a second biological experiment against *S. aureus* and *E. coli* was designed to screen out the behavior of AL-EU for longer deposition times, for 10, 60, and 120 min, while monitoring the bacterial growth for 1.5 (T1), 3(T2), and 4.5 (T3) hours. In the experiment against Gram-positive, after 4.5 h, both AL-EU-10 and AL-EU-60 samples showed antimicrobial action by reducing *S. aureus* cellular density by ¼ Log (about 2.1 and 2.7 times, respectively) compared to the bare PCL (ref. Figure 12 and Table 9). The effect on bacterial growth of AL-EU-120 (at 0.165 mg/cm^2 lignin density) was markedly greater, leading to a steeper decrease in bacterial counts of almost ½ Log, i.e., about 4.8 times compared to bare PCL. The dose-dependent impact of lignin deposition *on S. aureus* is significant.

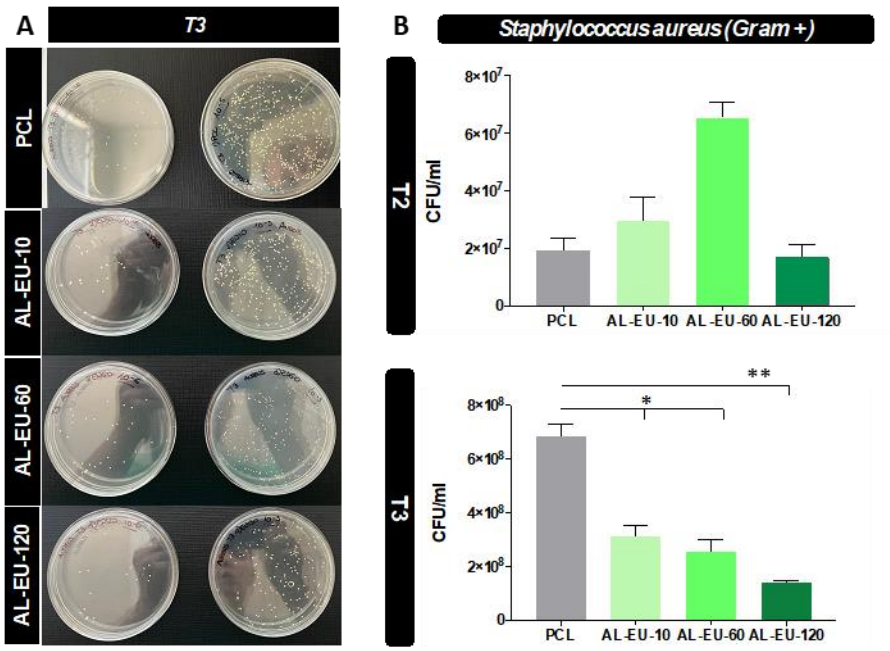

Figure 12. (A) Petri dishes obtained from *S. aureus* cultures with blank PCL and PCL-Lignin mats at two different serial dilutions (10^{-5} and 10^{-6}) and last sampled time (4.5 h); (B) *S. aureus* bacterial population (CFU/mL) measured for PCL and coated samples at different time points: 3 (T2) and 4.5 (T3) hours (* $p < 0.05$ or ** $p < 0.01$).

In the experiment against Gram-negative, both AL-EU-60 and AL-EU-120 samples exhibited antimicrobial activity after 3 h. However, only AL-EU-60 demonstrated a significant reduction in *E. coli* cellular density, achieving a decrease of 1/6 Log (approximately less than 2 times) compared to the untreated PCL, as indicated in Figure 13 and Table 10. The impact on bacterial growth became only slightly apparent after 4.5 h, with all samples exhibiting a modest, but not significant, reduction in bacterial counts compared to bare PCL. The deposition of lignin against *E. coli* is gradual and extremely subtle.

Despite AL-EU demonstrating its potential as an antibacterial agent against selected strains, it has been observed that its inhibitory effect on microbial growth is more pronounced against *S. aureus* compared to *E. coli*. This result aligns with a study conducted by Gregorova et al. [55], which highlights the antibacterial activity of lignin against both *S. aureus* and *E. coli* through agar diffusion tests. In their case as well, the inhibitory effect is observable on both selected strains, but *E. coli* shows greater resistance to the antibacterial action of lignin. This suggests that this effect may be attributed to the complex structure of the cell walls found in Gram-negative bacteria. Specifically, this resistance could be linked to the presence of the peptidoglycan layer on the outer membrane, which in *E. coli* is approximately 6–10 times thicker than in *S. aureus*, facilitating the entry of lignin into the bacterial cell [56]. This limited antibacterial effect against Gram-negatives was observed in another previous study where wood samples coated with a lignin-based formulation were subjected

to bacterial attack by *Pseudomonas aeruginosa*. In this case, bacterial colonies were numerous and well-developed, indicating that the coating did not demonstrate any antimicrobial effect [57].

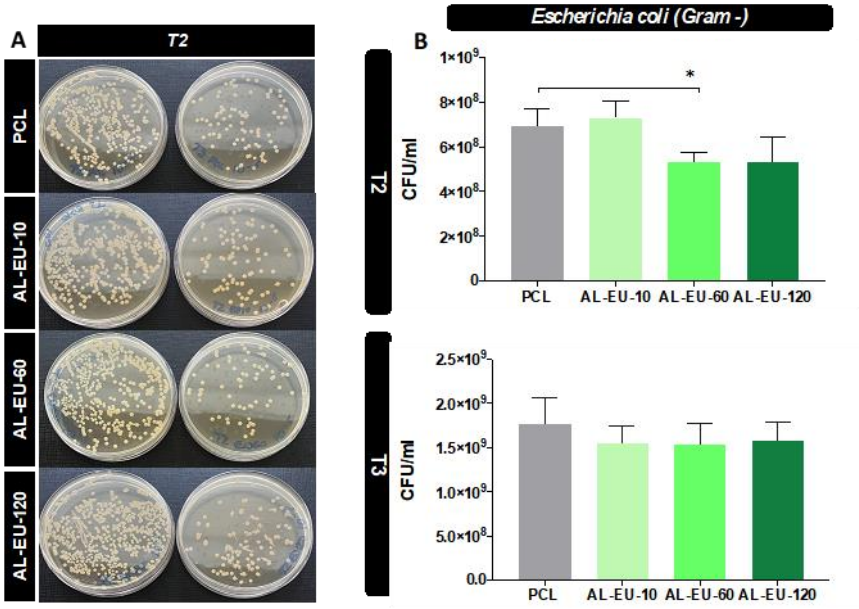

Figure 13. (A) Petri dishes obtained from *E. coli* cultures with blank PCL and PCL-Lignin mats at two different serial dilutions (10^{-5} and 10^{-6}) and the second last sampled time (3 h); (B) *E. coli* bacterial population (CFU/mL) measured for PCL and coated samples at different time points: 3 (T2) and 4.5 (T3) hours (* $p < 0.05$).

Table 9. Biological experiment 2 with *S. aureus*. Data are reported as mean values in the table and as mean value ± SEM from two independent experiments, each in triplicate, in the graph.

Time (h)	*S. aureus* CFU/mL (Means)			
	PCL	AL-EU-10	AL-EU-60	AL-EU-120
T0	1.1×10^6	1.1×10^6	1.1×10^6	1.1×10^6
T1: 1.5	5.5×10^6	2.2×10^6	4.6×10^6	8.2×10^6
T2: 3	1.9×10^7	2.9×10^7	6.5×10^7	1.7×10^7
T3: 4.5	6.8×10^8	3.1×10^8	2.5×10^8	1.4×10^8

Table 10. Biological experiment 2 with *E. coli*. Data are reported as mean values in table and as mean value ± SEM from two independent experiments, each in triplicate, in the graph.

Time (h)	*E. coli* CFU/mL (Means)			
	PCL	AL-EU-10	AL-EU-60	AL-EU-120
T0	5.2×10^6	5.2×10^6	5.2×10^6	5.2×10^6
T1: 1.5	4.2×10^7	3.2×10^7	2.9×10^7	3.0×10^7
T2: 3	6.9×10^8	7.2×10^8	5.3×10^8	5.3×10^8
T3: 4.5	1.7×10^9	1.5×10^9	1.5×10^9	1.5×10^9

In conclusion, the results from these two experiments suggest that, in principle, significant antibacterial activity can be achieved for relatively low lignin densities (here, in the order of ~0.1 mg/cm^2) and can be increased by increasing the lignin density. In the literature, the antibacterial

effects of lignin prepared by different fractionation methods were already investigated, with reports of an antibacterial effect of the lignin obtained by the acidolysis method higher than what we obtained. While more work is needed to perform a direct comparison to make and test such diverse lignin in the context of coating and under the same conditions, we observe that acidolysis leads to a lignin grade with greater exposure of active functional groups, such as phenolic hydroxyl and carboxyl groups [58], compared to the lignin examined in this work.

While the results indicate that lignin could indeed be further developed for anti-fouling applications and in filtration media, some performance gaps remain. Clearly, the antibacterial performance is considerably lower than other traditional mainstream options, such as, for example, the Ag nanocoating by magnetron sputtering, reported in recent literature by many and also by our group in the context of innovative nano-coatings [15,59]. However, key advantages of the proposed lignin-based antifouling coating strategy vs. Ag nanocoatings would include the following: (i) virtually no limitations in terms of scalability; (ii) semi-continuous manufacturing at ambient pressure in roll-to-roll mode; (iii) replacement of a metal-oxide coating by a biopolymer coating, which is more environmentally friendly and a definite advantage in the pervasive framework of circular economy. Hence, despite the lower performance achieved currently, the possibility of fabricating, on the same single electrospinning platform, an entire layered filter endowed with an antifouling coating from lignin represents an appealing and timely option with great potential impact.

Future work could expand on this investigation along many fronts and, for example, should include a more in-depth antibacterial evaluation to further characterize and optimize this new lignin coating for antifouling applications. Specifically, aside from studying the bacteria *E. coli*, which falls within the research scope, similar to the previously mentioned Ag nanocoating [15,25], one can explore the impact on other representatives within this bacterial group as well as against the Gram-positive group, as has already been carried out for *S. aureus*.

Conclusion

We investigated and proved the feasibility of a two-step electrospinning fabrication of a biocompatible and biodegradable polymer-on-paper layered system made of electrospun PCL fibers subsequently coated with electrosprayed lignin, all in one production line. The manufacturing of pure lignin coatings by solution electrospraying appears to be novel. In our investigation, lignin was responsible for two main functional properties: (i) the increase in wettability of the substrate towards both polar and apolar liquids, displaying a characteristic amphiphilic effect; (ii) the newly acquired antibacterial properties over the bare PCL membrane. The results achieved with either AL-OA or AL-

EU grade, for relatively small lignin densities of order 0.1 mg/cm^2, indicate that those properties can be tuned with relative ease by the amount of deposited lignin, which makes for an interesting alternative to other surface processing options entailing chemical transformations or physical transformations (e.g., plasma treatments). Also, our data highlight that lignin coatings did not change the overall porosity (a bulk property) of the membrane but reduced surface roughness and moderately reduced air permeability as lignin density increased, which is crucial for filtration applications.

Although the current antibacterial effectiveness of these coated surfaces is significantly inferior to well-established alternatives, such as Ag coatings, there is unquestionably potential for enhancement in these initial endeavours. For instance, when considering the efficacy against Gram-positive and Gram-negative bacteria, i.e., *S. aureus* and *E. coli*, there is certainly room for improvement compared to established options like said Ag coatings. More importantly, the deployment of electrosprayed lignin coating is worth exploring and developing further due to its scalability and potential to be deployed industrially in high-throughput manufacturing of sustainable layered mem-branes with antibacterial and antifouling properties, not just in the field of filtration. Finally, by highlighting the difference between two acidolysis lignin grades, i.e., *Quercus cerris* L. (AL-OA) and *Eucalyptus camaldulensis* Dehnh (AL-EU) lignins, our study points out that better lignin grades can be in principle carefully selected and engineered upstream to optimize the subsequent electrospraying process. Thus, the capability to make pure lignin coatings by electrospraying opens up and supports the possibility of using and reusing this natural polymer, overabundant and available from wood byproducts, for filtration and for circular economy applications in general.

References

1. Pendergast, M.M.; Hoek, E.M. A review of water treatment membrane nanotechnologies. Energy Environ. Sci. 2011, 4, 1946–1971. https://doi.org/10.1039/C0EE00541J

2. Lu, P.; Xia, Y. Maneuvering the internal porosity and surface morphology of electrospun polystyrene yarns by controlling the solvent and relative humidity. Langmuir 2013, 29, 7070–7078. https://doi.org/10.1021/la400747y

3. Abd Halim, N.S.; Wirzal, M.D.H.; Bilad, M.R.; Md Nordin, N.A.H.; Adi Putra, Z.; Sambudi, N.S.; Mohd Yusoff, A.R. Improving performance of electrospun nylon 6, 6 nanofiber membrane for produced water filtration via solvent vapor treatment. Polymers 2019, 11, 2117. https://doi.org/10.3390/polym11122117

4. Muller, A.-K.; Xu, Z.-K.; Greiner, A. Preparation and performance assessment of low-pressure affinity membranes based on functionalized, electrospun polyacrylates for gold nanoparticle filtration. ACS Appl. Mater. Interfaces 2021, 13, 15659–15667. https://doi.org/10.1021/acsami.1c01217

5. Cui, J.; Lu, T.; Li, F.; Wang, Y.; Lei, J.; Ma, W.; Zou, Y.; Huang, C. Flexible and transparent composite nanofibre membrane that was fabricated via a “green” electrospinning method for efficient particulate matter 2.5 capture. J. Colloid Interface Sci. 2021, 582, 506–514. https://doi.org/10.1016/j.jcis.2020.08.075

6. Khulbe, K.; Matsuura, T. Removal of heavy metals and pollutants by membrane adsorption techniques. Appl. Water Sci. 2018, 8, 1–30. https://doi.org/10.1007/s13201-018-0661-6

7. Yin, H.; Zhao, J.; Li, Y.; Huang, L.; Zhang, H.; Chen, L. A novel Pd decorated polydopamine-SiO2/PVA electrospun nanofiber membrane for highly efficient degradation of organic dyes and removal of organic chemicals and oils. J. Clean. Prod. 2020, 275, 122937. https://doi.org/10.1016/j.jclepro.2020.122937

8. Fahimirad, S.; Fahimirad, Z.; Sillanpää, M. Efficient removal of water bacteria and viruses using electrospun nanofibers. Sci. Total Environ. 2021, 751, 141673. https://doi.org/10.1016/j.scitotenv.2020.141673

9. Jaworek, A.; Sobczyk, A.; Krupa, A. Electrospray application to powder production and surface coating. J. Aerosol Sci. 2018, 125, 57–92. https://doi.org/10.1016/j.jaerosci.2018.04.006

10. Vatanpour, V.; Pasaoglu, M.E.; Kose-Mutlu, B.; Koyuncu, I. Polyacrylonitrile in the Preparation of Separation Membranes: A Review. Ind. Eng. Chem. Res. 2023, 62, 6537–6558. https://doi.org/10.1021/acs.iecr.3c00057

11. Parekh, S.A.; David, R.N.; Bannuru, K.K.; Krishnaswamy, L.; Baji, A. Electrospun silver coated polyacrylonitrile membranes for water filtration applications. Membranes 2018, 8, 59. https://doi.org/10.3390/membranes8030059

12. Essalhi, M.; Khayet, M. Self-sustained webs of polyvinylidene fluoride electrospun nanofibers at different electrospinning times: 1. Desalination by direct contact membrane distillation. J. Membr. Sci. 2013, 433, 167–179. https://doi.org/10.1016/j.memsci.2013.01.023

13. Abdelrasoul, A.; Doan, H.; Lohi, A.; Cheng, C.H. Morphology control of polysulfone membranes in filtration processes: A critical review. ChemBioEng Rev. 2015, 2, 22–43. https://doi.org/10.1002/cben.201400030

14. Raciny, I.; Zodrow, K.; Li, D.; Li, Q.; Alvarez, P. Addition of a magnetite layer onto a polysulfone water treatment membrane to enhance virus removal. Water Sci. Technol. 2011, 63, 2346–2352. https://doi.org/10.2166/wst.2011.551

15. Fiaschini, N.; Giuliani, C.; Vitali, R.; Tammaro, L.; Valerini, D.; Rinaldi, A. Design and Manufacturing of Antibacterial Elec-trospun Polysulfone Membranes Functionalized by Ag Nanocoating via Magnetron Sputtering. Nanomaterials 2022, 12, 3962. https://doi.org/10.3390/nano12223962

16. Kayan, G.Ö.; Kayan, A. Polycaprolactone Composites/Blends and Their Applications Especially in Water Treatment. Che-mEngineering 2023, 7, 104. https://doi.org/10.3390/chemengineering7060104

17. Mohamed, R.M.; Yusoh, K. A review on the recent research of polycaprolactone (PCL). Adv. Mater. Res. 2016, 1134, 249–255. https://doi.org/10.4028/www.scientific.net/AMR.1134.249

18. Bliley, J.M.; Marra, K.G. Polymeric biomaterials as tissue scaffolds. In Stem Cell Biology and Tissue Engineering in Dental Sciences; Elsevier: Amsterdam, The Netherlands, 2015; pp. 149–161. https://doi.org/10.1016/B978-0-12-397157-9.00013-8

19. Bartnikowski, M.; Dargaville, T.R.; Ivanovski, S.; Hutmacher, D.W. Degradation mechanisms of polycaprolactone in the context of chemistry, geometry and environment. Prog. Polym. Sci. 2019, 96, 1–20. https://doi.org/10.1016/j.progpolymsci.2019.05.004

20. Ghosh, S.K.; Pal, S.; Ray, S. Study of microbes having potentiality for biodegradation of plastics. Environ. Sci. Pollut. Res. 2013, 20, 4339–4355. https://doi.org/10.1007/s11356-013-1706-x

21. Azari, A.; Golchin, A.; Maymand, M.M.; Mansouri, F.; Ardeshirylajimi, A. Electrospun polycaprolactone nanofibers: Current research and applications in biomedical application. Adv. Pharm. Bull. 2022, 12, 658. https://doi.org/10.34172/apb.2022.070

22. Palacios Hinestroza, H.; Urena-Saborio, H.; Zurita, F.; Guerrero de Leon, A.A.; Sundaram, G.; Sulbarán-Rangel, B. Nanocel-lulose and polycaprolactone nanospun composite membranes and their potential for the removal of pollutants from water. Molecules 2020, 25, 683. https://doi.org/10.3390/molecules25030683

23. Cooper, A.; Floreani, R.; Ma, H.; Bryers, J.D.; Zhang, M. Chitosan-based nanofibrous membranes for antibacterial filter ap-plications. Carbohydr. Polym. 2013, 92, 254–259. https://doi.org/10.1016/j.carbpol.2012.08.114

24. Nivedita, S.; Joseph, S. Performance of polycaprolactone/TiO2 composite membrane for the effective treatment of dairy efflu-ents. Water Sci. Technol. 2021, 83, 2477–2485. https://doi.org/10.2166/wst.2021.143

25. Valerini, D.; Tammaro, L.; Vitali, R.; Guillot, G.; Rinaldi, A. Sputter-deposited ag nanoparticles on electrospun pcl scaffolds: Morphology, wettability and antibacterial activity. Coatings 2021, 11, 345. https://doi.org/10.3390/coatings11030345

26. Calvo-Flores, F.G.; Dobado, J.A. Lignin as renewable raw material. ChemSusChem 2010, 3, 1227–1235. https://doi.org/10.1002/cssc.201000157

27. Zhang, Y.; Naebe, M. Lignin: A review on structure, properties, and applications as a light-colored UV absorber. ACS Sustain. Chem. Eng. 2021, 9, 1427–1442. https://doi.org/10.1021/acssuschemeng.0c06998

28. Larrañeta, E.; Imízcoz, M.; Toh, J.X.; Irwin, N.J.; Ripolin, A.; Perminova, A.; Domínguez-Robles, J.; Rodríguez, A.; Donnelly, R.F. Synthesis and characterization of lignin hydrogels for potential applications as drug eluting antimicrobial coatings for medical materials. ACS Sustain. Chem. Eng. 2018, 6, 9037–9046. https://doi.org/10.1021/acssuschemeng.8b01371

29. Torres, L.A.Z.; Woiciechowski, A.L.; de Andrade Tanobe, V.O.; Karp, S.G.; Lorenci, L.C.G.; Faulds, C.; Soccol, C.R. Lignin as a potential source of high-added value compounds: A review. J. Clean. Prod. 2020, 263, 121499. https://doi.org/10.1016/j.jclepro.2020.121499

30. Wang, T.; Li, H.; Diao, X.; Lu, X.; Ma, D.; Ji, N. Lignin to dispersants, adsorbents, flocculants and adhesives: A critical review on industrial applications of lignin. Ind. Crops Prod. 2023, 199, 116715. https://doi.org/10.1016/j.indcrop.2023.116715

31. Cramariuc, B.; Cramariuc, R.; Scarlet, R.; Manea, L.R.; Lupu, I.G.; Cramariuc, O. Fiber diameter in electrospinning process. J. Electrost. 2013, 71, 189–198. https://doi.org/10.1016/j.elstat.2012.12.018

32. Faramarzi, A.-R.; Barzin, J.; Mobedi, H. Effect of solution and apparatus parameters on the morphology and size of elec-trosprayed PLGA microparticles. Fibers Polym. 2016, 17, 1806–1819. https://doi.org/10.1007/s12221-016-6685-3

33. Hohman, M.M.; Shin, M.; Rutledge, G.; Brenner, M.P. Electrospinning and electrically forced jets. I. Stability theory. Phys. Fluids 2001, 13, 2201–2220. https://doi.org/10.1063/1.1383791

34. Rutkowski, S.; Si, T.; Gai, M.; Frueh, J.; He, Q. Hydrodynamic electrospray ionization jetting of calcium alginate particles: Effect of spray-mode, spraying distance and concentration. RSC Adv. 2018, 8, 24243–24249. https://doi.org/10.1039/C8RA03490G

35. Basu, S.; Jassal, M.; Agrawal, A.K. Concept of minimum electrospinning voltage (MEV) in electrospinning of PAN–DMF system: Effect of distance. J. Text. Inst. 2013, 104, 158–163. https://doi.org/10.1080/00405000.2012.703797

36. Zong, H.; Xia, X.; Liang, Y.; Dai, S.; Alsaedi, A.; Hayat, T.; Kong, F.; Pan, J.H. Designing function-oriented artificial nano-materials and membranes via electrospinning and electrospraying techniques. Mater. Sci. Eng. C 2018, 92, 1075–1091. https://doi.org/10.1016/j.msec.2017.11.007

37. Liao, Y.; Loh, C.-H.; Tian, M.; Wang, R.; Fane, A.G. Progress in electrospun polymeric nanofibrous membranes for water treatment: Fabrication, modification and applications. Prog. Polym. Sci. 2018, 77, 69–94. https://doi.org/10.1016/j.progpolymsci.2017.10.003

38. Munir, M.M.; Suryamas, A.B.; Iskandar, F.; Okuyama, K. Scaling law on particle-to-fiber formation during electrospinning. Polymer 2009, 50, 4935–4943. https://doi.org/10.1016/j.polymer.2009.08.011

39. McKee, M.G.; Wilkes, G.L.; Colby, R.H.; Long, T.E. Correlations of solution rheology with electrospun fiber formation of linear and branched polyesters. Macromolecules 2004, 37, 1760–1767. https://doi.org/10.1021/ma035689h

40. Angammana, C.J.; Jayaram, S.H. Analysis of the effects of solution conductivity on electrospinning process and fiber mor-phology. IEEE Trans. Ind. Appl. 2011, 47, 1109–1117. https://doi.org/10.1109/TIA.2011.2127431

41. Bergamasco, S.; Zikeli, F.; Vinciguerra, V.; Sobolev, A.P.; Scarnati, L.; Tofani, G.; Scarascia Mugnozza, G.; Romagnoli, M. Ex-traction and Characterization of Acidolysis Lignin from Turkey Oak (Quercus cerris L.) and Eucalypt (Eucalyptus camaldulensis Dehnh.) Wood from Population Stands in Italy. Polymers 2023, 15, 3591. https://doi.org/10.3390/polym15173591

42. Deng, A.; Yang, Y.; Du, S. Tissue engineering 3D porous scaffolds prepared from electrospun recombinant human collagen (RHC) polypeptides/chitosan nanofibers. Appl. Sci. 2021, 11, 5096. https://doi.org/10.3390/app11115096

43. Di Carli, M.; Aurora, A.; Rinaldi, A.; Fiaschini, N.; Prosini, P.P. Preparation of Electrospun Membranes and Their Use as Sep-arators in Lithium Batteries. Batteries 2023, 9, 201. https://doi.org/10.3390/batteries9040201

44. Pozio, A.; Cemmi, A.; Carewska, M.; Paoletti, C.; Zaza, F. Characterization of gas diffusion electrodes for polymer electrolyte fuel cells. J. Fuel Cell Sci. Technol. 2010, 7, 041003. https://doi.org/10.1115/1.3119061

45. Freire, C.S.; Pinto, P.C.; Santiago, A.S.; Silvestre, A.J.; Evtuguin, D.V.; Neto, C.P. Comparative study of lipophilic extractives of hardwoods and corresponding ECF bleached kraft pulps. BioResources 2006, 1, 3–17. https://doi.org/10.15376/biores.1.1.3-17

46. Benouadah, N.; Pranovich, A.; Aliouche, D.; Hemming, J.; Smeds, A.; Willför, S. Analysis of extractives from Pinus halepensis and Eucalyptus camaldulensis as predominant trees in Algeria. Holzforschung 2018, 72, 97–104. https://doi.org/10.1515/hf-2017-0098

47. Wypych, G. Handbook of Adhesion Promoters; Elsevier: Amsterdam, The Netherlands, 2023. https://doi.org/10.1016/C2022-0-00535-3

48. Liu, W.; Walker, G.; Price, S.; Yang, X.; Li, J.; Bunt, C. Electrospun membranes as a porous barrier for molecular transport: Membrane characterization and release assessment. Pharmaceutics 2021, 13, 916. https://doi.org/10.3390/pharmaceutics13060916

49. Ahmadpour, M.; Mansourizadeh, A. Hydrophobic Modification of Polyetherimide Hollow Fiber Membrane Contactor by 2-(Perfluoroalkyl) Ethanol Coating for Carbon Dioxide Absorption. J. Appl. Membr. Sci. Technol. 2022, 26, 65–76. https://doi.org/10.11113/amst.v26n3.254

50. Borrega, M.; Päärnilä, S.; Greca, L.G.; Jääskeläinen, A.-S.; Ohra-Aho, T.; Rojas, O.J.; Tamminen, T. Morphological and wetta-bility properties of thin coating films produced from technical lignins. Langmuir 2020, 36, 9675–9684. https://doi.org/10.1021/acs.langmuir.0c00826

51. Notley, S.M.; Norgren, M. Surface energy and wettability of spin-coated thin films of lignin isolated from wood. Langmuir 2010, 26, 5484–5490. https://doi.org/10.1021/la1003337

52. Atifi, S.; Miao, C.; Hamad, W.Y. Surface modification of lignin for applications in polypropylene blends. J. Appl. Polym. Sci. 2017, 134, 45103. https://doi.org/10.1002/app.45103

53. Stefanović, I.S.; Džunuzović, J.V.; Džunuzović, E.S.; Dapčević, A.; Šešlija, S.I.; Balanč, B.D.; Dobrzyńska-Mizera, M. Compo-sition-property relationship of polyurethane networks based on polycaprolactone diol. Polym. Bull. 2021, 78, 7103–7128. https://doi.org/10.1007/s00289-020-03473-0

54. Kaur, R.; Uppal, S.; Sharma, P. Antioxidant and antibacterial activities of sugarcane bagasse lignin and chemically modified lignins. Sugar Tech 2017, 19, 675–680. https://doi.org/10.1007/s12355-017-0513-y

55. Gregorova, A.; Redik, S.; Sedlarik, V.; Stelzer, F. Lignin-containing polyethylene films with antibacterial activity. In Proceedings of the 3rd International Conference on Thomson Reuters of NANOCON, Brno, Czech Republic, 21–23 September 2011; pp. 21–23

56. Li, K.; Zhong, W.; Li, P.; Ren, J.; Jiang, K.; Wu, W. Antibacterial mechanism of lignin and lignin-based antimicrobial materials in different fields. Int. J. Biol. Macromol. 2023, 252, 126281. https://doi.org/10.1016/j.ijbiomac.2023.126281

57. Jusic, J.; Tamantini, S.; Romagnoli, M.; Vinciguerra, V.; Di Mattia, E.; Zikeli, F.; Cavalera, M.; Scarascia Mugnozza, G. Improving sustainability in wood coating: Testing lignin and cellulose nanocrystals as additives to commercial acrylic wood coatings for bio-building. Iforest-Biogeosci. For. 2021, 14, 499. https://doi.org/10.3832/ifor3782-014

58. Gao, H.; Sun, M.; Duan, Y.; Cai, Y.; Dai, H.; Xu, T. Controllable synthesis of lignin nanoparticles with antibacterial activity and analysis of its antibacterial mechanism. Int. J. Biol. Macromol. 2023, 246, 125596. https://doi.org/10.1016/j.ijbiomac.2023.125596

59. Badaraev, A.D.; Lerner, M.I.; Bakina, O.V.; Sidelev, D.V.; Tran, T.-H.; Krinitcyn, M.G.; Malashicheva, A.B.; Cherempey, E.G.; Slepchenko, G.B.; Kozelskaya, A.I. Antibacterial Activity and Cytocompatibility of Electrospun PLGA Scaffolds Sur-face-Modified by Pulsed DC Magnetron Co-Sputtering of Copper and Titanium. Pharmaceutics 2023, 15, 939. https://doi.org/10.3390/pharmaceutics15030939

60. ISO 21920-1:2022; Geometrical product specifications (GPS) — Surface texture: Profile — Part 1: Indication of surface texture. International Organization for Standardization ISO: Verier, Switzerland, 2022.

Conclusion and future perspectives

The highly versatile nature of lignin, with its structurally diverse and functionalized composition, has garnered increasing interest in recent years for utilizing lignocellulosic biomass waste, with a specific focus on valorizing its components. In the context of this research project, the primary objective was to highlight lignin extraction methodologies from Italian biomass sources such as oak and eucalyptus, aiming to obtain a material as pure as possible and adopting extraction processes with minimal environmental impact. Another significant challenge involved the application of lignin in creating new bio-based materials, leveraging nanotechnology processing techniques. Both aspects focused on utilizing lignin in the field of coatings but in different industrial contexts.

From this research, the following conclusions can be drawn:

- The treatments used to extract lignins from oak and eucalyptus wood demonstrate a significant impact on the chemical structure of the recovered material. While ensuring a high degree of purity for both processes, differences in substructures emerge, attributable to the distinct mechanisms involved during isolation.
- Despite the lower lignin yield from the ionic liquid treatment compared to acidolysis, NMR analysis revealed that the respective lignin contains less carbohydrate impurities.
- The use of lignin as a structural analogue for petrochemical polyols has paved the way for the creation of highly effective urethane coatings for wood. This innovative formulation provides the opportunity to modulate the chemical and physical properties of the material based on the concentration of lignin present. The proposed approach represents a significant step toward the development of sustainable and customizable coatings, thereby contributing to the creation of more eco-friendly solutions for the wood and related materials sector.
- Electrospraying proves to be an intriguing technique for producing lignin nanocoatings, with excellent results demonstrating the ability to modulate the properties of the underlying PCL membrane based on the amount of electrospun lignin. Compared to previous applications, this methodology requires considerably lower amounts of lignin, a crucial aspect for potential large-scale implementations, thus contributing to efficient resource management.

Future perspectives

The work carried out in this research project aims to promote the sustainable use of lignin in various application sectors, leading to innovative solutions with a positive environmental impact. Below are some key points to consider for future developments:

- To delve deeper into the extraction processes and explore possibilities for potential scaling up, the focus should be on green extraction methods such as ionic liquids. Investigate their recyclability at the end of the extraction process and optimize extraction yields.
- Explore and develop new applications for lignins in various sectors beyond coatings. Promote synergies between different disciplinary sectors to fully exploit the properties and potential of lignin.
- Invest in and explore emerging technologies for the production of nanocomposite materials.
- Plan a life cycle assessment (LCA) for both the extraction processes and extend it to the final products. Evaluate the environmental impact and sustainability of the entire life cycle of lignin-based materials.
- These strategies aim to enhance the efficiency, sustainability, and applications of lignin, contributing to its broader adoption in diverse industries.

List of publications

1. Bergamasco, S.; Tamantini, S.; Zikeli, F.; Vinciguerra, V.; Scarascia Mugnozza, G.; Romagnoli, M. Synthesis and characterizations of eco-friendly organosolv lignin-based polyurethane coating films for the coating industry. Polymers 2022, 14, 416, https://doi.org/10.3390/polym14030416

2. Tamantini, S.; Bergamasco, S.; Portoghesi, L.; Vettraino, A.M.; Zikeli, F.; Mugnozza, G.S.; Romagnoli, M. Detection, description, and technological properties of colour aberration in wood of standards and shoots from a chestnut (Castanea sativa Mill.) coppice stand. European Journal of Forest Research 2022, 141, 683-698, https://doi.org/10.1007/s10342-022-01468-2

3. Vettraino, A.M.; Zikeli, F.; Humar, M.; Biscontri, M.; Bergamasco, S.; Romagnoli, M. Essential oils from Thymus spp. as natural biocide against common brown-and white-rot fungi in degradation of wood products: Antifungal activity evaluation by in vitro and FTIR analysis. European Journal of Wood and Wood Products 2023, 81, 747-763, https://doi.org/10.1007/s00107-022-01914-3

4. Tamantini, S.; Bergamasco, S.; Zikeli, F.; Humar, M.; Cavalera, M.; Romagnoli, M. Cellulose Nano Crystals (CNC) as Additive for a Bio-Based Waterborne Acrylic Wood Coating: Decay, Artificial Weathering, Physical and Chemical Tests. Nanomaterials 2023, 13, 442, https://doi.org/10.3390/nano13030442

5. Zikeli, F.; Vettraino, A.M.; Biscontri, M.; Bergamasco, S.; Palocci, C.; Humar, M.; Romagnoli, M. Lignin Nanoparticles with Entrapped Thymus spp. Essential Oils for the Control of Wood-Rot Fungi. Polymers 2023, 15, 2713, https://doi.org/10.3390/polym15122713

6. Bergamasco, S.; Zikeli, F.; Vinciguerra, V.; Sobolev, A.P.; Scarnati, L.; Tofani, G.; Scarascia Mugnozza, G.; Romagnoli, M. Extraction and Characterization of Acidolysis Lignin from Turkey Oak (Quercus cerris L.) and Eucalypt (Eucalyptus camaldulensis Dehnh.) Wood from Population Stands in Italy. Polymers 2023, 15, 3591, https://doi.org/10.3390/polym15173591

7. Bergamasco, S.; Fiaschini, N.; Hein, L.A.; Brecciaroli, M.; Vitali, R.; Romagnoli, M.; Rinaldi, A. Electrospun PCL Filtration Membranes Enhanced with an Electrosprayed Lignin Coating to Control Wettability and Anti-Bacterial Properties. Polymers 2024, 16, 674, https://doi.org/10.3390/polym16050674